Thermomechanical Analysis of Ancient Roman Seawater Concrete

Torin Nicolas McCue

Czech Republic | 2019

ADVANCED MASTERS IN STRUCTURAL ANALYSIS
OF MONUMENTS AND HISTORICAL CONSTRUCTIONS

Master's Thesis

Torin Nicolas McCue

Thermomechanical Analysis of Ancient Roman Seawater Concrete

CTU

CZECH TECHNICAL
UNIVERSITY
IN PRAGUE

University of Minho

Czech Republic | 2019

UPC

ARCCHIP

Master's Thesis

Torin Nicolas McCue

Thermomechanical Analysis of Ancient Roman Seawater Concrete

CZECH TECHNICAL UNIVERSITY IN PRAGUE
Faculty of Civil Engineering
Thákurova 7, 166 29 Prague 6, Czech Republic

MASTER'S THESIS PROPOSAL

study programme: Civil Engineering

study branch: Advanced Masters in Structural Analysis of Monuments and Historical Constructions

academic year: 2018/2019

Student's name and surname: Torin Nicolas McCue

Department: Department of Mechanics

Thesis supervisor: Vít Šmilauer

Thesis title: Thermomechanical Analysis of Ancient Roman Seawater Concrete

Thesis title in English see above

Framework content: The main objective of this thesis is to analyze temperature and stress development in hardening massive Roman concrete piers. The objective was accomplished using a non-stationary thermal finite element (FE) analysis and a staggered thermomechanical analysis with ageing viscoelastic material law.

Assignment date: 1/04/2019   Submission date: 8/09/2019

If the student fails to submit the Master's thesis on time, they are obliged to justify this fact in advance in writing, if this request (submitted through the Student Registrar) is granted by the Dean, the Dean will assign the student a substitute date for holding the final graduation examination (2 attempts for FGE remain). If this fact is not appropriately excused or if the request is not granted by the Dean, the Dean will assign the student a date for retaking the final graduation examination, FGE can be retaken only once. (Study and Examination Code, Art 22, Par 3, 4.)

The student takes notice of the obligation of working out the Master's thesis on their own, without any outside help, except for consultation. The list of references, other sources and names of consultants must be included in the Master's thesis.

....
Master's thesis supervisor   Head of department

Date of Master's thesis proposal take over: July 2019

....
Student

This page is left blank on purpose.

DECLARATION

Name: Torin Nicolas McCue

Email: mccue.torin@gmail.com

Title of the
Msc Dissertation: Thermomechanical Analysis of Ancient Roman Seawater Concrete

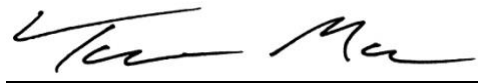Supervisor(s):   Vít Šmilauer

Year: 2019

I hereby declare that all information in this document has been obtained and presented in accordance with academic rules and ethical conduct. I also declare that, as required by these rules and conduct, I have fully cited and referenced all material and results that are not original to this work.

I hereby declare that the MSc Consortium responsible for the Advanced Masters in Structural Analysis of Monuments and Historical Constructions is allowed to store and make available electronically the present MSc Dissertation.

University: Czech Technical University in Prague

Date: July 8th, 2019

Signature:

This page is left blank on purpose.

ACKNOWLEDGEMENTS

I would like to thank my advisor, Dr. Vít Šmilauer, for being so supportive and over the top helpful throughout the extent of my thesis. You were always accessible, answering every question I had, and my thesis would certainly not be at the state it is without your strong guidance and support learning how to navigate the OOFEM code. Further thanks to Bořek Patzák and all other developers and contributors to the open source OOFEM code that made my analyses possible.

I would like to thank all of the professors from CTU, UMinho, UPC, and UNIPD who contributed their valuable time to lead the coursework, and all other faculty helping organize the program. I've learned a great deal in a short amount of time thanks to the well-presented content of the SAHC program.

My special thanks are extended to all my colleagues and friends also in the SAHC Masters in Prague and Guimarães, where it was a pleasure to study in such great company. It has been an unforgettable year that allowed me to experience many new parts of the world.

I would also like to give thanks to the SAHC consortium for the financial support provided by their gracious scholarship.

Finally, I would like to thank my family for their unwavering support leading up to and throughout my stay abroad. Without them I would not be anywhere near where I am today.

This page is left blank on purpose.

ABSTRACT

Ancient Romans were able to synthesize highly durable hydraulic concretes lasting over 2000 years while submerged in the Mediterranean Sea because of the formation of durable C-A-S-H gel, Al-tobermorite and phillipsite by alkali activation of alumina-rich volcanic materials. With hopes of being able to synthesize such robust phases within innovative concretes in the future, it is necessary to thoroughly understand the mechanism for how they form. Previous research has shown that two of the of the driving factors for their formation is the mineralizing effects seawater has in combination with the volcanic ash and the high temperatures that develop within massive concrete structures due to the pozzolanic reaction.

Using a non-stationary thermal finite element (FE) analysis this thesis has validated the studies looking into the evolution of temperature throughout a massive hardening Roman concrete pier and determined the secondary effects on temperature-rise due to partial replacement of slaked lime with quicklime, and a more realistic multi-day casting process required to pour the large volume of concrete.

Following thermal analyses, the stress development in the hardening concrete piers was analysed using a staggered thermomechanical FE analysis with ageing viscoelastic material law to understand any deleterious effects the large temperature rise may cause from a mechanical standpoint. Due only to the thermal expansion and contraction of the hydrating block, significant tensile stresses were found to occur at the outer portions of the block during early age, and at the core of the block during late age, likely suggesting cracking at various locations.

Keywords: Roman seawater concrete, thermomechanical analysis, stress development

This page is left blank on purpose.

ABSTRAKT

Termomechanická analýza starodávného římského betonu v mořské vodě

Starověcí Římané uměli vyrobit vysoce trvanlivý hydraulický beton, který ve Středozemním moři vydržel přes 2000 let. Dlouhá životnost se přičítá alkalické aktivaci vulkanických materiálů bohatých na hliník, které vedly k syntéze C-A-S-H gelu, Al-tobermoritu a filipsitu. Pro syntézu těchto robustních fází v inovativních betonech je nezbytné porozumět mechanismům jejich vzniku. Předchozí výzkum ukázal, že jsou důležité dva faktory k jejich vzniku, a to mineralizující účinek mořské vody a vysoké teploty, které vznikají uvnitř masivních betonů díky pucolánové reakci.

Tato práce používá metodu konečných prvků pro úlohu nestacionárního vedení tepla. Tou se ověřují předešlé studie teplot během tvrdnutí římských betonů na masivních mořských molech. Také se určují druhotné efekty jako náhrada hašeného vápna vápnem nehašeným, a více realistický několikadenní proces lití pro velkoobjemové konstrukce.

Po termální anlýze byla provedena slabě sdružená mechanická analýza tvrdnoucího betonu na molech pomocí metody konečných prvků. Použil se stárnoucí materiál s dotvarováním pro porozumění vývoje napětí díky nárůstu teplot. Díky termální expanzi a smrštění betonu došlo ke vzniku tahových napětí, v raných fázích zejména na povrchu betonu, v pozdějších fázích uprostřed bloku. Tato tahová napětí značí vznik trhlin v těchto místech.

Klíčová slova: římský beton v mořské vodě, termo-mechanická analýza, vývoj napětí

This page is left blank on purpose.

TABLE OF CONTENTS

LIST OF FIGURES

LIST OF TABLES

This page is left blank on purpose.

1. INTRODUCTION

Ancient Romans were able to synthesize highly durable hydraulic concretes lasting over 2000 years while submerged in the Mediterranean Sea because of the robust hydrate products formed through the hydration reaction, which have been the focus of many recent studies. These efforts have been successful in characterizing the unique chemical composition of the C-A-S-H gel, Al-tobermorite and phillipsite phases suspected of contributing to the durability of the concrete (M. D. Jackson, Chae, et al., 2013; M. Jackson et al., 2017). However, some questions still linger about the reaction mechanisms with most of the uncertainty relating to the temperature-time profile that the pozzolanic reaction developed within large blocks of the concrete.

Large blocks of the concrete material can be found submerged throughout harbors in the Mediterranean sea with the earliest dated structure tied back to the late 2nd century BC (Gazda & McCann, 1987). The ancient material was primarily used to construct sets of *pilae* (Latin for piers) surrounding beaches and harbors acting as breakwaters to stop large waves and disrupt tides. This meant they had to have adequate strength, excellent durability and large surface area, with the typical *pila* being measured as approximately 10m x 10m wide and of varying heights (Brandon, Hohlfelder, Jackson, & Oleson, 2014).

Figure 1. Typical *pila* being cored for experimental trials during the ROMACONS project. (J. Oleson et al., 2004)

The main objective of this thesis is to analyze temperature and stress development in hardening massive Roman concrete piers. The objective was accomplished using a non-stationary thermal finite element (FE) analysis and a staggered thermomechanical analysis with ageing viscoelastic material law.

Expanding upon the concept of temperature development, three subsets of the thermal analysis were conducted to compare independent variables based on unknowns about either the Roman concrete mix design, or the construction process. These analyses are as follows:

- The use of seawater versus freshwater for the concrete mix design
- The influence of a multi-day casting construction process
- The influence of including portions of quicklime for the concrete mix design

The heat of reaction for the material model was characterized by running short-term experimental tests using metakaolin-lime mortars designed to closely mimic the Roman seawater concretes.

2. ROMAN CONCRETE STATE OF THE ART

2.1 General Material Information

Concrete has long been regarded as one of the most impactful inventions throughout history and is certainly one of the most important building materials engineered to date, with worldwide production of more than 10 billion tons each year (Meyer, 2009). Concrete has long been one of the most implemented construction materials because of its excellent mechanical and durability properties, while still remaining easily available and highly affordable. One of the most important constituents of modern-day concrete is ordinary Portland cement (OPC), which is a binding material manufactured by burning and grinding a mixture of limestone and clay, that was first patented in 1824 (Ryan, 1929). However, looking back through history, literature has established that Roman builders discovered how to create hydraulic mortar much earlier, sometime in the 2nd or 3rd century BC (J. Oleson et al., 2004).

The critical similarity between modern-day concretes and the supposed hydraulic mortar used over 2000 years ago by the Romans, is the hydraulic nature of the two materials. Hydraulic mortars or concretes have two specific properties: the capacity of hardening upon the combination of the dry binder with water, and the ability for the mixture to set while completely submerged in water (Sabbioni, Bonazza, & Zappia, 2002). This distinguishing feature of the Roman concrete allowed for its use in the construction of maritime structures, a process that was previously impossible due to lime-based mortar's inability to set underwater.

The key to achieving such hydraulic reaction was the substitution of the pure silica sand for volcanic ash *pulvis puteolanus*, most often referred to as pozzolanic materials or simply pozzolans (J. Oleson et al., 2004). These materials are made up of chemically reactive aluminosilicates, which react with lime and water to form cementitious calcium aluminates and silicates (Cowper, 1927). This hydraulic reaction revolutionized concrete production in ancient Roman cities, especially those nearest to the many volcanoes around Italy.

Pozzolans are either natural or artificial materials that react with lime and water to produce calcium silicate and aluminate hydrates, which provides cementitious properties to the mix. Natural pozzolans can be classified by their origin and the primary phase associated with its reactivity as per the following list (Franco Massazza, 1998):

1. Volcanic, incoherent, rich in unaltered or partially-altered glass
2. Tuffs, where volcanic glass has been transformed, entirely or partially, into zeolitic compounds
3. Sedimentary, rich in opaline diatoms
4. Diagenetic, rich in amorphous silica, resulting from the weathering process of siliceous rocks

According to the chemical thermodynamic rules, any blend of silica, or silicates, with lime and water should synthesize calcium silicate hydrates, which is considered the *pozzolanic reaction* (F Massazza, 2002). However, for this reaction to be possible, one of three activation methods must be provided: thermal activation, mechanical activation, or chemical activation. Thermal activation is created by means of either calcination of the pozzolans, or by curing the material at high temperatures to increase reaction kinetics. Mechanical activation is created by prolonged grinding of the pozzolan to increase the effective surface area of the particles, thus leading to an increase in solubility. And chemical activation occurs when either the pozzolan is chemically treated to increase reactivity, or a chemical activator is added to the fresh-state mix (e.g. $Ca(OH)_2$, $NaOH$ or Na_2SO_4) (Shi, 2001).

For the Roman seawater concrete, it is suspected that the alkaline salts (primarily $NaCl$) in the natural seawater are the contributing activators. Thus, the fact that the concrete is cast underwater significantly effects the rate of hydration and likely the temperature developed within the material.
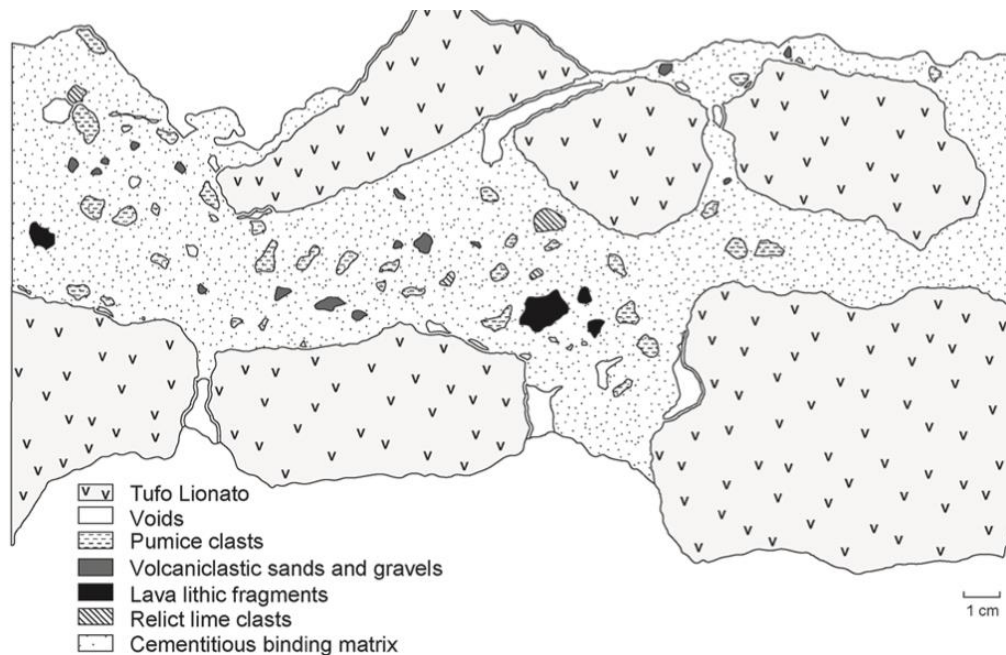
Figure 2. Macroscale map of a portion of Roman seawater concrete showing principal components. (Brandon et al., 2014)

The above photo illustrates a macroscale section cut of the typical Roman seawater concrete with each independent phase separately labeled. This clearly shows the difference between mortar and aggregate, with the presence of large decimeter sized aggregates at a typical mortar: aggregate ratio of about 1.7 (J. Oleson et al., 2004). It is also important to recognize the semi-frequent occurrences of small voids, which corresponds with the approximate porosity measured at 45% being significantly higher than modern-day OPC concrete.

The other takeaway is the presence of numerous relict clasts of either unreacted pumice, lime, or other pozzolanic materials. The Romans didn't perfectly grind the binder or perfectly fire the raw lime for every mix and were left with small chunks of material that didn't fully dissolve in the concrete mix and remained in-tact after the setting of the concrete. These relict clasts first seemed inconsequential, but later findings suggest that most of these clasts serve as nucleation sites for the synthesis of crystalline Al-tobermorite and phillipsite, both of which considerably improve the mechanical properties of the concrete (M. D. Jackson, Chae, et al., 2013; M. Jackson et al., 2017).

2.2 Ancient Roman Texts

Many famous Roman engineers, architects, and philosophers wrote detailed ancient texts serving as some of the first documentation of the over 2000-year-old Roman marine concretes, more specifically regarding proper material constituents, constituent ratios and origins, formwork and concrete pouring procedures, why they thought the hydration of quicklime gave off heat as it sets, and why the concrete developed its strength and durability (Brandon et al., 2014).

It all began with terrestrial concrete, where the generic term in Latin for concrete structural work was probably opus caementicium, although the term rarely comes up following the first-century BC (Brandon et al., 2014). The Romans focused more than modern-day builders on large aggregates (caementa) rather than the mortar mix (materia, materies, or calx harenatus), primarily from an economic standpoint because they realized using fist-sized aggregate leads to a much faster and cheaper building procedure (Janet DeLaine, 2002, pp. 236–239).

2.2.1 Vitruvius, *De architectura*

Probably the most important author for the modern understanding and recreation of Roman seawater concrete is Vitruvius, who wrote the only surviving ancient handbook of architecture, *De architectura*, likely published between 30 and 22 BC (Rowland & Howe, 2001). The collection of text is a series of ten books sometimes termed 'The Ten Books on Architecture', where the passages from the earlier books concern the material side of construction and architecture, whereas the later books concern building procedures.

Vitruvius reports in *De architectura* (2.5.1-3) the importance of preparing a proper lime from white stone or limestone that is made from dense and rather hard stone for the best use in concrete work. He then follows up immediately with proper ratios of *pozzolana* to lime binder as follows (2.5.1):

> Mix the mortar (*materia*) according to these formulae: if it is quarry sand (*harena fossicia*), mix three portions of sand to one portion of lime. If it is river or beach sand, mix two portions of sand with one of lime.

This specific formula has been interpreted by many as his mix proportions only for terrestrial concrete structures (Brandon et al., 2014). His later book (*De architectura* 5.12.1; Passage 9) is where he

specifies that the mix proportions for maritime concrete are two parts *pozzolana* to one-part lime (Lancaster, 2005: 55). Further comparisons with experimental data from extracted Roman concrete cores will be discussed later in this chapter. Although the comparisons determine the ratio is most likely closest to 2.7:1, which gives way to the assumption that quality control wasn't the top concern and that the terrestrial mix proportions could have been widely accepted by all builders no matter the scope of their project (J. P. Oleson et al., 2006).

After discussing the proportions of the material constituents, Vitruvius moved onto the sourcing of the materials and this seems to be the most important parameter studied by many Roman builders. He reports in his next book, *De architectura* that (2.6.1):

> There is a kind of powdery earth (*pulvis*) that by its nature produces wonderful results. It occurs (*nascitur*) in the neighborhood of Baiae and the territory of the municipalities around Mount Vesuvius. This material, when mixed with lime and rubble (*calce et caementa*), not only furnishes strength to other buildings, but also, when breakwaters (*moles*) are built in the sea, they set under water.

This statement reads that the origin of the Roman concrete *Puteolanus pulvis* is the region around Puteoli, and around the Bay of Pozzuoli in the Flegrean Fields volcanic district near Baiae, which is re-iterated upon about a century later by Pliny the Elder. He concludes the same section by explaining that the material properties of *pulvis* and tuff are developed through the action of extreme heat deep within the earth; whereas, hydrated lime is produced by heat in a man-made kiln. And therefore (2.6.1):

> When these three substances formed in a similar manner by the strength of fire are brought together into one mixture, and suddenly they are put in contact with [sea-]water, they cohere into a single mass, quickly solidifying, hardened by the moisture, and neither the force of the waves nor the effect of water can dissolve them.

The previous statement is the only relevant report regarding the use of water in the preparation of the mortar before pouring into the molds. Neither Vitruvius nor any other ancient literary source specifically differentiates between the use of seawater and fresh-water for the preparation of the mortar and because Vitruvius is so careful to specify the source and quality of the lime and pozzolans, it is assumed that he certainly would have specified fresh-water if it was necessary. Therefore, seawater from the harbor is assumed to be the only water source for the fresh-state Roman maritime concrete.

To summarize the texts from Vitruvius including numerous changes in proportions or protocols between the ten books, the most generally accepted specifications for Roman seawater concrete from *De architectura* are as follows:

- Lime:pozzolan (*calx:pulvis*) – 1:2 (by volume)
- Origin of pozzolan - Puteoli, and around the Bay of Pozzuoli in the Flegrean Fields volcanic district near Baiae

2.3   Current Research Findings

Up to date, numerous studies have looked into ancient Roman concrete with most of the studies before the 21st century analyzing terrestrial concretes, which aren't relevant for the scope of this thesis because of the significant difference in the mix design and the ensuing material properties. The earlier research studies specifically involving maritime Roman concretes were generally site-specific questions or historical surveys of architectural developments with little focus given to the material itself or material properties.

The first documented structural use of hydraulic concrete on land in central Italy was in the late 3rd century BC (Adam, 1994, pp. 79, 127–128), and the earliest surviving structure built with hydraulic concrete is located in the harbor at Cosa, a Roman colony ~150 km north of Rome (Gazda & McCann, 1987). The location of this port is highlighted by the green circle labeled as 2, shown in Figure 3 below, which visualizes the majority of the studied ancient Roman seawater concrete harbor sites across the Italian coast.
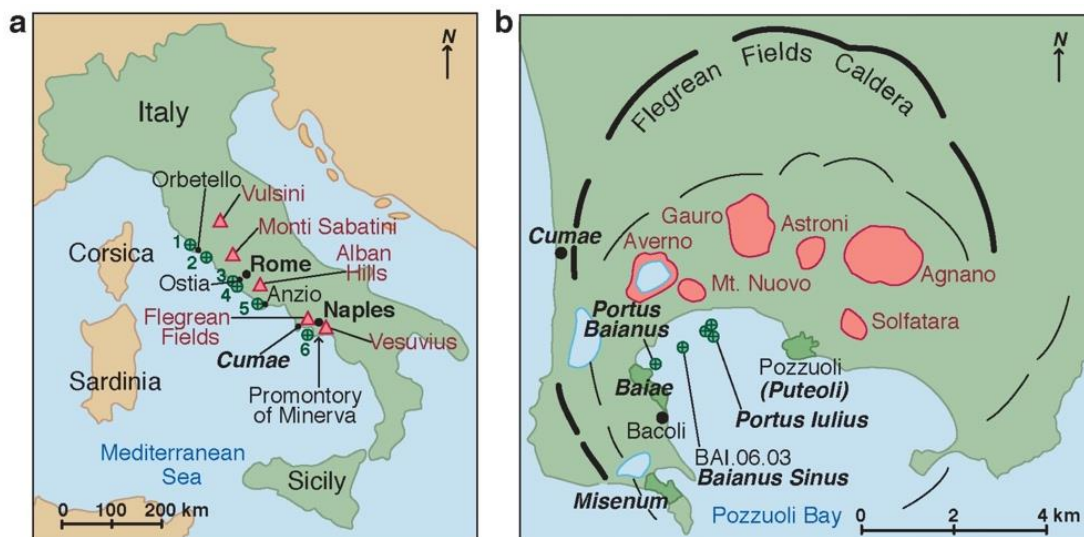
Figure 3. Ancient Roman seawater concrete harbor sites across the central Italian coast; (left) drill sites from ROMACONS project (green circles) and associated volcanic districts (red triangles); (right) Flegrean Fields caldera adjacent to the Pozzuoli Bay, where ROMACONS cores where extracted (green circles). (M. D. Jackson, Chae, et al., 2013)

2.3.1   Dating the Earliest Maritime Roman Concrete

Before much attention was given to studying the chemical composition or material and mechanical properties of the concrete, the material first had to be dated so that researchers knew the approximate

age of the maritime structures and the constituents. One of the first ground-breaking studies hoping to solve this question was the series of excavations by McCann et al. in the 1960's and 1970's.

Anna Marguerite McCann and her group of 21 other specialists conducted an almost decade long project from 1965-1972 involving numerous excavations both on land and underwater at the Roman harbor site with the earliest surviving hydraulic concrete structures, *Portus Cosanus* (Gazda & McCann, 1987). Their excavations firmly established that the port was first used by the Romans in the 3rd century BC and extending into the 3rd century AC, primarily by means of dating amphora sherds – a type of ceramic pottery found on site.

The team located five piers consisting of *tufo* and *pozzolana* concrete with amphora sherds of the ceramic jars showing up in the aggregate as well. The five piers form a line extending from the beach (Figure 4), presumably to act as docking facilities in addition to breakwaters for the prevailing beaches with three of the five appearing to be of the same size today as that of their original construction (Gazda & McCann, 1987). One of the five appears to have served as a quarry for building material as is apparent from missing portions of the pier observed by visual observation. The depth of the channel during ancient times was calculated to be approximately six meters, which provided an area of protected water large enough for ships about 30 meters or less in length (Casson, 1977). Comparison of the surveyed sea levels and surrounding geologic conditions of the bay with other studies by J. Lewis, estimates the ancient sea level to be approximately one meter below the present sea level (Lewis, 1972).
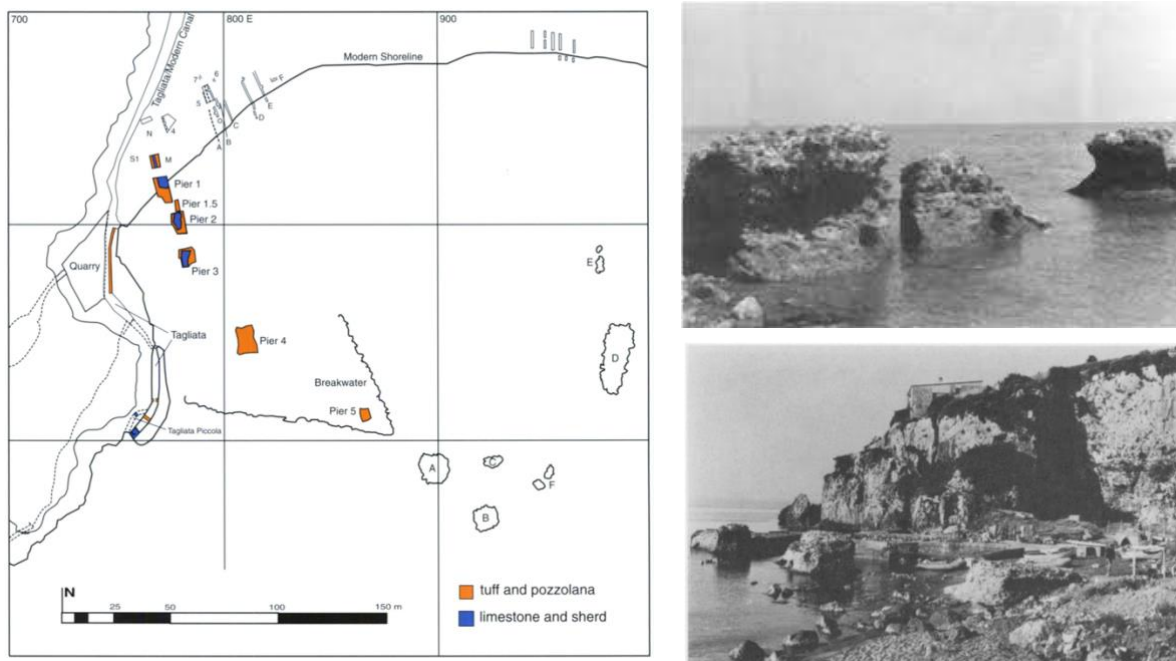
Figure 4. (left) Map of Portus Cosanus with the five piers highlighted; (right) two photos of the existing breakwaters. (Gazda & McCann, 1987)

Extensive surveying and documentation were conducted at numerous nearby inland structures built with either limestone or concrete as well as the concrete walls of an adjacent lagoon and fish tanks determined to have been used to keep fish awaiting market. The findings show that most inland structures making use of concrete or mortar used a different mix design (than that of the maritime structures) with amphora fragments as aggregate as well as other Italian glass fragments. However, all concrete in direct and constant contact with water was built with the *tufo* and *pozzolana* Roman maritime concrete mix with tuff aggregate. Both of those materials had to be imported to Cosa because the nearest Volsinian quarry containing *pozzolana* was about 35 kilometers away, although it is more likely that the imported *pozzolana* came from the region around Baiae and Puteoli as per Vitruvius and Pliny the Elder's ancient specifications (Gazda & McCann, 1987).

The excavations at *Portus Cosanus* of Cosa officially brought to light the earliest documented Roman harbor making use of the *tufo* and *pozzolana* concrete similar to the mix designs written about in ancient Roman literature. The material was no doubt discovered in the 3rd or 2nd centuries BC in the region of Puteoli, where the critical ingredients naturally appear. However, the successful dating of the amphora fragments found within the concrete aggregate of the maritime piers constitutes the earliest surviving and datable evidence of its use in water – sometime between the late 2nd century BC and the second quarter of the 1st century BC (Gazda & McCann, 1987).

2.3.2   Concrete Coring Campaign for Laboratory Testing

Following the excavation efforts of McCann and her team, there was still very little completed research put forth towards the material or mineralogical scale of the ancient Roman concretes. There was also very little collaboration between archaeologists and scientists, which was a necessary task in order to get an in-depth understanding of how this ancient concrete shows such outstanding durability compared to its modern OPC counterpart. However, to touch on all of these topics, the research community first needed quality samples of the ancient concrete to study in a laboratory setting. Although extracting over 2000-year-old seawater concrete was no simple task and usually not feasible for many small-scale studies.

To help provide these samples for the community, the ROMACONS project of the early 2000's spearheaded the first project developing a unique method to extract numerous cores from ancient maritime structures from all across the Italian coast (Figure 3 – map above). These cores would be first studied and documented by the ROMACONS team, and then stored at the laboratories of Italcementi of Bergamo, Italy, where they became easily accessible to numerous researchers moving forward. The easy access to such specific samples of ancient Roman seawater concrete led to numerous scientific breakthroughs down the road.

Christopher Brandon, John Peter Oleson, and Robert Hohlfelder founded the Roman Maritime Concrete Study (ROMACONS) in 2001, beginning an extensive coring effort to collect numerous large core samples of Roman maritime concrete at well-dated structures throughout the Mediterranean Sea (Hohlfelder, Brandon, & Oleson, 2008). Starting at the Bay of Naples in 2002 and ending in 2009, 36 cores were extracted from 12 different maritime sites to be used for analytical investigations using microscopy techniques, chemical analysis, and mechanical testing (Brandon et al., 2014). The ROMACONS project gave researchers access to ancient maritime hydraulic concrete samples for the first time in the form of full-length cores.

Previous material samples of the maritime structures were collected using a hammer and chisel, which was highly destructive when compared to the more complex task of extracting full-length cores. The hammer and chisel method required the removal of large surface areas of concrete just to collect small undisturbed samples, which left the historic fabric of some structures tarnished (Brandon et al., 2014). The coring method was a much more efficient means of collecting samples because the samples were obviously much larger and completely undisturbed making for ideal test specimens, while leaving almost no mark on the existing structures if proper repair protocols were followed. The ROMACONS protocol was to immediately fill the empty core holes with sea sand and seal them with a reinserted plug from the uppermost portion of the core, which was then set into place using a lean lime and *pozzolana* mortar (Brandon et al., 2014).

The ROMACONS team was meticulous in their selection of coring equipment in order to extract the samples as undisturbed as possible, while dealing with highly atypical coring conditions. The task of coring structures at sea, which are sometimes completely submerged, meant a pneumatic or hydraulically powered drill mounted on a rack and pinion rail was the best option as shown in Figure 5 and Figure 6. The selection of the drill bit was controlled by the fact that the team wanted to extract the standard 9 cm diameter core because that is what is used in most recognized civil engineering procedures.

Figure 5. *Portus Cosanus,* ROMACONS coring process at a hydraulic concrete *pila.* (Brandon et al., 2014)

Figure 6. *Portus Cosanus,* ROMACONS coring process at a hydraulic concrete *pila.* (Brandon et al., 2014)

Drill barrels were provided by a specialist drilling company (Xcalibre Equipment Ltd.) with four different barrel types, that were switched between throughout the project. All four of the barrel types used rugged diamond-tipped cutting surfaces to get through the mortar and tuff aggregate with ease. The coring was more difficult than modern concrete coring because of the large aggregate used within the pier, resulting in more heterogenous properties that sometimes led to fracturing of the cores within the barrel. While fractured cores were still extracted and used for testing, it was not optimal and was avoided as much as possible via continually refined drilling methods. Four specimens are shown in Figure 7, where one of the ROMACONS cores was divided into separate sub-cores that were all cut to the proper length for testing (175 mm).

Figure 7. Four sub-core specimens shaped from a ROMACONS full-length core with a typical diameter of 86.5 mm and a length of 175 mm. (Brandon et al., 2014; J. Oleson et al., 2004)

Another critical aspect of the coring procedure is the length of the barrel because the height of the pier ranged from a few meters up to around six meters. It was important to collect as long of a core as possible to get the most possible concrete for testing, while minimizing the amount of core holes. Full-length cores also gave a better look at the stratigraphic distribution of concrete composition from the base of the pier all the way to the top (Brandon et al., 2014). This was done using a continuous coring system that allowed 50cm or 1m sleeves to be incrementally screwed onto the start of the barrel to extend its overall length. This same procedure is used for modern concrete coring when greater depth is desired.

2.3.3   Mix Design

Upon excavation and initial analysis of the ROMACONS cores, numerous questions about the unique material were answered in regard to physical and mechanical properties, but the material had still not been accurately replicated and the only mix design proportions known were those documented by Vitruvius in *De architectura*.

To fill this void in the Roman concrete research, the ROMACONS team sought out to create an experimental campaign where they recreated a pier similar to the Roman *pilae* as closely as possible by following specifications by Vitruvius, while referencing findings from the extracted cores from the earlier research project. They built a roughly 8 m^3 pier in the harbor of Brindisi off the coast of Italy, using only materials believed to be available to the Romans at the time they constructed the original *pilae*.

Figure 8. (left) Prepared formwork for the Brindisi *pila*; (right) detailing the top surface*.* (J. P. Oleson et al., 2006)

Raw materials included lime paste, *pozzolana*, tuff aggregate, as well as seawater taken directly from the harbor as shown in Figure 9. The team matched the lime source as closely as possible to the lime analyzed in the ROMACONS cores and ended up using '*grassello di calce*', which is a form of slaked lime putty that arrived in 25-liter plastic bags. The pozzolan used was from a supplier from Bacoli, adjacent to Baiae, which is well within the region specified by Vitruvius. The coarse aggregate was also from Bacoli, but in the form of machine-sawn tuff blocks (30cm x 20cm x 10cm), which were later broken up into irregular 0.10-0.15 m diameter fragments.

Figure 9. Raw materials for the reproduction of the Brindisi pila; (left) lime putty; (middle) pozzolana; (right) tuff aggregate. (J. P. Oleson et al., 2006)

Three complications arise when basing mix proportions only off of translations from the Vitruvius specifications, which need further confirmation from literature:

- Did Vitruvius calculate the 1:2 lime:*pulvis* ratio based on weight or by volume?
- Did he consider slaked lime putty or dry quicklime?
- Did he consider wet or dry *pozzolana?*

When looking at the Vitruvius specifications, he never explicitly references slaked lime putty when reporting on maritime concretes, although in his specifications for terrestrial concretes (*De arch.* 2.5.1; pp. 16-17, Passage 6) he says, "once the lime has been slaked, mix the mortar (*materia*) according to these formulae: if it is quarry sand (*harena fossicia*), mix three portions of sand to one portion of lime". From this, it is assumed that for maritime concrete, slaked lime was aged and then combined with the *pozzolana,* at his maritime specification (*De arch.* 5.12.2) of two to one proportion, immediately before use. This was also the view that the team at ROMACONS took for the reconstruction of their test pier at the harbor of Brindisi (Brandon et al., 2014).

The ROMACONS team looked into the question of mixing dry versus wet *pozzolana* by mixing 16 batches of mortar with slightly different proportions from 1:2 to 1:2.7 *lime:pulvis*. The reason for these specific numbers is because the 25% volume change resulting from the addition of water to the *pozzolana* (J DeLaine, 1997, p. 23) means a 1:2 ratio of wet *pozzolana* is equivalent to a 1:2.7 ratio of dry *pozzolana*. Later comparison of the cores extracted from these varying batches of mortar shows that the chemical composition of the concrete with 1:2.7 ratio was closer to the original ROMACONS samples than any other mix (J. P. Oleson et al., 2006). Therefore, it is likely that Romans wet the *pozzolana* just before mixing it with the slaked lime at the volumetric ratio of 1:2 as specified by Vitruvius for maritime concrete.

None of the relevant ancient Roman literature discusses the concept of measuring proportions by mass or volume, although it is a safe assumption that they are always referring to volumetric measurements unless denoted otherwise. The process of weighing materials before combining in a mortar mix would have added an unnecessary step to the process, when they could simply (and most likely did) just measure based on baskets full of each different material (Brandon et al., 2014). Another study looking into the construction of the Roman Baths of Caracalla follows the same assumption, calculating labor requirements based on volume divided into basked loads (J DeLaine, 1997).

With all of those findings, the specified mix design deemed closest to the Vitruvius Roman maritime concrete used the following guidelines:

- All measurements for mortar proportions are done by volume
- Hydrated lime is combined with just enough water to make a firm lime putty
- The pozzolan is dampened just prior to mixing with the lime putty
- The dampened pozzolan and the lime putty are mixed at a volumetric ratio of 1:2.7 (lime:*pulvis*)
- Water is incrementally added at the bare minimum amount while mixing to form a stiff mix with little slump

Aside from the proportions of mix design, Vitruvius was also extremely specific about the origins of each material constituent making up the ancient concretes. To look into this, a study in 2013 by Jackson et al. performed a pyroclastic rock trace element analysis to determine two possible sources for pozzolanic aggregate and ash within a specimen from the ROMACONS coring project.

The team determined that the aggregate either originates from Neapolitan Yellow Tuff (NYT) having erupted at about 15 ka (15,000 years ago), or from Bacoli Tuff erupted at about 8.6 ka, both of which fall within the Flegrean Fields designation, which was the broadly specified origin for proper material sourcing by the ancient Roman texts (Fedele et al., 2011; M. D. Jackson, Chae, et al., 2013). The greyish orange pumices are most likely sourced from the Averno 2 pumice fall deposit, having erupted about 5.2 ka, but also possibly from Agnano crater pumice, having erupted at about 4.1 ka, although again both are considered Flegrean Fields pumices (Fedele et al., 2011; M. D. Jackson, Chae, et al., 2013).

These findings confirm that now the exact materials and the proper proportions are known for the mix design of the ancient Roman seawater concrete. This thesis will incorporate all of the discussed mix design findings for the preparation of a suitable mix design for experimental testing to develop material parameters for accurate thermal modeling.

2.3.4 Physical and Mechanical Testing

Following the 2002 and 2003 ROMACONS coring campaigns, a series of physical and mechanical tests was conducted on the retrieved concrete following ASTM standards at the laboratories of Italcementi of Bergamo, Italy. Physical and mechanical tests were conducted following internationally established procedures for modern concrete on shaped specimens taken from the full-length cores. Aside from that, chemical and mineralogical tests were done on the same concrete and petrographic examination was conducted by an external consulting firm. Mortar to aggregate ratios were determined by visual assessment of digital photos of the full-length cores. (J. Oleson et al., 2004)

All experimental parameters and their corresponding ASTM standard or test method are as follows:

- Young's modulus – ASTM C215, *Standard Test Method for Fundamental Transverse, Longitudinal, and Torsional Resonant Frequencies of Concrete Specimens*
- Compressive strength – ASTM C39, *Standard Test Method for Compressive Strength of Cylindrical Concrete Specimens*
- Density – ASTM C642, *Standard Test Method for Density, Absorption, and Voids in Hardened Concrete*
- Porosity – ASTM D4404, *Standard Test Method for Determination of Pore Volume and Pore Volume Distribution of Soil and Rock by Mercury Intrusion Porosimetry*
- Petrographic examination – ASTM C856, *Standard Practice for Petrographic Examination of Hardened Concrete*

- Mineralogical examination – X-ray diffraction
- Mortar to aggregate fractions – visual assessment from digital images

Results from the physical and mechanical testing show that Young's modulus and compressive strengths are low (as expected) and are about one-quarter that of modern OPC. Density is about two-thirds that of modern OPC, which is in line with decreased mechanical properties and the determination that the porosity is several times greater than modern OPC. Mortar to aggregate ratio by weight is about 1.7 on average, which for modern OPC is typically closer to 1.0. (J. Oleson et al., 2004)

Petrography shows well mixed and distributed constituents with micro cracking present, but all material was sound, as well as the presence of secondary ettringite. It is likely there is no visible distress related to the secondary ettringite because of the high porosity allowing for expansive material to prevail without excessive internal stress development. (J. Oleson et al., 2004)

X-ray diffraction shows differences in relative predominance of mineral phases, but no unusual phase development even considering the very small sample size of the concrete. Differences in phase predominance is deemed unimportant and most likely just due to small sample size (J. Oleson et al., 2004). Scanning electron microscope shows comparable values between ROMACONS specimens and similarities between samples extracted from piers at Cosa, where results showed pozzolans from the Bay of Naples region, and tuff from a nearby inland site (Gazda & McCann, 1987). This confirmation for the origin of the pozzolanic constituents follows the ancient specifications reported by Vitruvius in his handbook, *De architectura.*

Mortar to aggregate ratios were determined as a physical ratio, but the lime to aggregate ratios could not yet be determined without more detailed chemical analysis, thus the Vitruvius specification could not be checked for that parameter (J. Oleson et al., 2004).

Overall, the hydraulic concrete is relatively weak with high porosity, yet it is incredibly durable in the marine environment, a result in line with scientific observations. There were no apparent 'cold-joints' throughout the height of the core, which indicates the *pilae* were poured over a fairly continuous time frame. Estimated labor calculations determined that the Santa Liberata *pila*, with sides measuring 8.9, 9.0, 7.7, and 7.6 m and a height of 5.9 m (volume of 420 m^3), should have taken 13 days to fill the form with 16 unskilled workers actively pouring material, while 18 laborers mixed the mortar (Janet DeLaine, 2002). Even if labor stopped overnight between shifts, the slow-setting nature of the lime especially in such a large structure was not expected to show any separation or layers between pours. The overall homogeneity and lack of voids indicates that it was compacted by workers with long-handed tools after dumping the material from pouring baskets. (J. Oleson et al., 2004)

Summarized results from the Oleson et al. testing in 2004, are tabulated in Table 1 and Table 2 below:

Table 1. Physical and mechanical properties of the testing Roman subcores. (J. Oleson et al., 2004)

Core ID	Density (kg/m³)	Young's Modulus (MPa)	Comp Strength (MPa)
PO2	1583	5560	7.8
A1D	1549	6440	6.3
PTO2C	1665	7570	4.9
PCO1B	1624	7200	7.4
PCO2B	2163	18800	9.4
PCO3B-a	1652	7050	8
PCO3B-b	1587	8750	7.9
PCO4B-a	1589	6500	5.5
PCO4B-b	1557	5750	6.4
PCO4B-c	1635	4850	5.1
PCO4B-d	1542	6900	5.5
COV	3%	17%	19%
Average	1598	6657	6.5
modern OPC	2325	24820	27.6

Table 2. Physical and chemical properties of the testing Roman cores/subcores. (J. Oleson et al., 2004)

Core ID	Mortar:Aggregate	Subcore ID	Porosity (%)
POR.02.02	1.7	PO2	46.8
ANZ.02.01	1.9	A1D	49
PTR.02.02	1.9	PTO2C	52
PCO.03.01	2.2	PCO1A	42.3
	-	PCO1C	43.6
PCO.03.02	1.3	PCO2A	35.1
	-	PCO2C	37.1
PCO.03.03	3.4	PCO3A	44.7
	-	PCO3C	45.8
PCO.03.04	1.4	PCO4A	48.4
PCO.03.05	-	PCO5A	51.3
SLI.03.01	-	SLI1A	46.5
COV	20%	COV	11%
Average	1.7	Average	45.2

2.3.5   Hydrate Analysis

Multiple studies based around the chemical and mineralogical analysis of the unique cementitious hydrate phases found in Roman seawater concretes have been published in the last six or so years, with most being led by Marie Jackson of UC Berkeley. This collection of studies is the first of their kind when it comes to providing a detailed microscale and nanoscale understanding of ancient Roman seawater concrete and why the unique hydrate phases form in such an environment as well as how they lead to such durable concrete when compared to modern OPC concretes.

The results for these studies are primarily focused on the detailed chemical and mineralogical composition of the Al-tobermorite, which extends past the scope of this thesis, but are important concepts to understand at least on a qualitative level for proper understanding of how the material affects the behavior and performance of the Roman concrete, which it is known to form within. This section will briefly discuss only the results of the Jackson studies that are relevant to the development of this thesis.

2.3.5.1 Material Properties of Al-tobermorite

The first of the studies looks specifically at isolated Al-tobermorite crystal clusters from the ROMACONS cores, which has been previously reported by Vola et al. as a predominant cementitious phase in the binding matrix of Roman seawater concretes (Vola, Gotti, Brandon, Oleson, & Hohlfelder, 2011). Alumina substituted tobermorite (Al-tobermorite) is a calcium silicate hydrate mineral that is understood to be a key ingredient related to the durability of ancient maritime Roman concrete (M. D. Jackson, Moon, et al., 2013). Natural occurrences of Al-tobermorite occur quite rarely in geological environments, most often forming in hydrothermally altered basaltic rocks (Jakobsson & Moore, 1986) and some recent laboratory studies have successfully synthesized the crystal form of the material (Houston, Maxwell, & Carroll, 2009). Although up until this study, the material's interaction within concrete and the corresponding characteristic changes to the concrete weren't well known.

The 2013 Jackson et al. study analyzed 3-5 μm long clusters of Al-tobermorite, manually extracted from relict lime clasts within ROMACONS cores using multiple test methods to determine the material and elastic properties of the Al-tobermorite.

The nanoscale structure of Al-tobermorite clusters was analyzed using nanoscale tomographic reconstruction of the Al-tobermorite clusters, which shows both platey and elongated 1-2 μm crystals, similar to geological and laboratory synthesized tobermorite (M. D. Jackson, Moon, et al., 2013). The calculated porosity of the Al-tobermorite is 52%, although that's likely an overestimation due to the test methods used and when comparing to the 36-39% porosity of Al-tobermorite in autoclaved aerated concrete (Mitsuda, Sasaki, & Ishida, 1992).
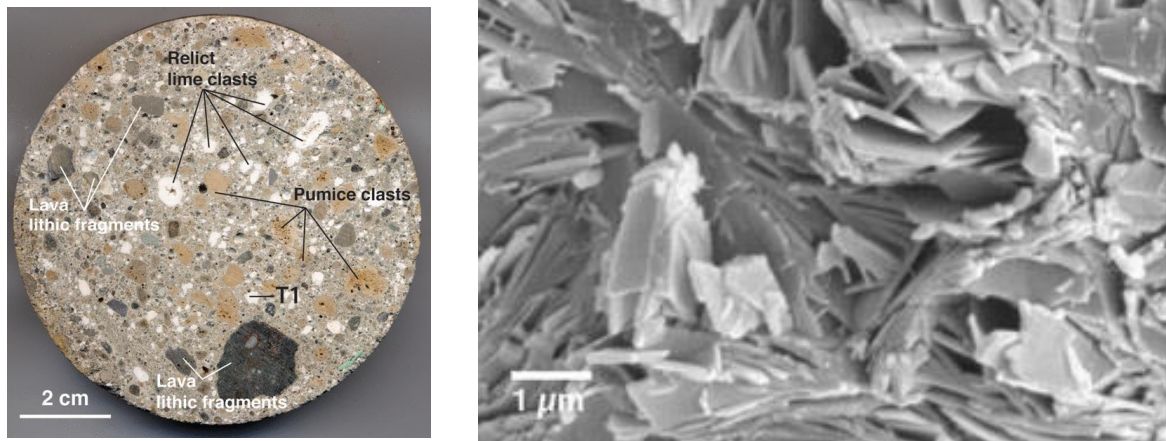
Figure 10. (left) Volcanic ash-hydrated mortar form the *Baianus Sinus pilae*; (right) Al-tobermorite crystals removed from a relict lime clast as shown by scanning electron microscope (SEM). (M. D. Jackson, Chae, et al., 2013)

Pressure-normalized data for the volume of Al-tobermorite crystals exposed to increasing pressure was fitted to a Birch-Murnaghan equation of state, yielding a calculated bulk modulus of 55 ± 5 GPa (M. D. Jackson, Moon, et al., 2013). This calculated value is slightly lower than the models of ideal tobermorite with a bulk modulus of 53 – 61 GPa (Manzano, Dolado, Guerrero, & Ayuela, 2007; Pellenq et al., 2009), most likely because of the change in bond characteristics that occur when Al^{3+} substitutes for Si^{4+} in the alumina substituted form of tobermorite. When comparing this bulk modulus to that of C-A-S-H: 35 ± 3 GPa, CSH: 34 ± 7 GPa (Oh, Clark, & Monteiro, 2011), and tobermorite-like CSH: 21-29 GPa (Manzano et al., 2007), it is clear that the bulk modulus of Al-tobermorite is significantly higher indicating that it could increase concrete stiffness.

2.3.5.2 Silicon Bonding Environments of Al-tobermorite

For a more in-depth analysis of the Roman concrete and more specifically the effects of the formation of Al-tobermorite, Jackson and her team expanded on the previous 2013 study with a broader overall scope to integrate interdisciplinary findings from mineral physics, geochemistry, engineering, and archaeological science fields. They looked deeper into the mineralogical properties of C-A-S-H gel and Al-tobermorite using the same concrete cores extracted from the Baianus Sinus breakwater from the Pozzuoli Bay, with specific focus given to the silicon bonding environments of Al-tobermorite.

The most important takeaways from the analyses of the silicon and aluminum bonding environments of the Al-tobermorite give good insight into why the Roman seawater concrete shows such durability in harsh maritime environments. Wide interlayer spacing of the *Baianus Sinus* Al-tobermorite, 11.49 Å, presumably provides cavities for Na^+ and K^+ cations derived from reaction of alkali-rich pozzolans and seawater-saturated lime (M. D. Jackson, Chae, et al., 2013). Additionally, the now well documented Al^{3+} substitution for Si^{4+} in the tetrahedral bonding environments of the Al-tobermorite produces a negative charge balance and increased silanol binding capacity (Taylor, Richardson, & Brydson, 2010). The

combination of these phenomena encourages irreversible binding of alkali cations in alkaline environments, such as those within the roman concrete, leading to increased resistance to chemical attack and increased chemical stability (M. D. Jackson, Chae, et al., 2013).

This unique mineralizing action of alkali cations, mainly Na^+ and K^+ from the pozzolans, and Na^+ and SO_4^{2-} from seawater counterintuitively has a beneficial effect through the formation of Al-tobermorite and C-A-S-H, which is a harsh contrast to modern OPC concretes where alkalis and sulfates commonly have highly damaging effects through secondary expansions (M. D. Jackson, Chae, et al., 2013). This breakthrough gives the first meaningful explanation as to why the ancient Roman maritime concretes are so much more durable than the modern-day concretes.

2.3.5.3 Post-pozzolanic Reaction and the Continuous Development of Hydrates

Now that it is well documented that Al-tobermorite was naturally synthesized in the ancient Roman concrete *pilae* across the Mediterranean sea, and that it leads to increased resistance to chemical attack while increasing concrete durability (M. D. Jackson, Chae, et al., 2013), it needs to be understood how it develops at such a low temperature in these ancient seawater concretes.

Following up on the 2013 set of Jackson and Moon studies, Jackson and a team of researchers published another study in 2017 demonstrating a much more in-depth look at the reaction kinetics and the microstructure of cementitious materials within Roman seawater concrete. Using more advanced experimental techniques with a much more focused scope, they were able to reveal why Roman concrete Al-tobermorite synthesized at such a low temperature over 2000 years ago, but similar reactions at equal temperatures haven't been observed in nature or replicated in laboratories. They also found evidence of un-discovered post-pozzolanic reactions occurring long after the initial reaction, involving crystallization of mineral phases that contribute to the strength and durability of the concrete, further explaining the durability of the 2000-year-old maritime structures.

The team studied ROMACONS cores that were extracted from 2002 – 2006 at nine different sites, one sample of basaltic tuff (BT) from a nearby quarry, and one sample of Neapolitan yellow tuff (NYT) also from a nearby quarry (M. Jackson et al., 2017).

Their first finding was that vesicles in the perimeter of a pumice clast in the mortar show signs of deep although incomplete dissolution of Flegrean Fields phillipsite, production of C-A-S-H and Al-tobermorite, and signs of an abrupt termination of the pozzolanic reaction before all of the phillipsite was consumed (M. Jackson et al., 2017). Cleary this proves the *Portus Cosanus* pumice recorded a rapid pozzolanic reaction just as Vitruvius described over 2000 years ago, but more importantly, this is evidence that the sealing of the surfaces of the phillipsite by the synthesis of C-A-S-H and Al-tobermorite stopped the pozzolanic reaction (M. Jackson et al., 2017).

Despite the evidence of the reaction stopping, the center of the same examined vesicle and adjacent vesicles contained Al-tobermorite crystals, suggesting a possible post-pozzolanic origin that has never been discovered. Further, the chemical composition of the post-pozzolanic Al-tobermorite crystals were also quite different than those previously isolated from lime clasts, with almost identical composition compared to Al-tobermorite crystallized in 15-year-old basaltic tuff (M. Jackson et al., 2017; Jakobsson & Moore, 1986).

Another piece of evidence confirming the post-pozzolanic production of new cementitious microstructures is the *in-situ* formation of coarse-grained fabrics of 100-200 μm phillipsite. X-ray microdiffraction analyses also indicates newly formed ettringite, a hydrous calcium-aluminum-sulphate often associated with modern concrete degradation in the form of delayed ettringite formation (M. Jackson et al., 2017). Previous studies confirmed that SO_4^{2-} and Cl^- were sequestered in ettringite near the perimeters of the lime clasts (M. D. Jackson, Chae, et al., 2013).

These findings prove that the alkaline fluids in Roman breakwater concretes produce precipitation of phillipsite and Al-tobermorite mineral cements. The natural synthesis of these mineral cements refines pore space, enhances bonding in pumice clasts, and sequesters alkali cations (M. Jackson et al., 2017). This is all in stark contrast to modern day OPC concretes where an overabundance of free alkali cations can lead to the development of expansive and destructive phases associated with damage in many modern-day concrete constructions.

The main takeaways from this in-depth study are summarized as follows:

- Low-temperature interactions between seawater-derived pore fluids and mineral components of the Flegrean Fields pozzolans drives zeolite (in the form of phillipsite) and Al-tobermorite crystallization in Roman marine concrete.
    - Laboratory synthesis of Al-tobermorite has not been successful at such low temperatures
    - The abundance of alkaline fluids in Roman marine concrete lead to the precipitation of mineral cements refining the concrete, whereas the same scenario is damaging to many modern-day OPC concretes
- The indications that post-pozzolanic reactions cycled in response to evolving fluid interactions over time, possibly leads to continually increasing mechanical resilience of the concrete similar to what Pliny the Elder reported in *Naturalis Historia,* "…becomes a single stone mass, impregnable to the waves and stronger every day..." (*35.166*)

2.3.6 Thermal Analysis

As discussed in the hydrate analysis section, Al-tobermorite synthesis appears to be dependent on high-temperature environments, meaning the temperature-time profile of the Roman concrete through the setting process is important to understand how and why the Al-tobermorite crystallized in 2000-year-old Roman structures, but not in any modern-day OPC concretes. Understanding the requirements for the concrete to produce the crystalline Al-tobermorite hydrate is important for the potential incorporation of the hydrate in new and innovative concretes meant to mimic the ancient Roman concrete.

During the 2013 study by Marie Jackson and her team, they modelled the temperature-time profile of a well-documented *pila* at *Baianus Sinus*, off the coast of Italy. They wanted to understand the progression of temperature throughout the large concrete block during the hydration and curing processes to see what maximum temperatures arose and allowed for the synthesis of Al-tobermorite.

To model the temperature-time profile of the 10m x 10m x 5.7m pier at *Baianus Sinus*, the initial concrete mix design was estimated based on recommendations by Vitruvius compared with results from past studies of excavations and core samples. Vitruvius initially specified that builders use a 1:2 lime:*pulvis* (lime:pozzolan) mix for maritime structures (*de Architectura* 5.12.2-3), but field studies and core analysis determined that Roman builders actually used a ratio much closer to 1:2.7 (J. P. Oleson et al., 2006). The discrepancy between the Vitruvius specification and the measured lime:pozzolan ratio from ROMACONS cores was determined to be due to the shrinkage of pozzolans after being dampened and the fact that Vitruvius doesn't explicitly specify whether or not to add dry or wet pozzolans to the mixture. Oleson et al. determined after their recreation of the *Brindisi Pila* in 2006, that the 1:2 ratio corresponds to wet pozzolana and the 1:2.7 ratio corresponds to dry pozzolana (J. P. Oleson et al., 2006).

For this model, the 1:2.7 volume ratio was assumed for the initial fresh-state concrete mix design which would have reacted and solidified into a concrete of the following hardened-state proportions by weight:

- 48 wt% - Neapolitan Yellow Tuff (NYT) – lithified tuff coarse aggregate (1300 kg/m^3)
- 45 wt% - Cementitious hydrates (average, 2200 kg/m^3)
- 7 wt% - Neapolitan Yellow Tuff (NYT) – ash pozzolan (1100 kg/m^3)

Material parameters for the seawater concrete model constituents were determined based on literature values for unit weight, thermal conductivity, and specific heat capacity as tabulated in Table 3. Material parameters for the whole concrete block included unit weight of the drilled core from the ROMACONS testing and calculated thermal diffusivity based on all combined material parameters (M. D. Jackson, Chae, et al., 2013). For the contribution of heat of hydration, Jackson et al. referenced experimental studies of pozzolanic concretes where volcanic ash replaces up to 50 wt% of OPC, which was deemed to be the heat of hydration experimental test closest to that of true Roman maritime concrete (F Massazza, 2002).

Table 3. Summary of Roman concrete constituent properties and FE material parameters assumed for the Jackson et al. thermal analysis.

	Unit Weight (kg/m³)	Thermal Conductivity (W/m/K)	Heat Capacity (kJ/kg/K)
NYT Coarse Aggregate	1300	0.49	2.48
Cementitious Hydrates	1100	0.27	2.75
NYT Ash Pozzolan	2200	0.98	1.69
ROMACONS Core	1494	-	-
FE Material Specification	1494	0.7	2.1

Boundary conditions were kept very simple for this study with a semi-adiabatic system where the concrete block was considered to be completely submerged thus isolated from the air above sea-level and the seafloor contribution to heat distribution was ignored. Two cases were analyzed with the first considering the seawater temperature constant at 14 °C which was deemed the minimum annual temperature and another case where the seawater temperature remains constant at 26 °C which was similarly deemed the maximum (M. D. Jackson, Chae, et al., 2013). Those seawater temperatures were taken from a range determined by Damiani et al. in a study on the Bay of Pozzuoli (Damiani et al., 1987). To account for the immediate and violent exothermic reaction brought on by the addition of quicklime to seawater, the weight percentage of lime (10%) was multiplied by an experimental rise in water temperature calculated by Moropoulou et al. when immersing a controlled mass of quicklime into water, thus giving an initial temperature rise of 5 °C for the model (Moropoulou, Bakolas, & Aggelakopoulou, 2001).

For the finite element semi-adiabatic model with all material parameters and boundary conditions aforementioned, the temperature-time profile was determined in chronological increments over three years as shown in Figure 11. The figure shows that under the minimum temperature condition (14 °C seawater), the maximum temperature at the center of the *pila* is 85 °C, and for the maximum temperature condition (26 °C seawater), the maximum temperature at the center is 97 °C (M. D. Jackson, Chae, et al., 2013). Highly similar values are expected for the initial modeling attempt used for this thesis, which will then be improved upon with calibration via experimental testing.
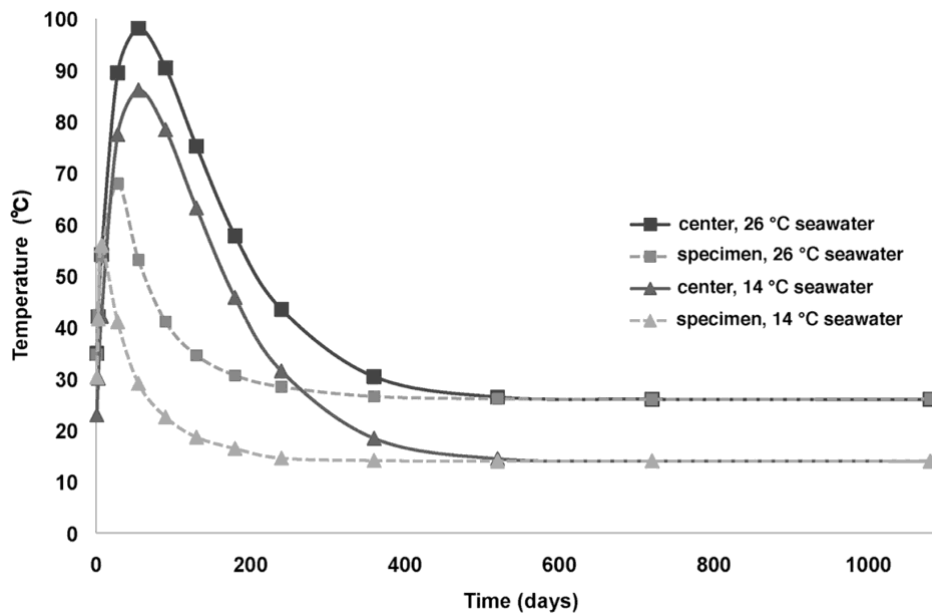
Figure 11. Temperature-time profile for the 10m x 10m x 5.7m *Baianus Sinus pila* model. (M. D. Jackson, Chae, et al., 2013)

This result shows high, yet feasible peak temperatures after the highly exothermic reaction of the model, but these results are based off of a heat of hydration curve for an experimental concrete formed with only 40 wt% volcanic pozzolan and 60 wt% Portland cement. The Portland cement dominates the reaction and therefore, the results aren't perfectly accurate from a thermal modelling standpoint when it comes to representing authentic Roman maritime concrete. For the thermal modelling portion of this thesis, a more accurate heat of hydration curve is necessary for a good representation of the behavior of the true Roman concrete.

More recently, Celik et al. conducted a more focused study to refine the heat of hydration curve representative of Roman maritime concrete by also replacing portions of OPC binder with pozzolanic substitutes to mimic Roman concrete. Although the study doesn't eliminate OPC entirely, it is the most recent isothermal calorimetry study on a concrete similar in nature to the Roman concretes.

The study by Celik et al. aims to analyze the effects of limestone powder (LP) and natural pozzolan (NP), used as a partial replacement for OPC binder, on reaction kinetics and products, as well as fresh and hardened material properties. The procedure involved replacing PC with 15 wt% of LP (85PC-15LP), 30 wt% NP (70PC-30NP), and 50 wt% NP (50PC-50NP) for experimental techniques including isothermal calorimetry (IC), thermogravimetric (TGA) and differential thermal analysis (DTA), as well as numerous other test methods to investigate chemical and mineralogical compositions.

The experimental natural pozzolan used was a basaltic ash obtained by finely grinding volcanic ash from Jabal Kadaha in Saudi Arabia. The particle size of the NP was chosen as 17 micrometers because that value is similar to the particle size of both the OPC and LP powders to allow for an accurate comparison of the reaction mechanics unrelated to particle size variation. Distilled water was used with a constant water-binder ratio of 0.5 for all specimens. (Celik, Hay, Hargis, & Moon, 2019)

Samples for the IC testing were made from cement pastes prepared in a vacuum mixer where the dry powder ingredients were mixed first and then mixed to completion with the water added. The mixed pastes were weighed into glass vials that were sealed right away and placed into the calorimeter to measure the heat flow for 162 hours at isothermal conditions (20 ± 0.02 °C). Sample proportions are shown in Table 4. (Celik et al., 2019)

Table 4. Mix proportions for cement paste specimens for IC testing for Celik et al., study.

Specimen ID	Proportions (by wt%)			
	PC	NP	LP	Water
100PC	1.00	-	-	0.5
85PC-15LP	0.85	-	0.15	0.5
70PC-30NP	0.70	0.30	-	0.5
50PC-50NP	0.50	0.50	-	0.5

Celik et al. found that replacement of OPC by LP or NP results in predominant filler effects and the formation of additional nucleation sites, which accelerates the hydration reaction for all specimens and amplifies heat flow peaks as shown in Figure 12 (Celik et al., 2019). The pozzolanic reactions of the NP were confirmed with chemical analysis due to the time-dependent reduction of calcium hydroxide. Contribution of cementitious phases from the NP and LP was also confirmed by the overall reduction in compressive strength of the specimens that was less than the expected loss due to the reduction in OPC content.
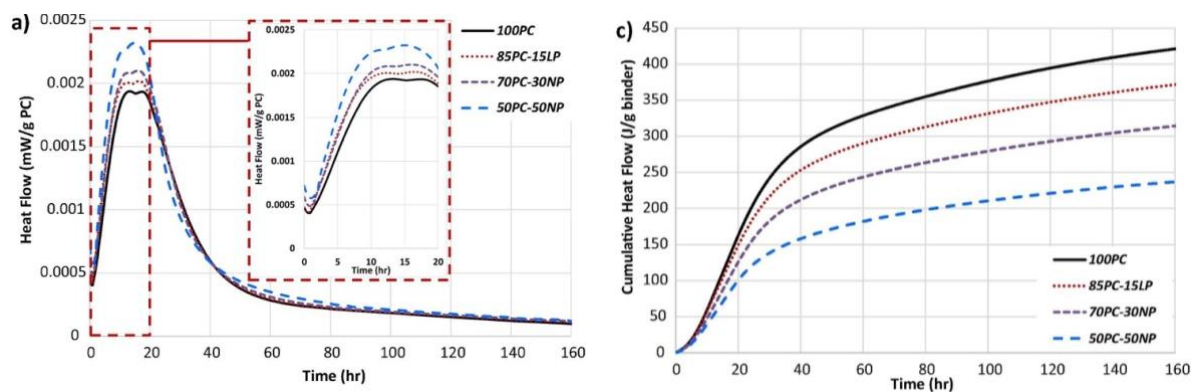
Figure 12. Isothermal calorimetry data from blended binder specimens (left) heat flow; (right) cumulative heat normalized to the binder content. (Celik et al., 2019)

Although this study gives a detailed look into the heat of hydration for an experimental mortar paste with a 50 wt% replacement of OPC binder with pozzolanic ash, the presence of any quantity of OPC is still troubling for the thermal analysis. No studies have been found to use isothermal calorimetry to analyze the heat of hydration for a concrete containing only hydrated lime and pozzolans mimicking the mix proportions of the Roman seawater concretes. This thesis aims to accomplish such a task in order to most accurately calibrate material parameters for the FE model.

2.4   Summary of Results from Research Findings

Overall, the collection of past studies on Roman seawater concrete is thorough and explains a lot about a material that has not been perfectly recreated in over 2000 years. Review of the ancient texts by Vitruvius and Pliny the Elder gives insight as to what proportions of each ingredient were being specified for the concrete mixes as well as the specific origin of the pozzolanic ash. Multiple studies within the past 15 years have been able to validate proportions and material origins specified in the ancient texts (M. D. Jackson, Chae, et al., 2013; J. Oleson et al., 2004; J. P. Oleson et al., 2006)

The ROMACONS coring campaign starting in the early 2000's gave researchers access to the first full-length concrete cores for more accurate and robust research on the material scale. This initially allowed for the characterization of physical, chemical, and mechanical properties of the concrete and later transitioned into a more detailed analysis of the hydrate phase compositions and morphology to better understand why the concrete shows such great durability.

Studies later revealed the widely accepted explanation for the highly durable properties of the material, which is the presence of Al-tobermorite, Phillipsite, and other zeolitic compounds having formed on a microscopic level (M. D. Jackson, Chae, et al., 2013; M. Jackson et al., 2017). The mechanism for how the crystals formed within pores and relict lime clasts is the more difficult determination. On a broad scale, the two studies suggest the crystals formed due primarily due to the unique chemical compositions of the source materials reacting in the presence of the highly alkaline seawater at elevated temperatures.

Al-tobermorite hasn't been successfully synthesized in a laboratory in low temperature environments, so it is suggested that the heat of reaction caused by the pozzolanic hydration reaction could raise temperatures within the concrete high enough for the crystals to form. This thesis aims to validate past studies determining the temperature rise within the hydrating Roman concrete *pilae*.

3. EXPERIMENTAL TESTING

Prior to implementing the Roman seawater concrete into a finite element analysis, experimental tests were conducted to characterize certain material properties. Mechanical testing was done to compare the flexural and compressive strengths of three experimental mix designs as well as to validate the overall mechanical properties by comparing to similar studies also using lime-pozzolanic mortars. Then, thermal testing by means of isothermal calorimetry was conducted to characterize heat evolution from the hydration reaction of each mix design to compare mixes and more importantly calibrates material parameters for the FE model.

3.1 Mix Design

Three mix designs were developed for all of the experimental tests to study the effects of two primary soluble salts found in seawater, sodium chloride and sodium sulfate. This was done by keeping the solid constituents constant for all three mixes but changing the concentrations of the two salts within the mix water to replicate fresh water, seawater, and a variant of seawater. The reasoning for controlling the mix water instead of the solid mix proportions is because literature demonstrates a good understanding of the solid constituents and mix proportions, but the only knowledge surrounding the use of mix water is found in Vitruvius' *de Architectura* (2.6.1) where any mention of mix water is ambiguous and it isn't known with certainty whether fresh water or seawater were used in the original concrete mix design. The comparison of the fresh water and seawater mix design aims to answer this uncertainty.

For the solid constituents, the three mixes were designed to replicate the Roman seawater concretes as closely as possible, although the highly specific Flegrean Fields pozzolanic ash described by Vitruvius and confirmed by Jackson et al. (M. D. Jackson, Chae, et al., 2013) could not be obtained for this experiment. Instead, the closest accessible alternative, metakaolin, was used, which is the calcined form of the clay mineral kaolinite and is considered one of the most effective pozzolanic materials for use in concrete. The other primary difference between the experimental mix design and the typical Roman concrete is the presence of coarse aggregate. For the Roman concretes, decimeter sized Neapolitan Yellow Tuff was used for coarse aggregate as also described by Vitruvius and Jackson et al., but due to the small size of the specimens used for this experimental campaign, coarse aggregates were neglected and instead a comparable mortar with a standard distribution of quartz sand was mixed for the mechanical testing and a comparable paste was mixed for the calorimetry testing.

Following the 1:2.7 lime:pozzolana ratio and the 45:55 mortar:aggregate ratio previously determined to be the most accurate proportions for the Roman concrete according to primary findings during the ROMACONS excavations and the Jackson et al. studies, Table 5 shows the fresh-state concrete constituent mass and volume per cubic meter for an ideal comparison to Roman seawater concrete. The use of quicklime versus slaked lime is another question mark that is not well answered by academic or ancient literature and will be explored further in the modeling phase.

Table 5. Ancient Roman seawater concrete constituents for one cubic meter of fresh-state mix.

	Skeletal ρ (kg/m³)	Bulk ρ (kg/m³)	Mass (kg)	Dry Mass %	Volume (m³)
Quicklime	3340	880	0	0%	0.000
Slaked Lime	2350	1050	111	11%	0.047
Pozzolan Ash	2392	1172	333	32%	0.139
NY Tuff	1223	-	582	57%	0.476
Seawater	1000	-	337	-	0.337
		Total:	1364	100%	**1.00**

For the actual mix prepared for the mechanical tests, the fresh-state constituent mass and volume per cubic meter is summarized in Table 6.

Table 6. Volumetric and mass proportions for each experimental mortar mix (excluding soluble salts).

	Skeletal ρ (kg/m³)	Mass (g)	Volume (m³)	Dry Mass %
Slaked Lime	2350	131	0.056	8%
Metakaolin	2300	315	0.137	19%
Sand	2650	1240	0.47	74%
Water	1000	339	0.34	-
Superplasticizer	1200	1.0	0.001	-
	Total:	2025	1.00	100%

The lime component used was a dried slaked lime powder from Vápenka Čertovy schody that follows Czech technical standard ČSN EN 459-1 and contains at least 90% pure calcium hydroxide, $Ca(OH)_2$. The pozzolanic component used was a dry Mefisto L05 metakaolin powder from Čéské Lupkové Závody that follows Czech standard ČSN EN 72 1300. The grain size distribution chart from the manufacturer, as well as the chemical proportions of the metakaolin, are both shown in Figure 13.
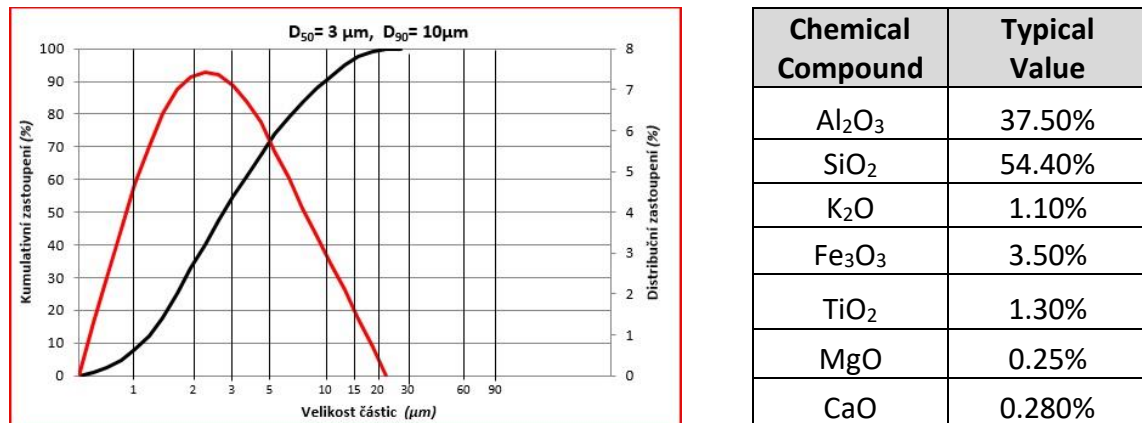
Figure 13. (left) Grain size distribution for the Mefisto L05 metakaolin mix; (right) chemical compound proportions for the same metakaolin mix. (Česke Lupkové Závody, n.d.)

The aggregate component was a standard mixture of sand proportioned with a sand to binder ratio of 2.8:1. Additionally, a superplasticizer was included with a dose of 0.23 wt% of the binder, in order to keep the water to binder ratio within a reasonable amount.

As previously mentioned, the three different mix designs contain the same proportions of dry constituents but have different concentrations of alkaline salts in the mix waters as summarized in Table 7. The first mix water is plain tap water from the civil engineering laboratory at Czech Technical University with no additives. The second mix water is meant to closely mimic seawater by including two of the most predominant and easily accessible soluble salts found in seawater, sodium chloride, and sodium sulfate, with proportions of the two salts following ASTM D1141 *Standard Practice for the Preparation of Substitute Ocean Water.* Seven other salts should be added to the mixture according to the ASTM standard for an exact ocean water substitute, but six of the seven salts are added with concentrations at or significantly below 0.12% and were therefore neglected from the mix designs as the inclusion would likely be inconsequential. The other salt excluded from the mix design was magnesium chloride hexahydrate, which was not kept out by justification of it being inconsequential, but rather due to the lack of access to the chemical.

The third and final mix water only contains sodium sulfate with its weight percentage matching the sum of sodium chloride and sodium sulfate from the first mix water. This mix is intended to provide an adequate amount of alkaline activation for the lime-metakaolin binder combination, while excluding the chloride ion contribution from sodium chloride, which is known to have deleterious effects in modern, reinforced concrete.

Table 7. Mix-water proportions per liter of water for all three mix designs.

	H_2O (g)	NaCl (g)	Na_2SO_4 (g)
Mix 1 - Freshwater	1000	0	0
Mix 2 - Seawater	1000	24.53	4.09
Mix 3 – Na_2SO_4	1000	0	28.62

3.2   Specimen Preparation

Mortar was prepared and tested in the Experimental Center at Faculty of Civil Engineering of Czech Technical University in Prague with assistance from Ing. Pavel Reiterman, PhD. The lime powder, metakaolin, and sand were weighed out and blended together using a standard auger drill to combine the dry ingredients before the addition of water. Each mix water was also weighed out for the same water to binder ratio (0.76), with the proper concentrations of the soluble salts and the addition of superplasticizer. The solutions were combined with the dry constituents and thoroughly mixed until the mix was highly homogenous. The three mortar mixes were prepared separately one after the other, but all with the same procedure and within the same hour of time.

Before pouring the mortar into molds, the consistence of each mix was checked using a flow table following standard EN 1015-3. This procedure involved placing a mold (60mm height, 100mm base diameter, and 70mm top diameter) on the center of the flow table and pouring two layers of tamped mortar into the mold. The mold is then removed, and the table is jolted 15 times at a constant rate of one jolt per second and the final diameter of the spread mortar is measured. The resulting final diameters for each mix are as follows: Mix 1 – 170mm, Mix 2 – 165 mm, Mix 3 – 170mm. The test setup and a representative photo of the spread mortar are shown in Figure 14.

Figure 14. (left) Flow table setup with empty mold; (middle & right) spread mortar after completion.

3.2.1   Mechanical Testing Specimens

The first series of experimental tests to be carried out was three-point bending tests to evaluate the flexural strength of the mortar, and as such specimens were cast in 40mm x 40mm x 160mm three-gang standard molds shown in Figure 15. A total of twenty-seven specimens were cast, with nine for each mix design, and three from each mix intended for a series of 7-day, 14-day, and 28-day bending tests. The samples were covered in plastic to prevent carbonation and left to cure at 20 °C.

Figure 15. (left) Empty three-gang mold; (right) mortar-filled molds for Mix 1.

3.2.2   Isothermal Calorimetry Specimens

Apart from the previously mixed mortar, a highly similar paste was mixed with the same proportions of lime, metakaolin, and water; however, without any sand. Three different pastes were mixed consecutively for each mix design and then immediately poured into small 20 ml plastic vials as seen in Figure 16. The vials were sealed and placed into a TAM Air isothermal calorimeter as soon as possible, which was 25 minutes after the first mix began to set. Two vials were prepared for each of the three mix designs.

Figure 16. Six 20ml paste specimens immediately before entering the isothermal calorimeter.

3.3   Mechanical Tests

3.3.1   Three-point Bending Tests

In order to determine the flexural strength of the mortar mixes meant to mimic Roman seawater concrete, a series of three-point bending tests was conducted using the twenty-seven 40mm x 40mm x 160mm prisms at 7, 14, and 28 days after casting. The tests were all carried out following the standard EN 1015-11 *Determination of Flexural and Compressive Strength of Hardened Mortar* and using an MTS Criterion Model 43 universal test system. Prior to testing, all specimens were weighed and measured for width and height for accurate density and strength calculations.
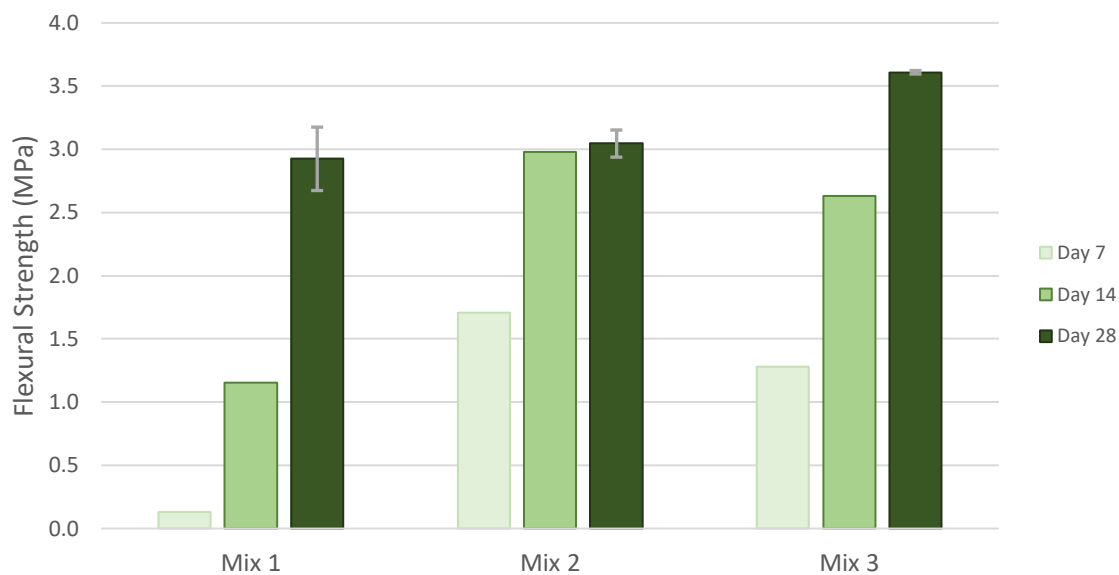
Figure 17. Three-point bending test results for all three mix designs at 7, 14, and 28 days after casting.

All twenty-seven specimens failed due to cracking along the bottom surface in the standard loading orientation (Figure 18), meaning all failures were controlled by tension and they all showed similar cracking patterns very close to the midpoint of the span. After the tests, each specimen was pulled apart by hand into two moderately even halves to be used for the compressive tests.
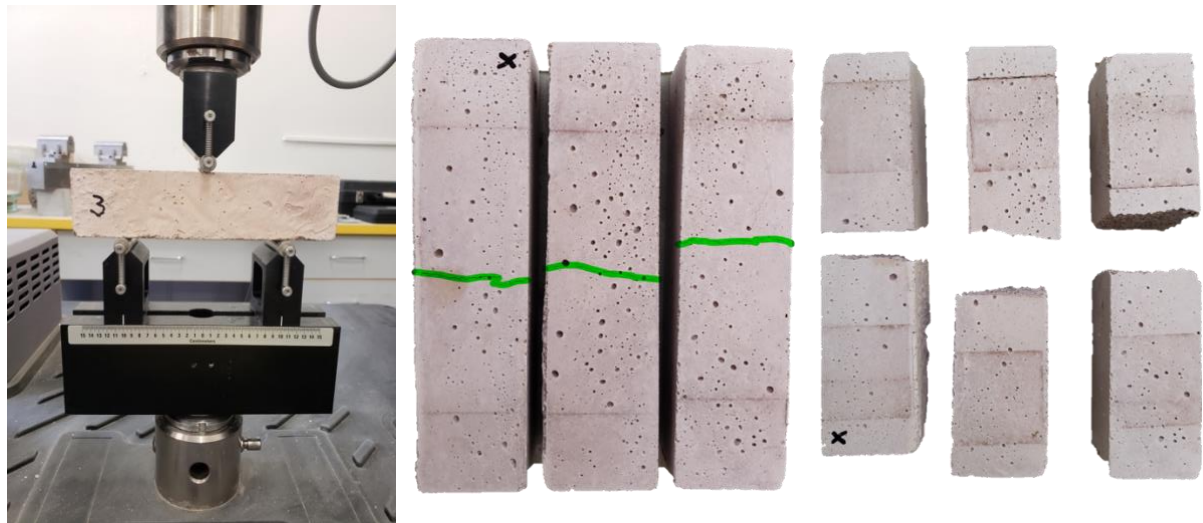
Figure 18. (left) Three-point bending test setup; (middle) three specimens just after bending test, where green highlights the crack pattern; (right) same specimens just after snapping in half for compressive testing.

3.3.2 Compressive Tests

The now fifty-four specimens were all tested to determine the compressive strength of the mortars in a series of compressive tests following standard EN 1015-11 while using a Heckert tester. Each specimen was loaded on the faces corresponding to the vertical walls in the three-gang mold because this minimizes any unwanted effects from sand segregation during the curing process. The results from the compressive tests are shown in Figure 19 and Table 8.
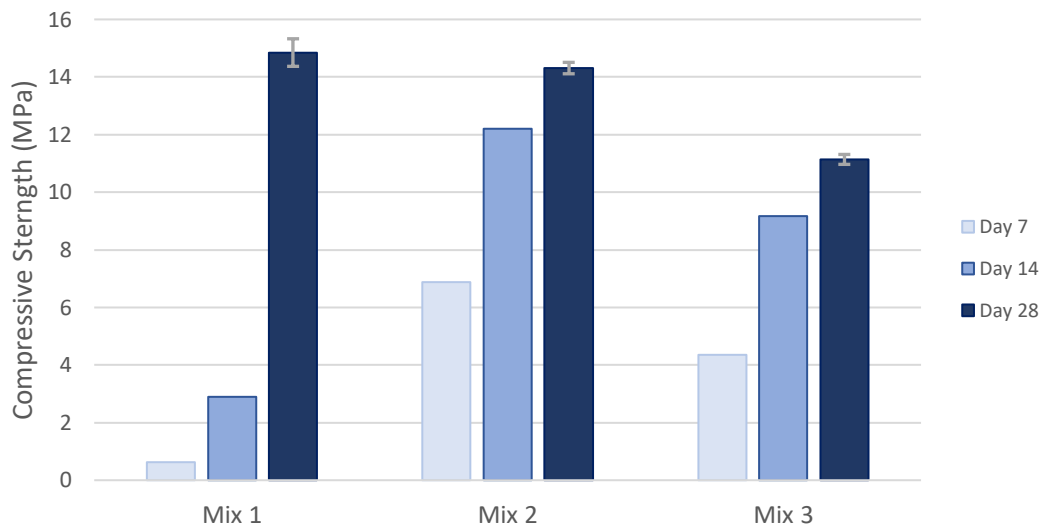
Figure 19. Compressive testing results for all three mix designs at 7, 14, and 28 days after casting.

3.3.3 Combined Mechanical Testing Results

Table 8. Summary of results from mechanical testing.

Density (kg/m³)	7-Day	14-Day	28-Day
Mix 1	1987	2034	1991
Mix 2	1987	1994	1982
Mix 3	1986	2007	1999
Flexural Strength (MPa)	7-Day	14-Day	28-Day
Mix 1	0.13	1.15	2.92
Mix 2	1.71	2.98	3.05
Mix 3	1.28	2.63	3.61
Compressive Strength (MPa)	7-Day	14-Day	28-Day
Mix 1	0.63	2.89	14.8
Mix 2	6.87	12.2	14.3
Mix 3	4.35	9.16	11.1

3.4 Isothermal Calorimetry Tests

Characterizing the total heat of hydration is crucial for developing an accurately calibrated thermal finite element model to properly represent heat generation and flow for the ancient Roman seawater concrete upon their casting nearly 2000 years ago. To collect this heat flow profile, isothermal calorimetry tests were conducted on the three experimental lime-metakaolin pastes, meant to mimic the ancient concrete mix as closely as possible, using a TAM Air isothermal calorimeter.

The process works by continuously exchanging the heat produced by the cementitious paste with the surroundings in the calorimeter. This essentially keeps the temperature of the paste constant to the manually specified baseline, while the device uses heat flow sensors to record the exchange of heat between the specimen and the surrounding heat sink. The heat flow, also considered heat power, can then be integrated and normalized to determine the cumulative heat flow in Joules per gram of binder.

For this experiment, the baseline of the calorimeter was set at 20 °C and two vials from each mix design were placed in the device 25 minutes after the paste was mixed. The device begins recording heat flow immediately, but it doesn't begin the integration process until 45 minutes have passed because the initial hydration releases energy and the temperature of the samples needs to be equilibrated to the heat sink.

The experimental test with the isothermal calorimeter ran for 311 hours or just under 13 days before the six vials were removed for inspection and data was collected. The heat flow data was automatically integrated by the data logger and thus output data included heat flow in Watts, and cumulative heat in Joules for each of the six specimens. The error between the two specimens for each different mix design was essentially negligible due to the high accuracy of the testing equipment and the homogeneity of the mixes. The heat flow curves are shown in Figure 20 and the total heat curves are shown in Figure 21.
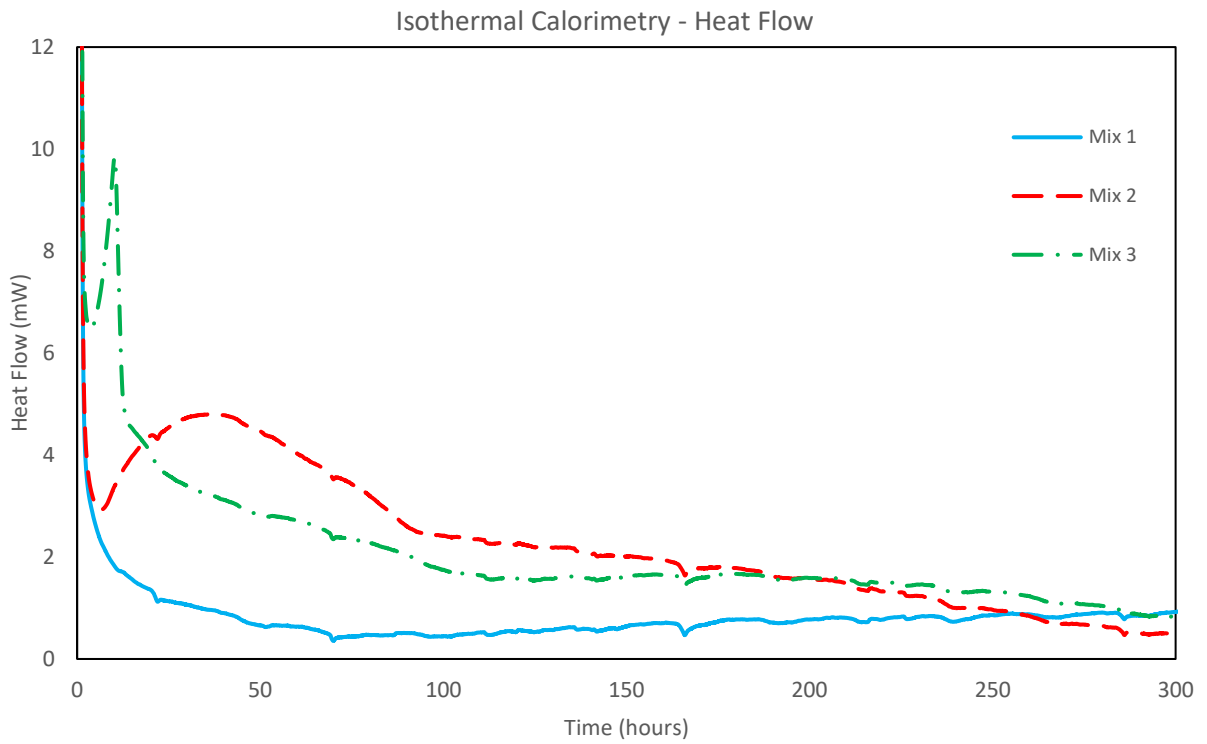
Isothermal Calorimetry - Heat Flow

Figure 20. Heat flow data from the isothermal calorimetry test for all paste mixes.

Isothermal Calorimetry - Total Heat
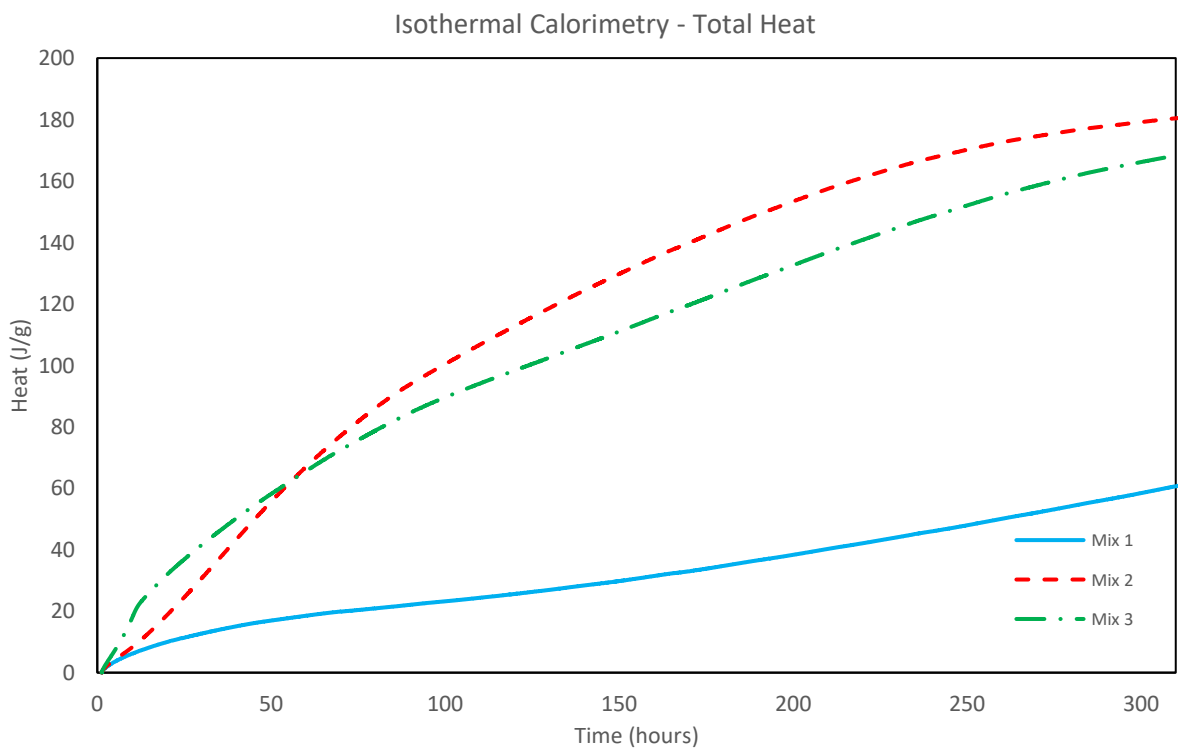
Figure 21. Total heat data for all paste mixes normalized per gram of binder.

3.5   Discussion

Overall, both the mechanical and thermal testing showed good, consistent data with little error due to experimental procedures; however, there is obviously a significant difference in material properties as a result of the different mix waters and this shows through in all test methods. The lack of any alkali additives to the fresh water used for Mix 1 resulted in very slow and incomplete hydration of the paste, which was most clear from the isothermal calorimetry data and the fact that the material was still moist and crumbly after being removed from the plastic vials 14 days after the paste was mixed.

Figure 22. All three paste mixes after being cut out of their plastic vials 14 days after being mixed.

The mechanical tests show how a very large difference in early flexural and compressive strength when comparing the fresh water mortar (Mix 1) to the artificial seawater mortar (Mix 2). This trend of fresh water mortar lacking early strength is again apparent at the 14-day mark and only catches up to the seawater mortar at the 28-day mark where the two mixes have very similar compressive and flexural strengths. Mix 3 seems to be somewhere between the two other mixes in terms of the development of its mechanical properties.

When looking at the isothermal calorimetry data, Mix 1 and Mix 3 both show highly unusual heat flow and total heat curves when compared to typical concrete mixtures. Mix 1 has no significant acceleration of heat flow after the rapid initial hydration phase shown before in Figure 20, although it does keep a relatively constant and non-zero heat flow through to the end of the test. This along with the strength only fully developing at the 28-day mark may indicate a significantly delayed hydration with very little early strength.

The other non-typical heat flow curve is that from Mix 3, where it shows very rapid acceleration of hydration starting after about four hours and lasting only six hours before decelerating at a similar rate. Both mechanical tests show that despite Mix 3 exerting more early heat flow in the first day when compared to Mix 2, it also shows lower mechanical properties at all time intervals except flexural strength at 28 days. For the material parameters characterized by these experimental tests, there appears to be no benefit to using the sodium sulfate solution from Mix 3 instead of the more conventional artificial seawater from Mix 2.

Mix 2 appears to be the only mix without any striking behavior dissimilar to typical OPC based concretes and as such, these tests seem to answer the question of whether it's more likely ancient Romans used seawater or fresh water for their maritime concrete mixes. The experiments show no significant improvement when using fresh water and rather mostly diminutive early-age mechanical properties for the fresh water mix. This lesser behavior along with the fact that logistically and economically, using fresh water makes far less sense when compared to taking seawater directly from the construction site at no cost, indicates that ancient Romans most likely mixed their concretes with seawater.

Going forward to FE modeling, Mix 1 will be considered the freshwater mix by default and Mix 2 will be considered the seawater mix. The mix water proportions of Mix 2 match seawater the closest, and the heat curves are more similar to OPC concretes then the slightly different Mix 3.

4. FINITE ELEMENT MODEL DEVELOPMENT

After completing the isothermal calorimetry experiments, all necessary information had been gathered for the preparation of the finite element model for both thermal and mechanical analyses. The two primary analyses to be conducted are a standalone thermal analysis, and subsequently a staggered thermomechanical analysis. All FE models were developed as text-only input files, which are processed using the open source OOFEM code, utilizing the transient transport module for thermal analyses, and a combination of the transient transport and structural modules for the thermomechanical analyses (Patzák, 2012).

Both primary models began development using the Tab Block Temperature interface of a program called ConTemp, where basic input parameters allowed for the program to create an initial input file to be refined and built upon to best simulate each specific subset of analysis (e.g. freshwater vs. seawater concrete mixtures).

4.1 Thermal Model

4.1.1 Geometry

The geometry of the FE model was primarily based on measurements of the *Baianus Sinus pila* taken by Oleson et al. during the ROMACONS project and simplified in a manner that matches the thermal analysis conducted by Jackson et al. to allow for direct comparisons and validation of their model.

The pier was measured to be 8.9m x 9.0m x 7.7m x 7.6m in plan view and 5.7m tall, which was simplified to 10m x 10m x 5.7m tall (Brandon et al., 2014). In order to reduce the computational load of the analysis and to easier visualize results at the center of the block, it was reduced to one quarter of the full structure as shown in Figure 23, thus making the final geometry 5m x 5m x 5.7m tall. With the proper boundary conditions put in place, this reduction shouldn't cause any change in the results.
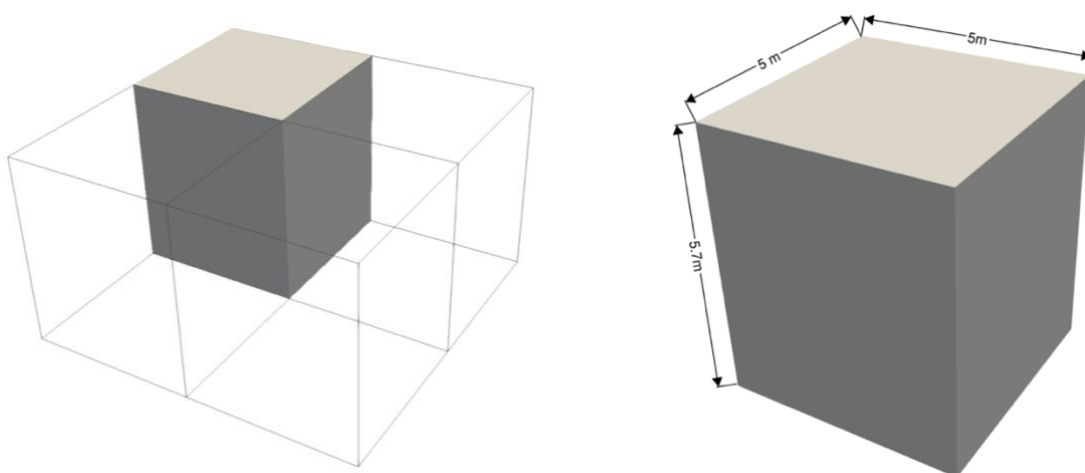
Figure 23. (left) Representation of the full 10m x 10m *pila* shown in wireframe with the solid quarter being the true geometry of the model; (right) dimensioned geometry.

In preparation for a secondary analysis, which will explore the effects of an instantaneous versus multi-day concrete casting scenario, a non-stationary geometry was also modeled. This analysis will require that the geometry of the block is divided into thirteen even layers along the height of the block (Z-axis) to simulate a construction scenario closer to reality, where it takes thirteen days to pour the entire concrete block (Janet DeLaine, 2002).

To distinguish between both modeling approaches, the basic block geometry will only be referred to as the 'solid block', and the non-stationary, layered geometry will only be referred to as the 'layered block' when comparing results. Portions of the layered block are shown after being meshed in Figure 26 within Section 4.1.2 below.

4.1.2 Meshing

After specifying block geometry in ConTemp, the program created the initial input file with a list of nodes and their XYZ coordinates and a list of elements and their corresponding nodes. The thermal model was meshed using hexahedral 3D elements containing eight nodes with one degree of freedom for each node, and with linear approximation between nodes. The one degree of freedom at each node is defined as temperature for all heat transfer analyses. This type of element is characterized in the OOFEM element library manual as a 'Brick1ht' element as shown in Figure 24 (Patzák, 2012).
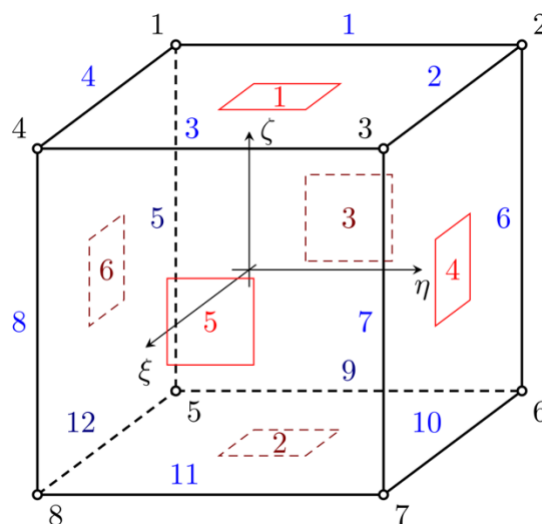
Figure 24. 'Brick1ht' element as defined by OOFEM. (Patzák, 2012)

Element size was determined based upon a general level of fineness required for good accuracy, while choosing a size that evenly distributes throughout the overall geometry of the block in order to keep all elements the exact same size and orientation. The block was divided into 10,400 elements in a 20x20x26 pattern meaning there are 20 elements along the edges in the X and Y directions, but 26 elements along the longer edge in the Z direction. Thus, the size of each mesh element for all thermal analyses is 25cm x 25cm x 21.9cm.

The distribution of elements in the Z-direction was controlled by an analysis using the layered block geometry, where thirteen non-stationary layers will incrementally be meshed over time. It was important to keep the aspect ratio of the elements close to 1.0 to avoid irregular meshing, while still providing an even distribution of elements along the Z-axis for each individual layer to prevent any inconsistencies amongst elements. To comply with both of those requirements, the best option was to use 26 elements distributed along the Z-axis. Two different instances of the time-dependent mesh for the layered block are shown in Figure 26, with both one layer and two combined layers displayed.

Figure 25. (left) Fully meshed solid block geometry with 10,400 elements; (right) zoomed in and dimensioned individual element.

Figure 26. Layered block mesh; (left) single layer (time = 0hrs); (right) two layers (time = 24hrs).

4.1.3 Material Characterization

Characterizing ancient Roman seawater concrete is not as straightforward of a process as is typical for modern materials because there are far more unknowns, especially when it comes to thermal transport parameters. The approach to properly define material properties in the FE model involv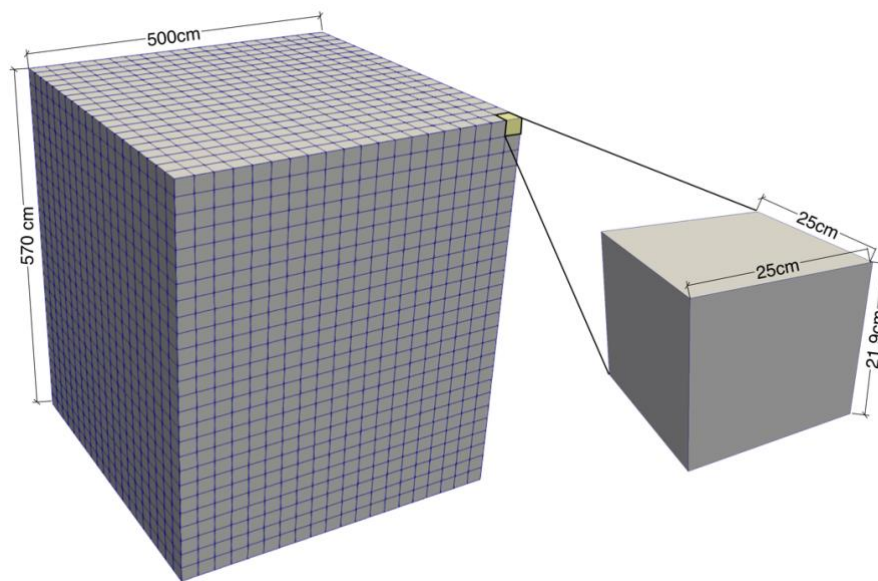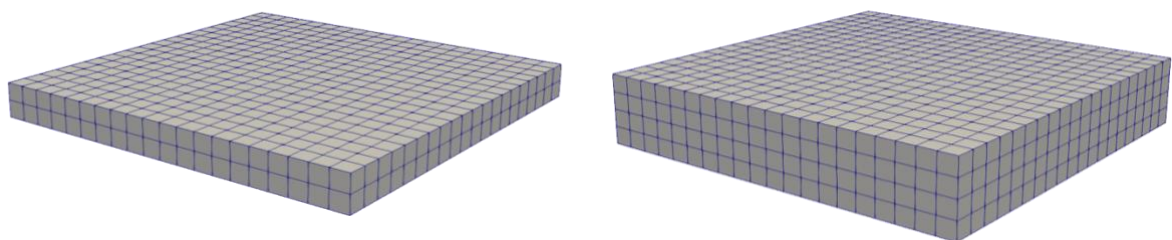ed using past studies on the ancient seawater concrete or and similar modern concrete mixes, performing calculations based on concrete mix proportions, and implementing the data collected from isothermal calorimetry experiments.

For the thermal transport FE analysis, the material must also be dynamic in the sense that the hydration reaction of the concrete needs to be taken into account to properly calculate the progression of temperature rise and fall throughout the block. This is handled in OOFEM by using a material that implements the chemical affinity model to evaluate the incremental solution for heat release dependent upon the evolution of hydration degree. The final solution for each time step is the released heat obtained from the following equation:

$$Q(t) = DoH * Q_{pot} \tag{1}$$

Equation (1) requires two material parameters for the OOFEM code to properly run, which are the potential hydration heat (Q_{pot}), and the mass of cement per cubic meter of concrete. Q_{pot} is expressed in kJ/kg of cement and is based on another input for mass of cement, which in our case will be represented instead by the mass of lime and metakaolin per cubic meter. As previously determined by literature, the ancient Roman seawater concrete most likely contains approximately 444 kg/m^3 of lime-pozzolana binder (M. D. Jackson, Chae, et al., 2013).

The potential hydration heat for the Roman seawater concrete has not been experimentally tested, so for this model, Q_{pot} is selected as the standard value in the ConTemp program for a pozzolanic cement, 360 J/g (Šmilauer et al., 2016). This value can be justified by doing a rough calculation using the standard enthalpy equation considering ΔH_f = -780 J/g for the S $\rightarrow$ C-S-H reaction (Waller, De Larrard, & Roussel, 1996) and the technical data sheet for the experimental metakaolin used for calorimetry shows 54.1% SiO$_2$ (Čéské Lupkové Závody, n.d.) while also considering that this accounts for only 75% (by mass) of the complete lime-metakaolin binder mix. Thus, the effective SiO$_2$ content in the binder mix is approximately 40.6% and when multiplying that by ΔH_f, the calculated Q_{pot} value is 316.49 J/g.

Looking back at Equation (1), the degree of hydration, DoH, still needs to be solved by using the chemical affinity model, which when considering hydration under isothermal temperature 25 °C is as follows:

$$\frac{dDoH}{dt} = \tilde{A}_{25}(DoH) \tag{2}$$

This is where the experimentally determined heat flow curve, q(t), and total heat curve, Q(t) become relevant because using the following set of equations the experimental data allows for an approximation of the chemical affinity model.

$$\frac{Q(t)}{Q_{pot}} \approx DoH \tag{3}$$

$$Q(t) = DoH \cdot Q_{pot} \tag{4}$$

$$\frac{1}{Q_{pot}} \frac{dQ(t)}{dt} = \frac{q(t)}{Q_{pot}} \approx \frac{dDoH}{dt} = \tilde{A}_{25}(DoH) \tag{5}$$

The analytical form of the normalized affinity can be calculated by introducing four new variables, all of which will be crucial input parameters for the OOFEM model. The Q(t) set of data can be fit to a four-parametric model using B_1, B_2, coefficients, DoH_∞ being the ultimate hydration degree, and the η parameter representing microdiffusion of free water through hydrate phases (Šmilauer et al., 2016). The analytical form is shown in the following equation:

$$\tilde{A}_{25}(DoH) = B_1 \left(\frac{B_2}{DoH_\infty} + DoH\right) (DoH_\infty - DoH) f_s \exp\left(-\bar{\eta}\frac{DoH}{DoH_\infty}\right) \tag{6}$$

In order to determine these four new variables, the isothermal calorimetry data was imported into the ConTemp program where it uses an iterative curve fitting algorithm to match the input data by defining the B_1, B_2, and eta parameters. The program also requires manual input of the Q_{pot}, activation energy, DoH_∞, and initial conditions. This is where the only differences arise for the material parameters when comparing the seawater mix (Mix 2) to the freshwater mix (Mix 1). As discussed earlier, the sodium sulfate mix (Mix 3) will not be used for FE analysis going forward and as such the primary comparison is Mix 1 to Mix 2.

For both mixes, the Q_{pot} value was set to 360 J/g as described before, and they also both had the same initial conditions. The initial sample temperature was 20 °C for both because that was the experimental temperature chosen for the isothermal calorimeter. They also both had the same initial offset time of 1.28 hours, which represents the time between initial mixing and the start of the test, combined with the neglected rapid hydration period that occurred before heat flow integration began.

For Mix 1, the activation energy was set to 66,000 J/mol based on a similar study using metakaolin-lime mortars with different alkali additives (Shi & Day, 1993). The DoH_{inf} was set to 0.80 because of the delayed and incomplete hydration reaction. The curve fitting result from ConTemp is shown in Figure 27. Obviously, this mix did not yield a good curve fitting result because of the slow and incomplete reaction that caused the heat flow and resultant total heat curves to have atypical shapes when compared to standard concretes that were used to calibrate the program.
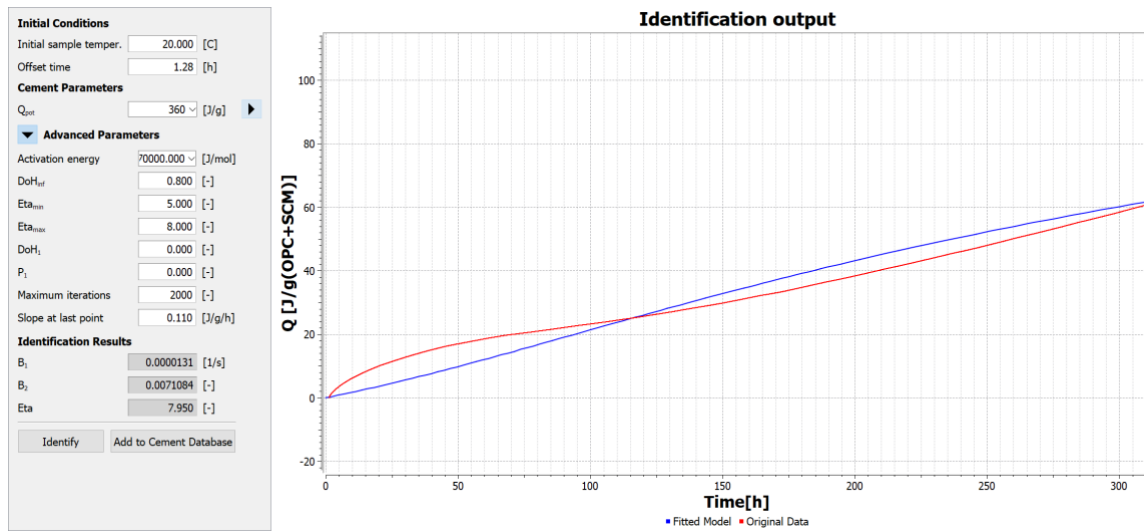
Figure 27. ConTemp curve fitting result for the fresh-water paste mix (Mix 1).

For Mix 2, the activation energy was set to 75,000 J/mol based on the same study (Shi & Day, 1993) and the DoH_{inf} was set to 0.90 because that is typical for standard concretes and the heat flow curve showed a typical hydration reaction based on the shape and values from the curve. The curve fitting result from ConTemp is shown in Figure 28. This is a much better result with an accurate representation of the empirical data using the four-parametric model.
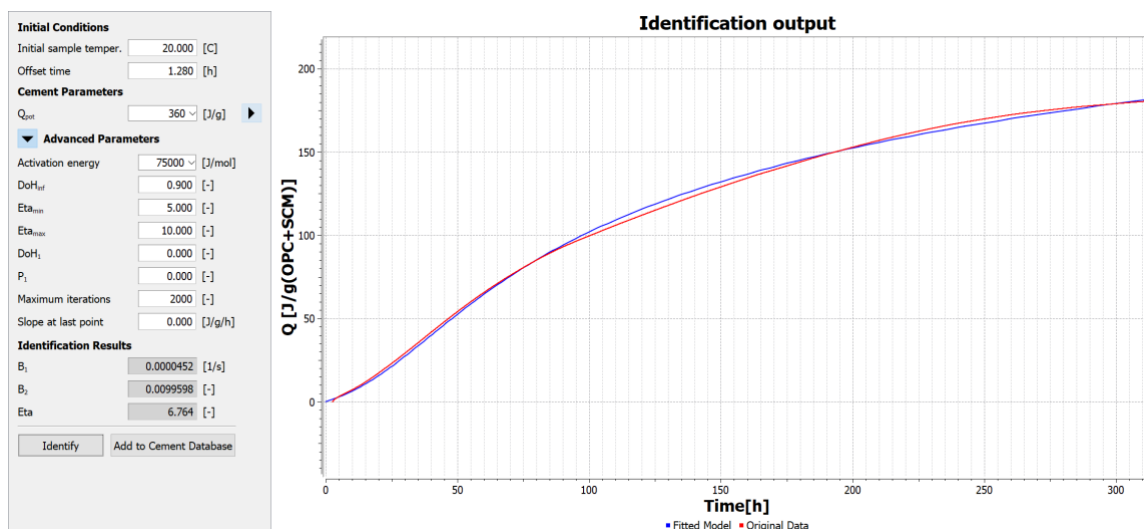

Figure 28. ConTemp curve fitting results for the seawater paste mix (Mix 2).

The last set of material parameters that needs to be characterized for the ancient Roman seawater concrete is the thermal conductivity, λ, and the heat capacity, c. Again, there are no studies that have researched these specific properties for the over 2000-year-old concretes, so the values were calculated based on the thermal properties of the concrete constituents and their mix proportions.

ConTemp is used to homogenize all constituent parameters and calculate one constant conductivity value for the whole of the concrete based upon what is technically a composite material with varying conductivity properties throughout the block. ConTemp performs this calculation by homogenizing properties from two constituents at a time and then upscaling to the next constituent down a list of six material combinations. The list has been reduced to only the three relevant combinations for the Roman seawater concrete, which reads as follows:

1.   Binder Paste = lime-pozzolan + water [HS]

2.   Paste with entrapped and entrained air = 1 + air [MT]

3.   Concrete = 2 + coarse NYT aggregate [HS]

Each of these three upscaling calculations are performed following the average of Hashin-Shtrikman bounds (HS) and the Mori-Tanaka scheme (MT) with the following equations:

$$k_{lower} = k_1 + \frac{f_2}{\dfrac{1}{k_2 - k_1} + \dfrac{f_1}{3k_1}} \tag{7}$$

$$k_{upper} = k_2 + \frac{f_1}{\dfrac{1}{k_1 - k_2} + \dfrac{f_2}{3k_2}} \tag{8}$$

$$k = \frac{k_{lower} + k_{upper}}{2} \tag{9}$$

Where the k_1 and k_2 variables represent the independent conductivity values of each of the two components being homogenized for each upscaling calculation, and the f_1 and f_2 variables represent each volume fraction.

Mix 1 and Mix 2 both have the same solid constituents so they have the same value of conductivity, which according to the inputs shown in Table 9 and the homogenization calculations performed by ConTemp, is 0.580 W/m/K.

Table 9. Material constituent inputs with output conductivity and capacity from ConTemp.

	Mass (kg)	Density (kg/m³)	Volume (l)	Conductivity (W/m/K)	Capacity (J/kg/K)
Water	337	1000	337	0.604	4180
Air	0.06	1.2	50	0.001	0.001
Lime-pozzolana	444	2382[a,b]	186	1.55[c]	790[e]
NYT Aggregate	582	1223[d]	476	0.4[d]	1380[d]
Total - Concrete	1363	1299	1049	0.580	1623

[a,b] - (National Lime Association, n.d.; Sabir, Wild, & Bai, 2001); [c] - (M Neville, 1997); [d] - (Heap et al., 2018); [e] - (Faria, Azenha, & Figueiras, 2006)

Calculating the homogenized heat capacity is much simpler and doesn't require any upscaling or incremental calculations. The final heat capacity is just the weighted average of all constituents, dependent on their mass contribution and independent heat capacity. This calculation yields a total heat capacity value of 1623 J/kg/K. It is important to note that the calculated heat capacity and thermal conductivity were both kept constant throughout the FE analysis.

To summarize all of the material properties that are included in the thermal analysis for both experimental mixtures, Table 10 displays all values and their corresponding input string into the OOFEM code.

Table 10. Summary of all material parameters for thermal analysis.

	Mix 1	Mix 2	Units	OOFEM ID
Density	1494	1494	kg/m³	d
Heat Capacity	1623	1623	J/kg/K	c
Thermal Conductivity	0.58	0.58	W/m/K	k
Potential Hydration Heat	360	360	J/g	qpot
Binder Mass	444	444	kg/m³	masscement
B_1 Parameter	1.31E-05	4.52E-05	-	b1
B_2 Parameter	7.11E-03	9.96E-04	-	b2
Eta Parameter	7.95	6.76378	-	eta
Ultimate Hydration Degree	0.8	0.9	-	dohinf
Activation Energy	66000	75000	J/mol	activationenergy

4.1.4 Boundary Conditions

The boundary conditions of the *pila* residing in the Pozzuoli Bay were modeled to closely match real-life weather and seawater temperatures, while the effects due to geometry and formwork were represented as well. Initially, two sets of analyses were run to predict model behavior under both winter and summer conditions for the specific geographic location of the block. However, as expected, the only difference between the two analyses was a simple shift up or down in maximum temperature within the block. Because the purpose of the thesis is based more on the maximum temperatures in the block and some mechanical effects from the temperature rise, the winter scenario was deemed unnecessary and will not be discussed further.

The boundary conditions for all thermal analyses are meant to match the average temperatures during the summer, which is kept to a constant 24-hour cycle of varying temperatures for the model. The average air temperature in the Pozzuoli Bay during the summer is 26 °C with ~4 °C of variance according to Meteostat's statistical weather database (Meteostat, n.d.). The average seawater temperature for this same time and location is approximately 26 °C with little archived information on the variance over a 24-hour cycle, and as such will be modeled as a constant 26 °C (Seatemperature.org, n.d.). The last surface in need of temperature data is the seafloor where the bottom of the block lays, which is modeled as a constant 18 °C according to data from the ArcGIS archive on seafloor temperatures.

Now that all applicable temperature sets are known, the boundary conditions can be properly applied to the block in sets broken up by exposure conditions, which depends based on the location of the block. Based on observations during the ROMACONS survey and a review of images from Vitruvius' *de Architectura* (Figure 29), it seems likely that formwork wasn't removed after construction as evidenced by multiple instances of researchers finding at least partially in-tact formwork on the outer surface of *pilae* (Hohlfelder et al., 2008). There also serves no logistical purpose to removing the formwork as it continues to provide at least some protection from the crashing waves, while only wasting time and resources to remove. That said, formwork is assumed to be present on all four vertical faces of the block for this analysis, although because only one-quarter of the block is being modelled, only the two outer faces should see effects from formwork.
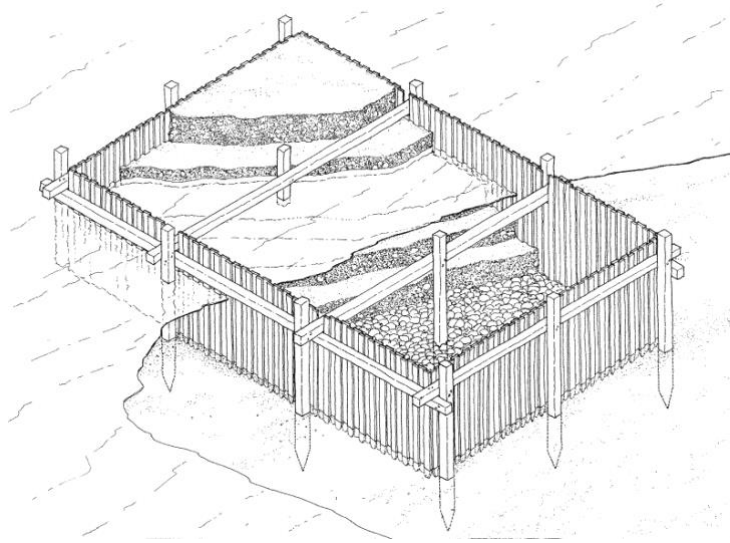
Figure 29. Representation of Vitruvius' formwork scheme for seawater concrete pours. (Hohlfelder et al., 2008)

The last notable occurrence that changes the boundary conditions is the fact that not all of the pier is completely submerged similar to the pier shown in Figure 30. According to the ROMACONS survey, there is a large variance in *pilae* size and depth below or height above the water surface and as such the model follows the measurement from the *Baianus Sinus pila* (J. Oleson et al., 2004). The proposed real-life conditions of the concrete block being modelled are shown in Figure 31.

Figure 30. Coring effort at a Roman pier during the ROMACONS study. (Brandon et al., 2014)
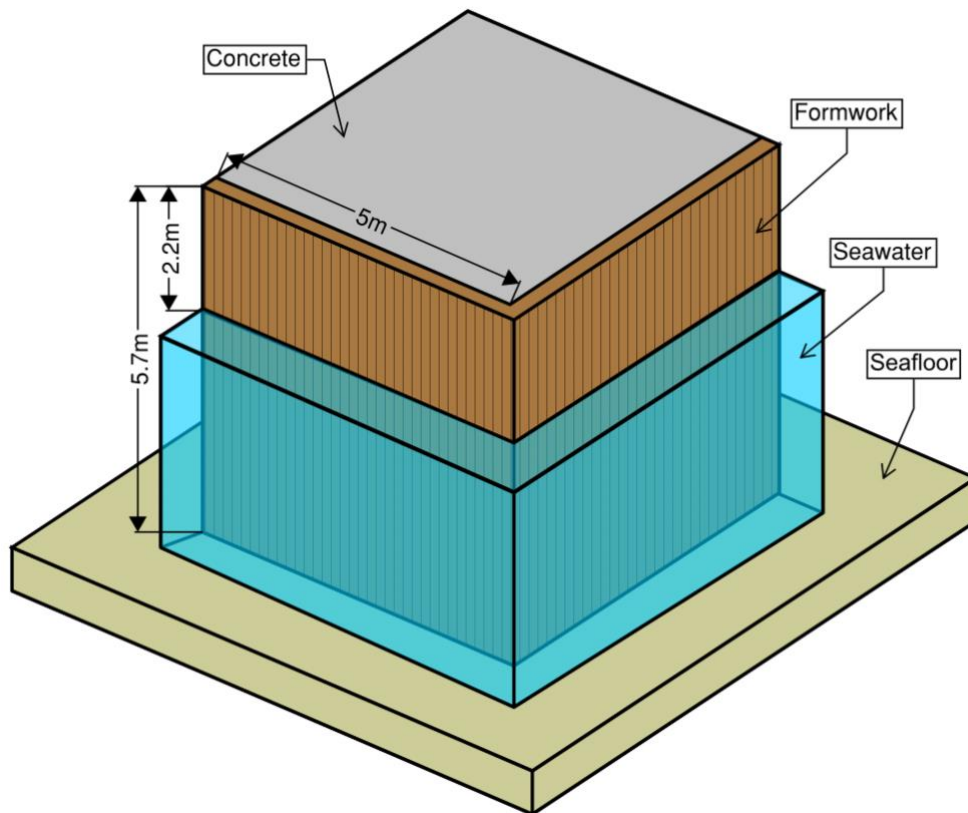
Figure 31. Representation of real-life conditions being implemented into the model as boundary conditions.

Based on the above Figure 31, the exposure of the block can be broken down into five different sets as follows:

- **Set 1 –** Top surface – Direct exposure to air with fluctuating temperature

- **Set 2 –** Outer surfaces above sea-level – Indirect exposure to air with fluctuating temperature (barrier provided by formwork)

- **Set 3 –** Outer surfaces below sea-level – Indirect exposure to seawater with static temperature (barrier provided by formwork)

- **Set 4 –** Bottom surface – Direct exposure to seafloor with static temperature

- **Set 5 –** Interior surfaces – No exposure; virtual surfaces that only exist to make use of symmetry

As shown in the list above, sets 3 and 4 are both represented in the model as interfaces with a fixed temperature. This is defined in the analysis as a Cauchy's boundary condition where heat convection around the concrete body is based upon an equivalent heat transfer coefficient calculated from the homogenization of the interface and the boundary layer between mediums (e.g. concrete + formwork + seawater) as visualized in Figure 32.

Figure 32. Homogenization of multiple boundary layers into one cohesive heat transfer coefficient. (Šmilauer et al., 2016)

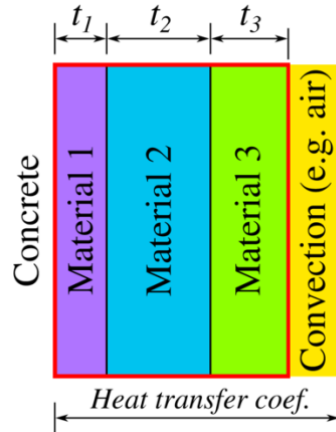The homogenization is performed using a harmonic mean equation implemented in ConTemp that calculates the equivalent heat transfer coefficient. Each constituent of the boundary layer is assigned a partial heat transfer coefficient using the following formula:

$$h_i = \frac{\lambda_i}{t_i} \tag{10}$$

Then the total equivalent heat transfer uses the harmonic mean equation as follows:

$$\frac{1}{h_{eq}} = \sum_{i=1}^{n} \frac{1}{h_i} = \frac{1}{h_1} + \frac{t_2}{\lambda_2} + \cdots \tag{11}$$

From there, the equivalent heat transfer coefficient is used to calculate the heat flux at the surface by following Newton's law on body surfaces using the following equation:

$$n(x)^T q(x) = h(x)\, (T(x) - T_\infty) \tag{12}$$

Where $n(x)^T$ is a unit normal vector perpendicular to the surface, and T_∞ is the ambient temperature specified for the adjacent medium (e.g. seawater or seafloor temperature).

For sets 1 and 2, the same principle boundary condition applies, and the same process is used to determine the equivalent heat transfer coefficient, but another equation is introduced to incorporate the fluctuating temperature corresponding with the chosen 24-hour day cycle. The equation is composed of two sine functions and a Heavyside step function, H(t), to create a 24-hour day and night cycle with the maximum temperature specified occurring at 14:00, the minimum at 2:00, and the average at both 8:00 and 20:00. The equation is as follows:

$$T(t) = T_{avg} + \left[T_{avg} - T_{min} + \left(T_{max} - 2T_{avg} + T_{min} \right) \cdot H \left(\sin \frac{2\pi t}{24} \right) \right] \cdot \sin \frac{2\pi t}{24} \qquad (13)$$

After defining these boundary conditions, all inputs for the differential equations are fulfilled and the thermal transport finite element analysis can be completed. Table 11 summarizes all boundary condition parameters for each block surface broken down by sets as described in the list above.

Table 11. Summarized boundary conditions parameters for the defined sets of surfaces on the block.

	h_{eq} (W/m^2/K)	T_{min} (°C)	T_{avg} (°C)	T_{max} (°C)
Set 1	16.8	22	26	30
Set 2	1.25	22	26	30
Set 3	1.21	-	-	-
Set 4	12	-	-	-
Set 5	-	-	-	-

4.2   Mechanical Model

4.2.1   Geometry

The geometry of the finite element model for the mechanical portion of the staggered analysis was kept exactly the same as the geometry for the thermal model. The intent is to study the effects of thermal and mechanical behavior concurrently on the same modeled *pila* so there is no need to make any modifications. The final geometry of the mechanical model is 5m x 5m x 5.7m tall.

4.2.2   Meshing

Although highly similar to the mesh element used for the thermal model, a different type of element had to be used for the mechanical model because the OOFEM structural module operates using a completely different selection of materials and elements. The intent was to again model the structure using 3D elements, which was determined to be best represented using 'LSpace' elements according to their description in the OOFEM Element Library (Patzák, 2012). They are described as linear isoparametric 3D brick elements containing eight nodes with three degrees of freedom for each node, and linear approximation between nodes with eight integration points used during the analysis. The three degrees of freedom for the structural mechanics module are u-displacement, v-displacement, and w-displacement. The diagram for the LSpace element according to the OOFEM manual is shown in Figure 33.
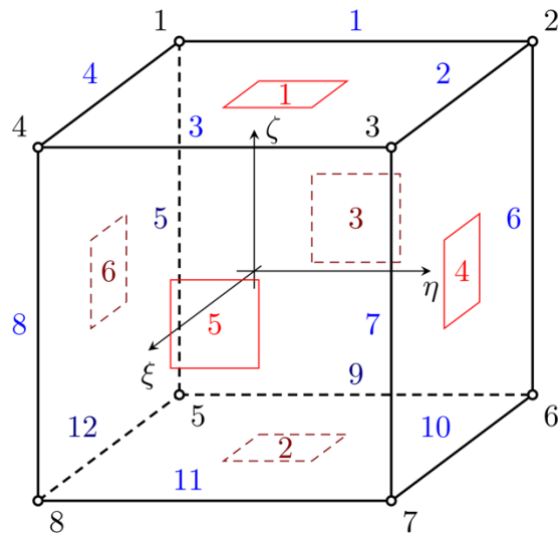
Figure 33. 'LSpace' element as defined by OOFEM. (Patzák, 2012)

The element size for the mechanical model was reduced because of the more robust LSpace element, which was defined with eight integration points making for accurate results with slightly coarser meshes. The final mesh was divided into 1000 elements in a 10x10x10 pattern with 10 elements evenly distributed across all edges. Thus, the size of each mesh element for all mechanical analyses is 50cm x 50cm x 57cm as shown in Figure 34.
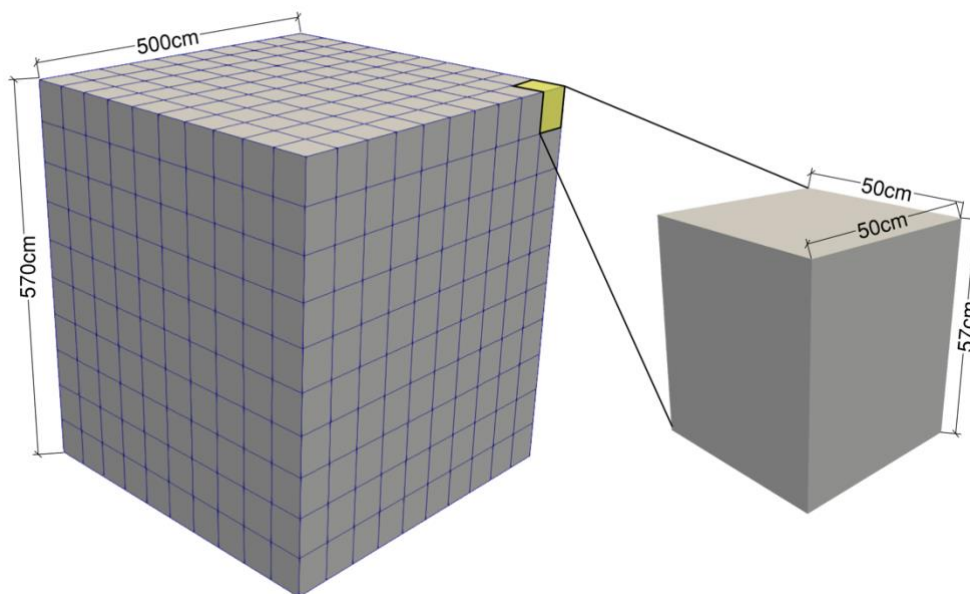
Figure 34. (left) Complete mesh for the mechanical analysis; (right) zoomed in single element.

It should be noted that the mechanical model's mesh could be simplified and contain nodes with coordinates different from those of the thermal model's mesh because OOFEM automatically uses linear interpolation across the entire thermal model to determine temperature values to be referenced at each node in the mechanical model according to their coordinates. Matching the two meshes exactly would have no benefit to the analysis.

4.2.3   Material Characterization

For the mechanical model, the Roman concrete was characterized primarily according to experimental values obtained during the ROMACONS study, and concrete constituent proportions according to literature, supplemented with experience from the experimental calorimetry trials. The basis of the mechanical model is to use a staggered analysis that incorporates the data from the thermal analysis for each timestep, which then gets incorporated into the stress calculations for the structural module. Because elevated temperatures and prolonged periods of time are crucial factors for the analysis, it makes the most sense to define the model with an aging viscoelastic material that can incorporate basic creep properties affected by temperature.

The material model selected for use with the OOFEM code is the 'MPS' material, which is based on the microprestress-solidification theory and is a more recent improvement upon the aging viscoelastic B3 model for concrete creep and shrinkage developed by Prof. Bažant and coworkers at Northwestern University (Bazant & Baweja, 2000). The rheological model consists of four parameters $q_1 - q_4$, which are all based upon concrete compressive strength and the proportions of the concrete constituents. The equations for each of the four parameters are as follows:

$$q_1 = 126.77 \, \bar{f}_c^{-0.5} \; [10^{-6}/MPa] \tag{14}$$

$$q_2 = 185.4 \, c^{0.5} \, \bar{f}_c^{-0.9} \; [10^{-6}/MPa] \tag{15}$$

$$q_3 = 0.29 \, (w/c)^4 \, q_2 \; [10^{-6}/MPa] \tag{16}$$

$$q_4 = 20.3 \, (a/c)^{-0.7} \; [10^{-6}/MPa] \tag{17}$$

For these equations, the compressive strength was specified as 6.5 MPa as per the experimental testing on ROMACONS cores (J. Oleson et al., 2004), which is the best accessible data on Roman seawater concrete strength. The water to binder ratio, w/c, was specified as 0.76 because that was determined to be a good ratio during the experimental trials with the lime-metakaolin mortars. The binder content, c, was specified as 444 kg/m^3 and the aggregate to binder ratio as 1.32, both according to the constituent proportions from literature (Brandon et al., 2014; M. D. Jackson, Chae, et al., 2013). It is important to note that some of these material parameters are probably beyond the validity range of the B3 model primarily meant for OPC concretes (Bazant & Baweja, 2000).

The three other parameters required for the structural module to run are density, Poisson's ratio, and the coefficient of thermal expansion. The density value was set at 1494 kg/m^3 as per the same ROMACONS study (J. Oleson et al., 2004). Poisson's ratio was set at 0.2, which is a common value for most concretes, and the coefficient of thermal expansion at 12 x $10^{-6} \, m/m \cdot K$ (Jeong, Zollinger, Lim, & Park, 2012). All material parameters for the mechanical model are summarized in Table 12.

Table 12. Summary of material parameters for the mechanical model.

Density	1494	kg/m³
Poisson's Ratio	0.2	-
Thermal Expansion Coeff.	1.2E-05	1/K
Compressive Strength	6.5	MPa
Elastic Modulus	6657	MPa
Binder Mass	444	kg/m³
Water/Binder Ratio	0.76	-
Aggregate/Binder Ratio	1.32	-

4.2.4 Boundary Conditions

Boundary conditions for the quarter block modeled after the *pila* were kept simple with the analysis attempting to replicate real-life conditions where the base of the block is unconfined in the X- and Z-axes meaning the block can expand and contract freely along the seafloor. The two vertical faces of the block representing planes along the interior of the entire 10m x 10m block need boundary conditions as well to properly mimic the 3D behavior of the full block, while modeling just one-quarter. To do so, the interior surface parallel to the X-axis was confined in Y-direction (orange surface in Figure 35), while vice versa was specified for the interior surface parallel to the Y-axis (pink surface in Figure 35). These two boundary conditions replicate the influence of the other ¾ of the block that has not been modeled directly. A schematic for the boundary conditions is shown in Figure 35.
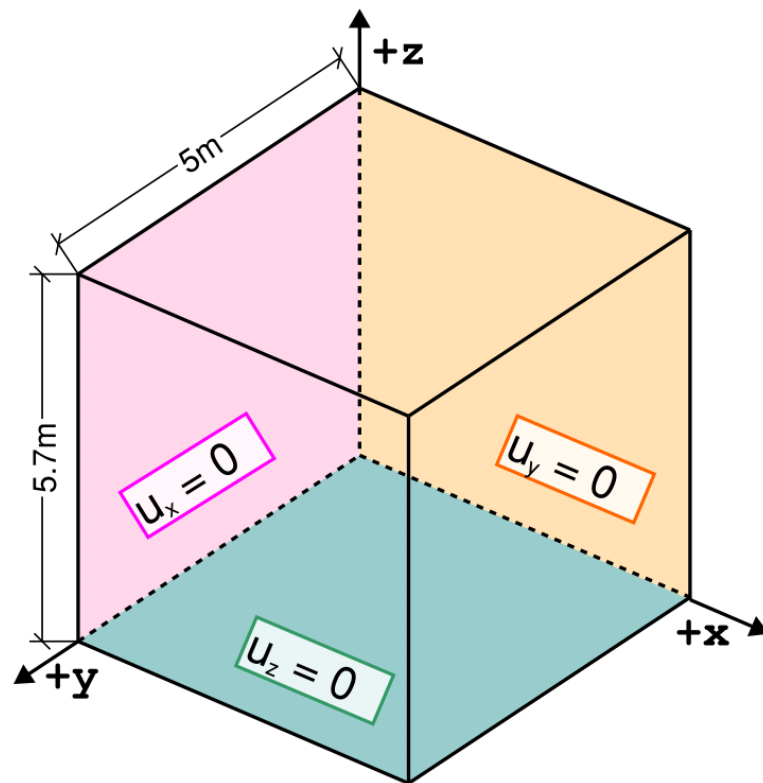
Figure 35. Boundary conditions for the structural module.

4.2.5 Loading

Although this analysis uses a structural module to calculate the development of stress as the result of displacements due to loading, the input file is written such that no physical load is applied to the block and all stress development is purely due to effects from thermal expansion and contraction. The dead load of the concrete has also been neglected as it is deemed inconsequential when compared to the thermal loads. This makes it so the model is closely representing the real-life conditions of the existing ancient Roman *pilae* distributed throughout the Mediterranean Sea as free-standing structures with no applied loads. All stress development is completely controlled by the hydration process of the concrete.

5. THERMAL ANALYSES

Three different thermal analyses were conducted using the transient transport module of the OOFEM finite element code, with temperature as the primary variable for all degrees of freedom. Heat was generated for each model by means of a hydrating concrete block and due to any influence from the surrounding environment as controlled by boundary conditions. The goal for each analysis is to calculate the evolution of temperature throughout the 3D block, with the primary takeaway typically being the peak temperature resulting from the independent analysis parameters.

Results from the thermal analysis model deemed most representative of the Roman seawater concrete will be implemented into the staggered thermomechanical analysis in the proceeding chapter.

5.1 Freshwater Mix vs. Seawater Mix

As made clear by the design of the experimental campaign, one of the primary objectives of the thermal analyses is to understand the effect that mixing the concrete with seawater, instead of freshwater, has on the time-dependent temperature profile of the modeled concrete pier. This analysis serves to compare two different models with completely different OOFEM input files; however, with the same heat transfer problem, time domain, mesh geometry, and boundary conditions. The only difference between the two models is the material parameters, with one characterizing a freshwater based concrete mixture and the other characterizing a seawater based concrete mixture, both mimicking as closely as possible all other material parameters known for ancient Roman seawater concretes.

5.1.1 Results

When comparing the freshwater mix (Mix 1) versus the seawater mix (Mix 2) with an identical transient transport analysis, the evolution of temperatures shows a clear difference as visualized in Figure 36.
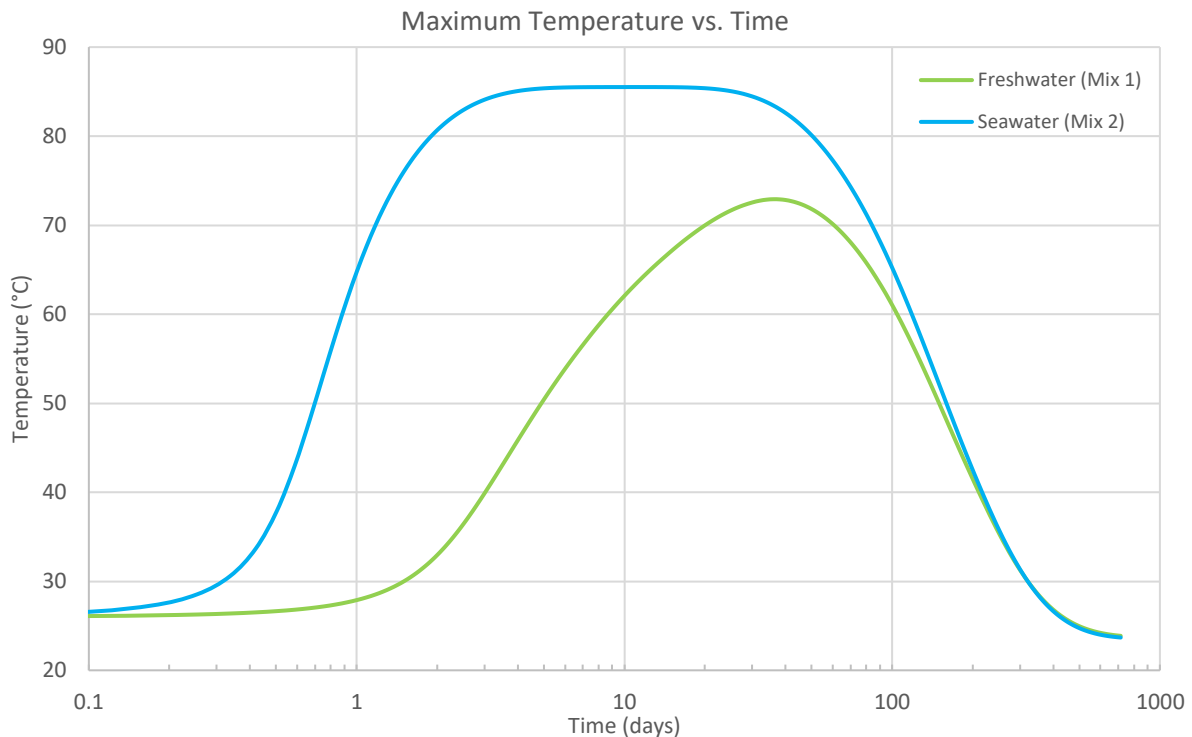
Figure 36. Maximum temperature within the concrete block versus time for both Mix 1 and Mix 2.

The seawater mix shows much larger and faster temperature rise with the centermost node of the block reaching 65 °C after only one day, and then at about six days it reaches its peak temperature of 85.5 °C where it holds constant for an extended period of time. The freshwater mix only reaches 27.9 °C after one day and a peak temperature of 72.9 °C after about 34 days. The two models both cool down to the ambient temperature of the surrounding seawater, 26 °C, around the same time, both taking approximately 434 days to do so.

Based upon the experimental isothermal calorimetry heat flow and total heat curves, the temperature rise shown in Figure 36 follows the expected pattern of the seawater model reaching much higher temperatures. The peak change in temperature for the seawater mix is 59.5 °C and for the freshwater mix is 46.9 °C.

Because of the large size of the structure, the centermost node is extremely close to experiencing purely adiabatic conditions due to the mass of the surrounding concrete. This means if virtually no heat from the centermost node is lost to the surrounding environment (e.g. seawater), according to the first law of thermodynamics, the temperature change must increase linearly with the heat added and scaled by the heat capacity of the material, as in the following equation:

$$\Delta Q = mc\Delta T \tag{18}$$

The heat capacity of the concrete, c, was already calculated in the material parameters section and is known to be 1623 J/kg/K, however the change in heat, ΔQ, still needs to be determined. To do so, the heat of hydration curve from the isothermal calorimetry tests can be used to get the expected ΔQ based upon the time at which the model reaches the peak temperature, 8 days. However, one extremely important detail is that the time needs to be scaled to an equivalent time, T_{eq}, because as the concrete hydrates, the production of heat further encourages the hydration reaction to accelerate. Essentially it is a self-exacerbating reaction that exponentially increases the equivalent time based primarily on the Arrhenius equation with the analytical form as follows:

$$T_{eq}(T) = exp\left[\frac{E}{R}\left(\frac{1}{T_0} - \frac{1}{T}\right)\right] \tag{19}$$

Where E is the activation energy of the reaction (J/mol), R is the universal gas constant (8.314 J/mol·K), and T_0 is the reference temperature. For the freshwater model, the activation energy is 66,000 J/mol, for the seawater model it is 75,000 J/mol (Shi & Day, 1993), and the reference temperature for both is 293 K. Equivalent time was calculated for both mixes and is plotted versus time in Figure 37.
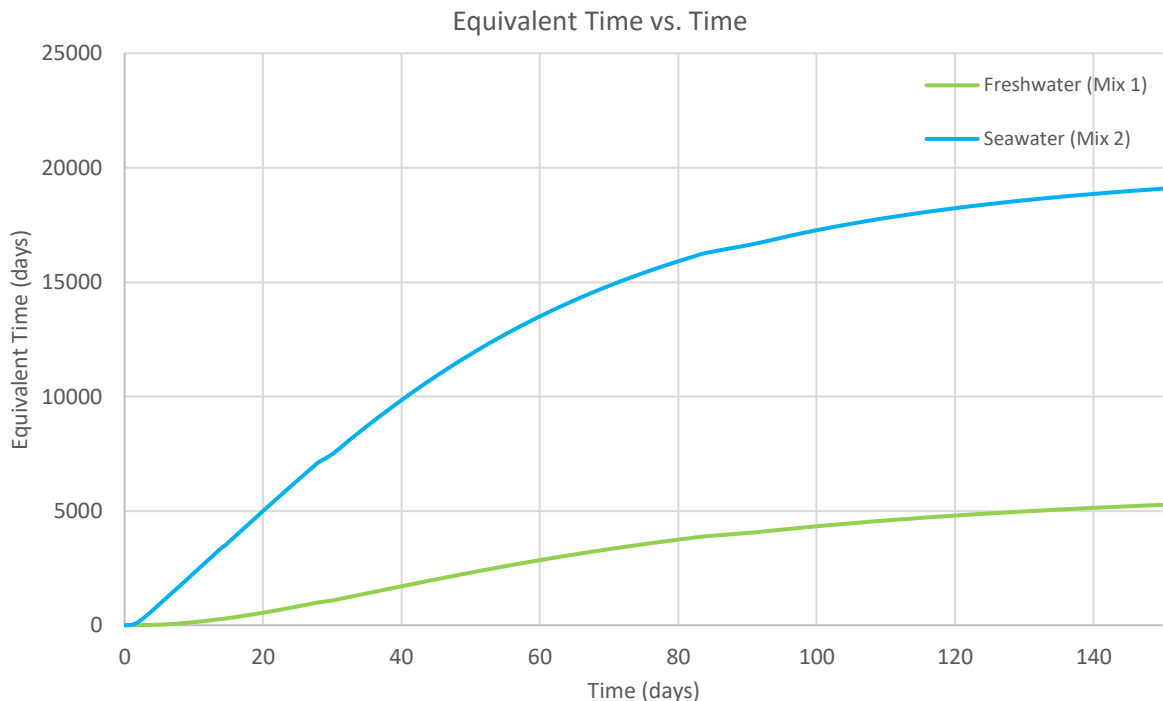

Figure 37. Equivalent time versus real time for both models.

Looking at the equivalent time calculation for each mix, the peak temperature for the freshwater mix occurs at an equivalent time of 2099 days, and for the seawater mix it occurs at an equivalent time of 2427 days. Now these values should be compared to the isothermal calorimetry dataset to find what the corresponding ΔQ would be, but that presents a problem. The experimental test was only conducted for thirteen days so there is no value to correspond to the equivalent times, but this can be solved by taking the four-parametric model curve that was fit to each dataset using ConTemp and then extrapolating out the curve to the necessary equivalent time as shown in Figure 38 and Figure 39.
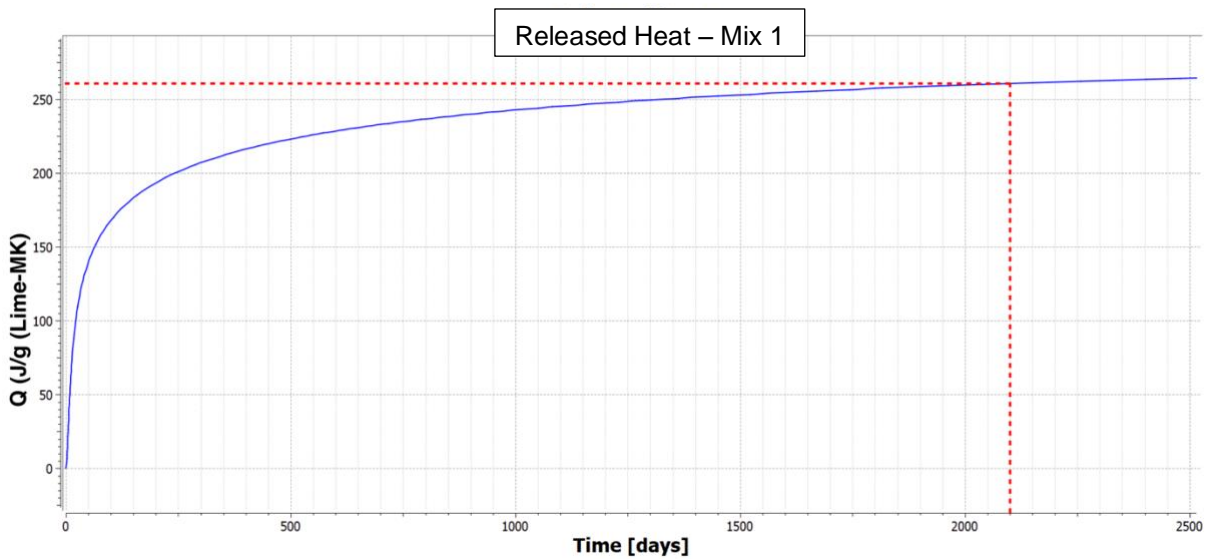

Figure 38. Extrapolated four-parametric model curve of heat vs. time - freshwater mix.
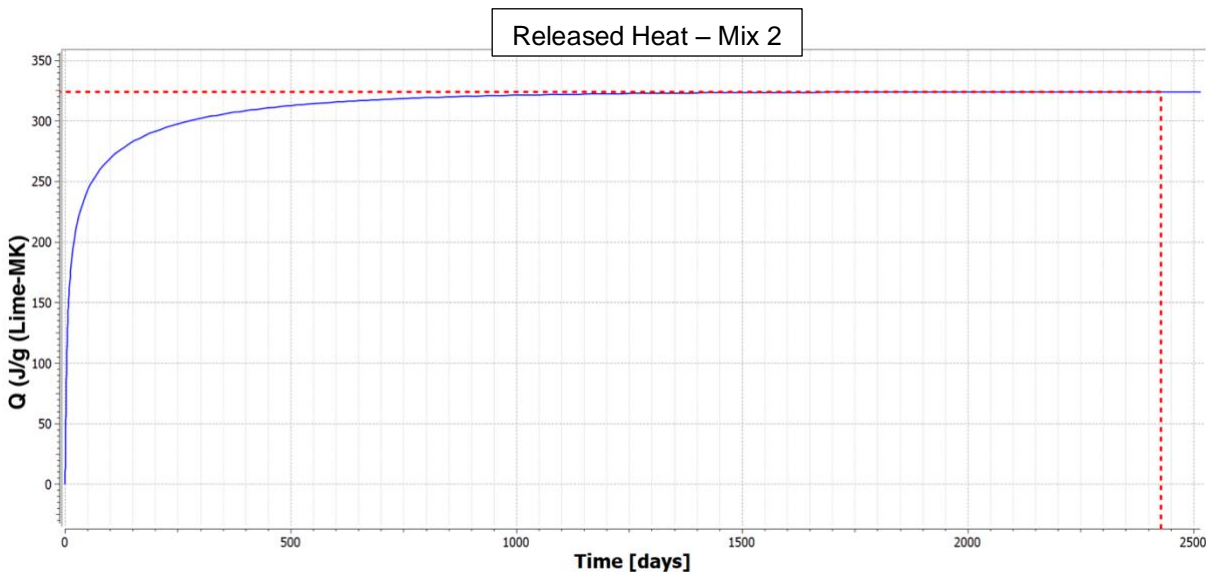

Figure 39. Extrapolated four-parametric model curve of heat vs time - seawater mix.

The datasets shown in Figure 38 and Figure 39, are then used to determine that the expected ΔQ for the freshwater and seawater mixes at their peak temperature are as follows:

- Freshwater (Mix 1): $\Delta Q = 260.8 \left[\frac{J}{g}\right]$

- Seawater (Mix 2): $\Delta Q = 323.9 \left[\frac{J}{g}\right]$

Going back to Equation (18), ΔT can be calculated and added to the initial temperature (26 °C) of the model to determine the theoretical peak temperature, assuming perfectly adiabatic conditions at the center of the block. These results are compared to the peak temperatures from the model and summarized in Table 13 below.

Table 13. Theoretical adiabatic peak temperature versus FE model peak temperature results.

	Mix 1	Mix 2	
Binder Mass	444	444	(kg)
ΔQ	260.8	323.9	(kJ/kg)
Density	1494	1494	(kg/m^3)
Heat Capacity	1.623	1.623	(kJ/kg/K)
ΔT	47.8	59.3	(°C)
Adiabatic T$_{max}$	73.8	85.3	(°C)
FE Model T$_{max}$	72.9	85.5	(°C)
% Error	1.2%	0.2%	(%)

Further visualization of the temperature gradients across the entire block for both separate models is better represented with 3D animations, which were prepared using the ParaView program (Ahrens, Geveci, & Law, 2005). To give an idea of the progression of temperature in 3D, screenshots were taken of the two models at four identical times during the analysis, 12 hours, 1 day, 7 days, and 34 days. These screenshots are compared side by side in the following Table 14, where all visualizations are showing temperature in degrees Celsius.

The 12-hour and 1-day timesteps are general representations of early development of internal temperatures, while the 7-day timestep corresponds to the peak temperature for the seawater model, and the 34-day timestep corresponds to the peak temperature for the freshwater model. All screenshots have the same orientation looking slightly from above and with the nearest edge along the Z-axis representing the vertical centerline for the overall 10m x 10m *pila*. The origin shown on the first screenshot represents the center of the 10m x 10m *pila* at the seafloor elevation.

Table 14. Screenshots displaying 3D temperature gradients for both models at four incremental timesteps.
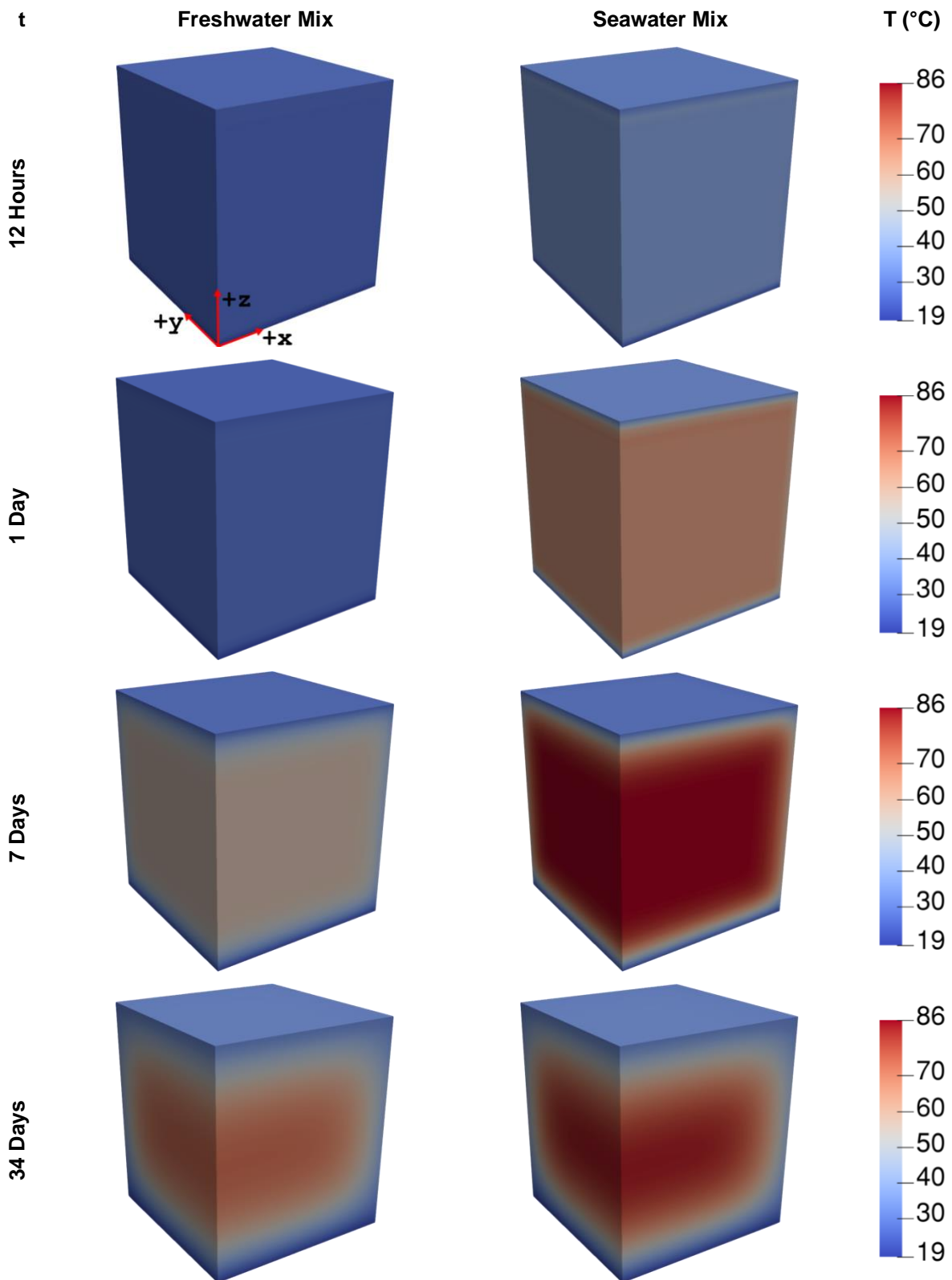
5.2 Instantaneous vs. Multi-day Concrete Casting

As discussed earlier, it has been estimated that the modeled *pila* would have taken approximately 13 days to pour given the contribution of 16 skilled workers and 18 laborers, amongst other assumptions regarding construction techniques and tools (Janet DeLaine, 2002). The previous analysis in Section 5.1, operates under the assumption that all 420 m^3 of concrete appears instantaneously in the formwork, which is an obvious simplification of the construction process for which an exact timeline is uncertain. However, when considering the slower hydration reaction of the lime-pozzolan binder when compared to modern-day OPC concretes, the differences between an instantaneous casting scenario versus a more realistic 13-day casting scenario could have a significant impact on the temperature profile of the concrete block.

This analysis serves to compare two different models with different input files using the same heat transfer problem, time domain, material properties, and boundary conditions. Following the results of the previous analysis, the seawater concrete (Mix 2) will be used to define the material parameters for this model and moving forward for all thermal analyses. The only difference between the two models is the mesh geometries and the subsequent casting times for portions of the concrete block.

The more simplified model of the two is the solid block geometry with all of the concrete being cast instantaneously and thus starting the hydration reaction at moment the analysis starts. The other model uses the layered block geometry, which starts with one layer being cast instantaneously the moment the analysis starts, and each subsequent layer is cast instantaneously 24 hours after the last. After 13 days and the final layer has been cast, there are absolutely no differences between any model parameters going forward and all changes in temperature-profiles are entirely dependent on the impact of the time-dependent layered casting.

5.2.1 Results

The superimposed temperature-time profiles for the layered block and solid block geometries are shown in Figure 40. It is important to note that for the solid block, all temperature values are taken from the centermost node because it is always the maximum temperature throughout the block. However, for the layered block, a direct comparison is not possible because for the first six days the node in question does not exist and therefore has no temperature data. To provide the closest comparison between the two models, data from the centermost column of 27 nodes on the layered block is isolated and set to record the maximum temperature for each time step at any one of the 27 nodes. This means that the temperature-time profile for the layered block corresponds to multiple different nodes throughout the block, while this does not occur for the solid block model. It is still comparing the absolute maximum temperature-time profile for each model.
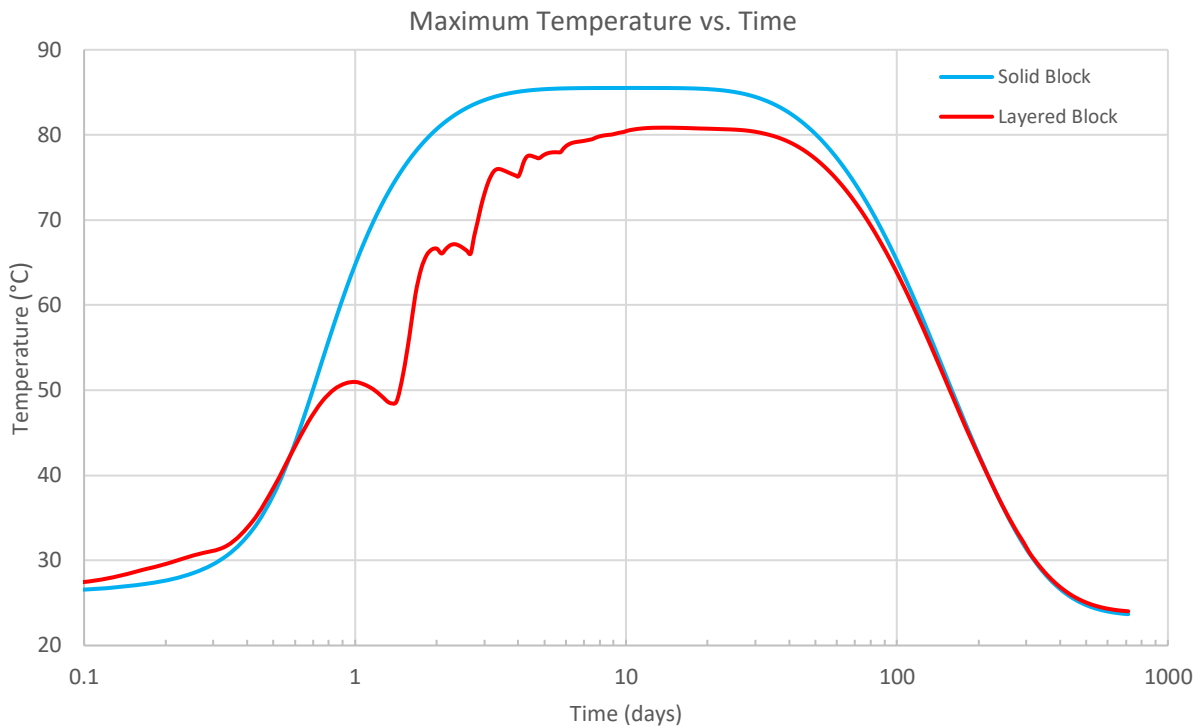
Figure 40. Maximum temperature versus time for both the solid block and layered block geometries.

When looking at the superimposed temperature-time profiles, it is obvious that the multi-day casting process has a significant effect on the maximum temperature throughout the concrete block. Only for the first ~6 hours of the analysis, the layered block has a slightly higher maximum temperature than that of the solid block because the heat flux contribution from the fluctuating air temperature above the block has much more of an influence on the node being evaluated. This is simply because the existing geometry of the single layer for this brief stretch of time is only ~44cm tall so the heat flux from above has much less distance to travel through the layer. However, after this short stretch of time, the layered block shows significantly lower maximum temperatures due to the prolonged casting process.

As mentioned in the previous analysis, the solid block model reaches a peak temperature of 85.5 °C after approximately six days, whereas this analysis shows the layered block reaching its peak temperature of 80.8 °C after approximately thirteen days. When subtracting out the initial condition of 26 °C, the solid block shows $\Delta T = 59.5\ ^{\circ}C$ and the layered block shows $\Delta T = 54.8\ ^{\circ}C$, meaning the introduction of the multi-day casting procedure reduces the maximum temperature by approximately 8%, while more than doubling the amount of time required to reach the peak temperature. The cooling processes for both models show very similar profiles and they both drop down to the ambient temperature of the surrounding seawater at the same time.

5.3   Effects of the Partial Use of Quicklime

One of the primary constituents of the ancient Roman seawater concrete is lime, or the as Vitruvius writes in *de Architectura*, *calx*. It is well understood from literature that this lime component makes up one-quarter of the lime-pozzolan binder mixture by volume (M. D. Jackson, Chae, et al., 2013); however, it is not known with certainty whether any of the lime product was slaked or not.

Most researchers suggest that slaked lime was used because quicklime can increase in volume 350 to 400% when slaked with water (Lancaster, 2005), and such expansion would cause discrepancies between observed volumetric ratios from coring and ancient specifications from Vitruvius, which is not the case. Further reading into the translations of Vitruvius specifications for terrestrial concretes (*De arch.* 2.5.1; pp. 16-17, Passage 6) shows an explicit mention of slaking lime before mixing the mortar, which although is not a direct specification for maritime concrete, strongly suggests the process is similar.

Looking from the other perspective, it has been well documented that relict lime clasts appear somewhat regularly throughout cored specimens of ancient Roman concrete (M. D. Jackson, Chae, et al., 2013), which could mean the slaking reaction was incomplete, or possibly some small additions of quicklime could explain the relict clasts. The thermal model effort conducted by Jackson et al., which the primary thermal analysis of this thesis serves to validate, calculated thermal parameters based on assumptions considering the use of quicklime instead of slaked lime.

To look into how the addition of quicklime, substituted for slaked lime, affects the temperature rise within the block, modifications were made to the FE model to simulate the slaking process. The previous analysis discussed in Section 5.1 operates under the assumption that 100% of the lime product is slaked before adding it to the concrete mixture, but this section seeks to explore the effects of replacing 10% of the total lime with pure quicklime. The value of 10% was chosen based on the assumption that the quicklime is an additive meant to contribute to the release of heat, and that it shouldn't be the predominant lime constituent. The model can easily be scaled to change the assumed percentage of quicklime.

In order to incorporate such an assumption into the FE model, a comparative model was developed with the only difference being an additional thermal body load applied to all nodes for a defined length of time beginning at the start of the analysis. This time-dependent method was chosen because studies have shown that the reaction time for quicklime to fully convert into $Ca(OH)_2$ takes anywhere from a few minutes to ten minutes depending on initial temperatures and the study referenced (Hassibi, 1999; Moropoulou et al., 2001). For this modeling scenario, the reaction will be simulated at a constant rate from $t = 0$ through $t = 300\ seconds$, which is input as a simple Heavyside function with time in seconds:

$$f(t) = 1 - h(300)$$

Now that the method of implementation via body loads and time of loading has been determined, the value of the load needs to be calculated based upon the heat of enthalpy for the slaking reaction of quicklime as follows:

$$CaO + H_2O \rightarrow Ca(OH)_2 \qquad \Delta H_f^\circ = -65.3 \; kJ/mol$$

Knowing that the molar mass of pure CaO is 56.08 g/mol,

$$Q = \frac{\Delta H_f^\circ}{molar \; mass} = -\frac{65.3 \frac{kJ}{mol}}{56.08 \frac{g}{mol}} \times 1000 \frac{g}{kg} = 1164.4 \frac{kJ}{kg}$$

Looking back at the concrete constituent proportions, 110kg of lime product are required per cubic meter of concrete, so the assumption of 10% quicklime equates to 11kg of quicklime per cubic meter. Then, the total heat of reaction can be calculated per cubic meter:

$$Q = 1164.4 \frac{kJ}{kg} \times 11 \frac{kg}{m^3} = 12808 \frac{kJ}{m^3}$$

Then considering that the heat is produced at a constant rate over a 300 second interval, the constant power per cubic meter can be calculated and then directly implemented into the model:

$$P = \frac{Q}{t} = \frac{12808 \frac{kJ}{m^3}}{300 \; sec} = 42695 \frac{W}{m^3}$$

The preceding calculations are summarized in Table 15.

Table 15. Summary of calculations for the thermal body load to simulate the reaction for lime slaking.

% Unslaked	10%	%
ΔH	-65.3	kJ/mol
Molar Mass CaO	56.08	g/mol
Q	1164.4	kJ/kg
Mass of CaO	11	kg/m³
Total Q	12808	kJ/m³
rxn Time	300	sec
Constant Power	42695	W/m³

5.3.1 Results

The temperature-time profile for the comparative model simulating the contribution of a 10% substitution of quicklime for slaked lime is superimposed with the standard mix with 0% quicklime in Figure 41.
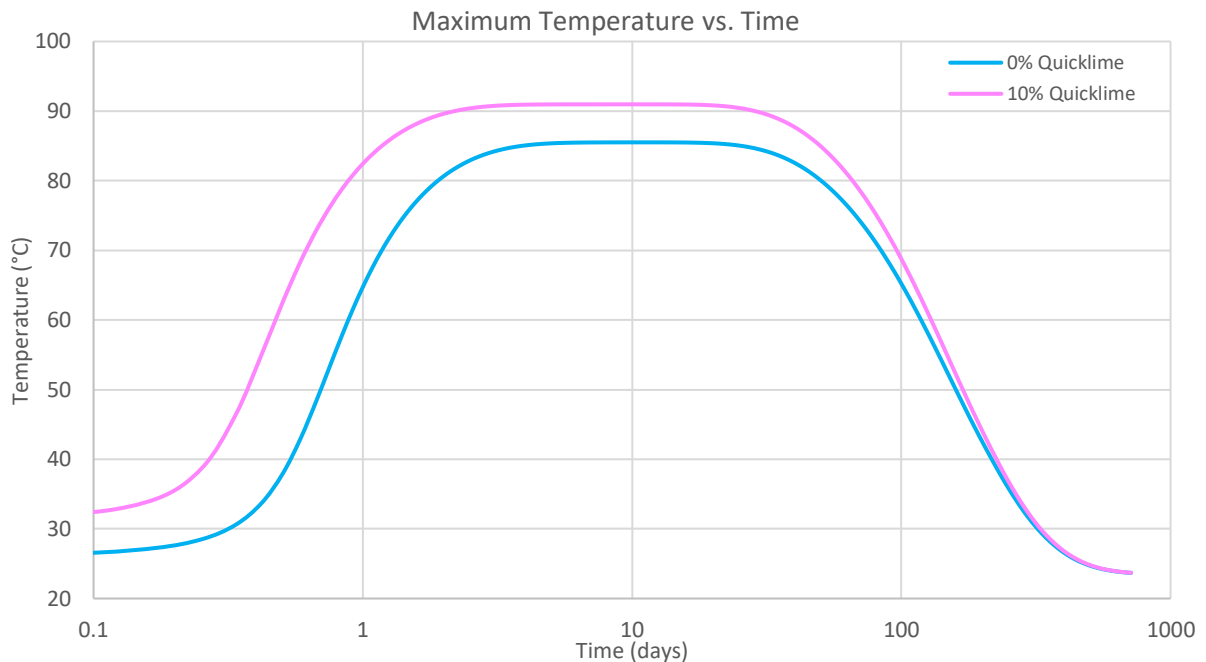

Figure 41. Maximum temperature versus time for the models with 0% and 10% quicklime.

When looking at the superimposed temperature-time profiles, it appears that the replacement of 10% quicklime accelerated the hydration process even quicker and appears to shift the temperature curve up approximately 5.5 °C while holding at the maximum adiabatic temperature for a longer period of time than the control model (0% quicklime). This behavior is in line with what was expected as a rapid production of additional heat in the first five minutes of casting should of course shift the temperature profile up to match what is basically an elevated initial condition.

When looking at the specific values, the peak temperature of the 10% quicklime model is 91.0 °C versus 85.5 °C for the control model meaning the corresponding ΔT values are 65.0 °C for the former and 59.5 °C for the latter. Because both are being held at their maximum adiabatic temperature for an extended period of time, another simple method was done to validate the results for the 10% quicklime model. This was done through another comparative model keeping all inputs the same as the control, and instead of adding a constant body load for 300 seconds, the initial condition was just scaled up to account for the total energy of the slaking reaction previously calculated. This will work by adding the same amount of energy as the body load method but instantaneously and in a more robust and failproof method, which serves well for validation.

To properly scale the initial boundary condition for this secondary validation, Equation (18) can be referenced again with the new ΔQ value simply being the contribution from quicklime slaking. The calculation is as follows:

$$Q = mc\Delta T$$

$$\Delta T = \frac{12808 \ \frac{kJ}{m^3}}{1494 \ \frac{kg}{m^3} \times 1.623 \ \frac{kJ}{kg*K}} = 5.3 \ °C$$

The comparison between the first comparative model with the replacement of 10% quicklime implemented using body loading, and this validation with a simple change in boundary conditions is shown in Figure 42.
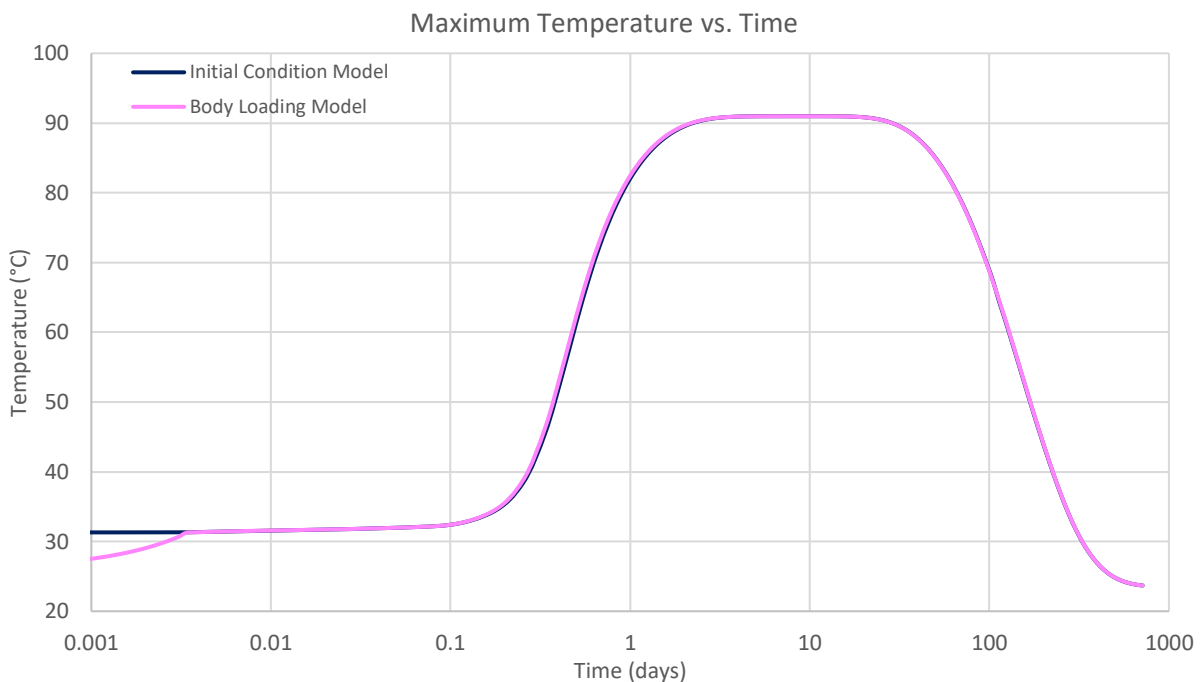

Figure 42. Maximum temperature versus time for the two comparative models, both implementing the effects of a 10% substitution of quicklime for slaked lime to the original model.

As clearly shown in the comparison between the original method using body loads, and the validation effort using a simple change in initial condition, the difference in the temperature-time profile is virtually zero. The only difference occurs during the first 300 seconds, where the body load is being introduced at a time dependent rate, whereas, the initial condition is an instantaneous increase in temperature. All things considered, these both have the exact same result and they both result in the same 5.5 °C increase in peak temperature when compared to the control model with 0% quicklime.

6.   MECHANICAL ANALYSIS

Following the thermal analyses, the same model was implemented into an OOFEM staggered thermomechanical FE code, now using both the original transport module for the thermal analysis alongside the structural module for the mechanical portion. In order to accurately model any effects on the mechanical analysis as result of the rise and fall of temperatures from the hydration process, a material model was selected that implements concrete creep based on time and temperature. Additionally, thermal expansion and contraction was part of the module, thus creating thermal strains to govern stress development. Aside from the creep aspect of the material model, it begins as a linear isotropic material without any strength reduction mechanisms, essentially following a linear viscoelastic isotropic material law. All other aspects of the thermal model were kept the same including geometry, basic material properties, and time domain.

The goal of the analysis is to calculate the compliance function in order to quantify effects related to concrete creep and then to track stress development over time throughout the 3D block. The governing calculation for mechanical assessment should be tensile strength, which is expected to be significantly affected by the concurrently implemented thermal analysis.

The following equation shows the general stress-strain incremental formulation for the viscoelastic analysis:

$$\Delta\sigma \ = \ E D_V (\Delta\varepsilon - \Delta\varepsilon'' - \Delta\varepsilon_T) \tag{20}$$

Where $\Delta\sigma$ is an increment of nominal stress, E is the incremental elastic modulus, $\Delta\varepsilon$ is incremental strain, $\Delta\varepsilon''$ is incremental strain due to creep, and $\Delta\varepsilon_T$ is incremental thermal strain. D_V represents a unit elastic stiffness matrix with a constant Poisson's ratio.

6.1   Compliance Function

Concrete creep is often quantified using what is called a compliance function, $J(t, t')$ $[1/MPa]$, where the constant stress applied to the material can be correlated to the resultant strains as a function of two variables: time (t), and the time loading is applied (t'). This analysis neglects both autogenous and drying shrinkage, making the only associated strains related to the load application and the thermal expansion or contraction of the concrete block. As such, the general form of the compliance function is as follows:

$$\varepsilon(t) = \ \varepsilon_e + \ \varepsilon_c(t) \ + \ \alpha\Delta T(t) = \ \hat{\sigma} J(t, t') \tag{21}$$

Where ε_e is the instantaneous strain from the application of stress, $\hat{\sigma}$, and $\varepsilon_c(t)$ is the strain due to concrete creep. The change in temperature, to later be associated with the staggered thermal analysis, is captured by ΔT and thermal expansion by α.

Further, the conventional elastic modulus at age t' can be related to the inverse of the compliance function as a separate function of $t' + \Delta t$, where Δt is taken as 0.01 days for this analysis. This equation is as follows:

$$E_c(t') = 1/J(t' + \Delta t, t') \tag{22}$$

The compliance function for this analysis will be solved using the B3 model, an aging viscoelastic model for basic concrete creep, which is based on the solidification theory (Bazant & Baweja, 2000). This method offers a simple solution to a complex problem, making use of empirical formulae solely dependent on the $q_1 - q_4$ parameters predicted based on the composition of the concrete mix and its 28-day compressive strength.

The general form of the total compliance function is essentially the summation of three primary components of basic creep, all of which are calculated as their own partial compliance functions. The first of which is the contribution from the non-aging viscoelastic response of the solidifying material, written as $J_v(t, t')$, which in its simplest form is expressed as:

$$J_v(t, t') = q_3 \ln \left[1 + \left(\frac{t - t'}{\lambda_0} \right)^n \right] + q_2\, Q(t, t') \tag{23}$$

Where λ_0 is typically set to 1 day but is defined as 86400 seconds in the OOFEM analysis because the default unit of time for the transient transport module is seconds instead of days, and that time domain is used for the staggered analysis. Parameter n is an empirical constant set to 0.1 for the B3 model (Šmilauer et al., 2016).

The second partial compliance function corresponds to a non-aging elastic spring, which is meant to capture instantaneous deformation from the application of load. This is the simplest of the three and is expressed as follows:

$$J_e(t - t') = q_1 \cdot H(t - t') \tag{24}$$

Where $H(t - t')$ is a Heavyside function defined such that at any time before the application of the load, $H(t - t') = 0$, and any time after, $H(t - t') = 1$. Thus, making that portion of the compliance function simply equal to q_1 for all relevant timesteps.

The last compliance term corresponds to late-stage creep and it essentially scales a semi-logarithmic function of time by a scalar related to flow, which is dependent on the aggregate to cement ratio used in the q_4 calculation. The compliance term is expressed as follows:

$$J_f(t, t') = q_4 \cdot \ln \left(\frac{t}{t'} \right) \tag{25}$$

Finally, summing up the three terms gives the general form of the total compliance function for basic creep and is expressed as such:

$$J_b(t,t') = J_e(t-t') + J_v(t,t') + J_f(t,t') \tag{26}$$

The following Table 16 summarizes the concrete constituent inputs specified for the solution of the compliance function, and then Table 17 displays the resultant $q_1 - q_4$ parameters. After calculating the four parameters, the only missing variable for the solution is the time of loading.

Table 16. Concrete constituent proportions and material strength inputs.

f_c	6.5	MPa
c	444	kg/m^3
a/c	1.32	-
w/c	0.76	-

Table 17. Four-parameter output values used for B3 model compliance function.

q1	49.7	10^{-6}/MPa
q2	724.7	10^{-6}/MPa
q3	70.1	10^{-6}/MPa
q4	16.7	10^{-6}/MPa

Calculating for compliance using the four parameters described in Table 17, with a specified time of loading at 28 days after casting, yields the compliance function shown in Figure 43.
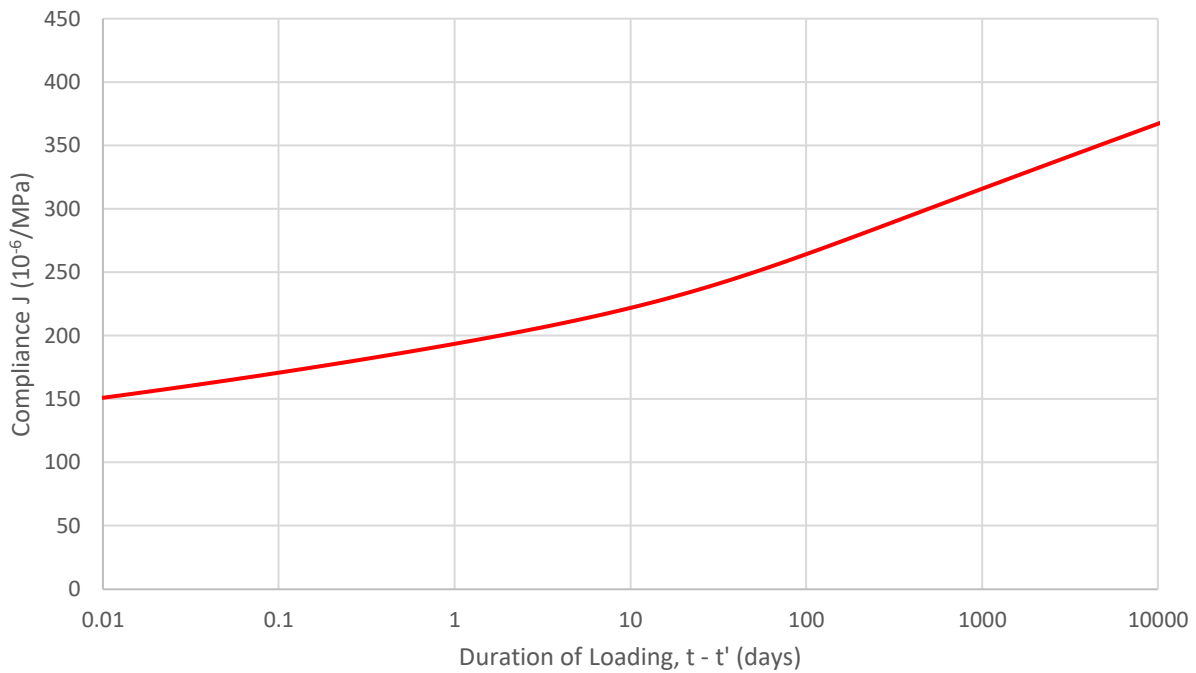
Figure 43. Compliance function for the modelled Roman seawater concrete, given t' = 28 days.

Then comparing the effects of time of loading, t', the compliance function has been solved for three different times of loading: 7, 14, and 28 days. Figure 44 shows these three compliance functions superimposed on the same chart.
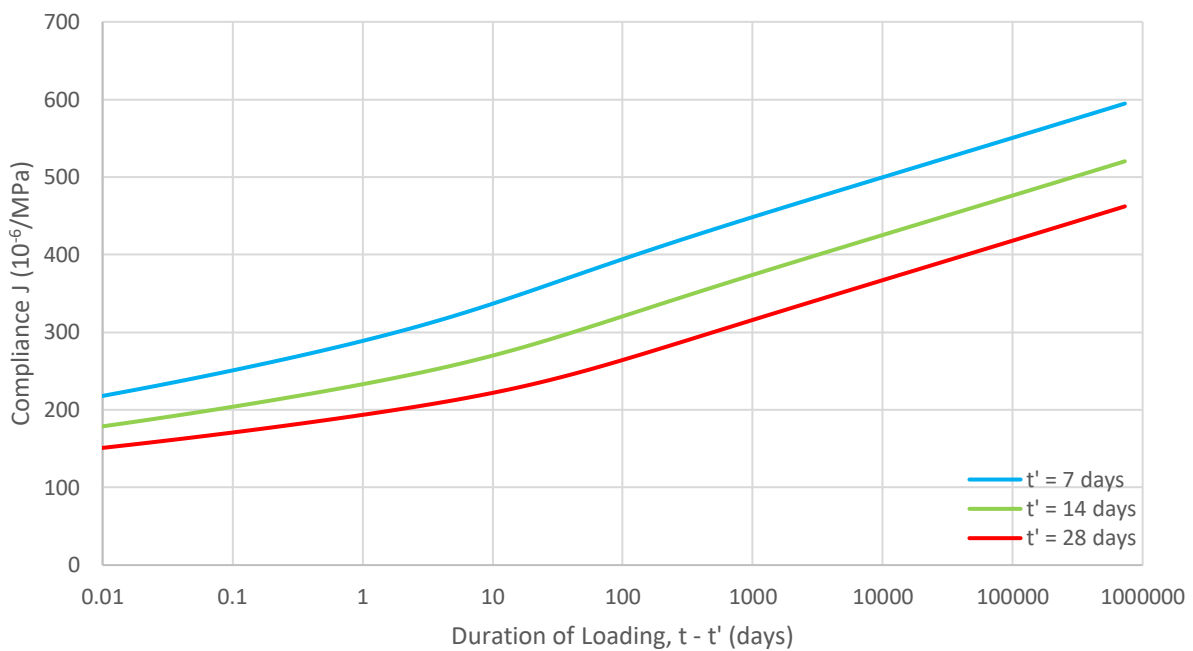

Figure 44. Superimposed compliance functions for three different times of loading: 7, 14, and 28 days.

Now, looking back at Equation (22), the compliance function can be used to incrementally plot the theoretical curve for the evolution of elastic modulus over time, as shown in Figure 45.
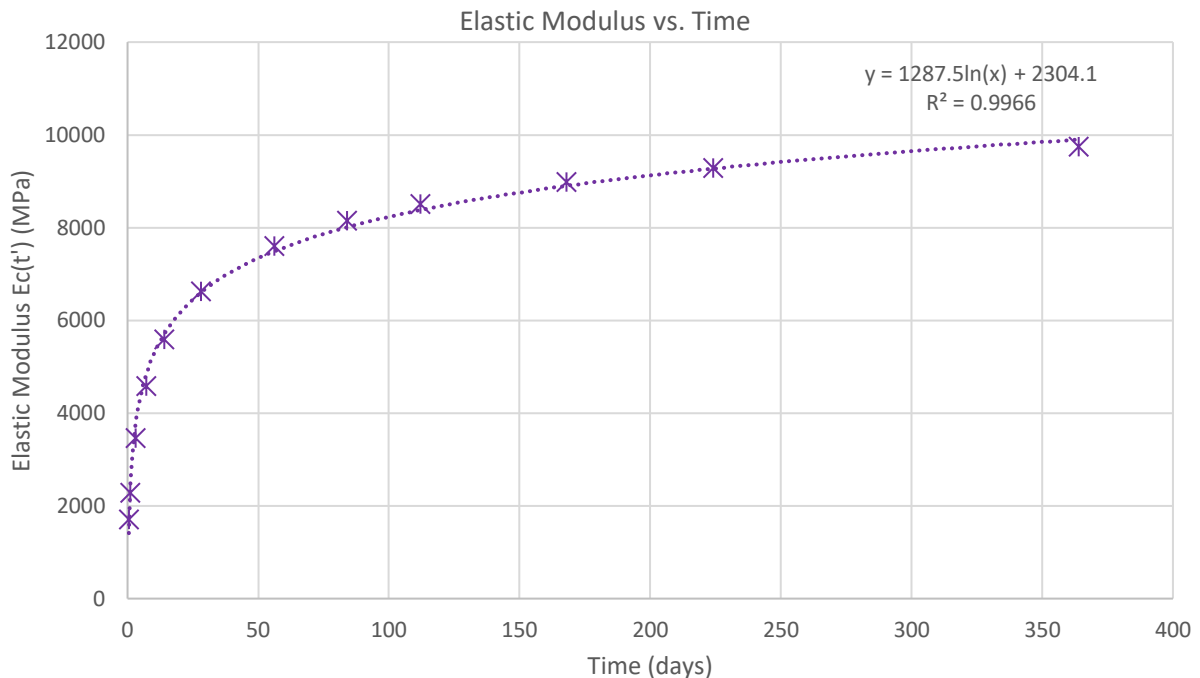

Figure 45. Theoretical evolution of the Elastic Modulus for the Roman seawater concrete.

Looking at the predicted evolution of elastic modulus, it is apparent that the B3 concrete creep model is a powerful tool, but not well calibrated for the Roman seawater concrete as evidenced by the difference between the predicted elastic modulus at 2000 years being 11,837 MPa, whereas the experimental value was measured to be 6657 MPa (J. Oleson et al., 2004). This is not surprising primarily because the B3 model is calibrated for concrete mixtures with OPC binder instead of only lime-pozzolana binder, and the compressive strength of the Roman concrete, 6.5 MPa (J. Oleson et al., 2004), falls outside of the suggested limits of the B3 model (Bazant & Baweja, 2000). Although not calibrated for the material of study, it is still useful for the overall thermomechanical analysis.

6.2   Stress Development

After solving the compliance function, the model can be checked for the development of stresses over time throughout the 3D block. No external loads have been applied to the block and dead load is ignored so all stress development is the result of thermal expansion and contraction due to the hydration reaction of the concrete. As such, both compressive and tensile stresses were expected to develop throughout the block and change throughout time with tension being the governing factor due to the brittle nature of concrete.

When looking into the directionality of the stresses, it is clear that the stresses in the X- and Y-directions are the highest due to block being almost twice as wide as it is tall (10m x 10m x 5.7m). This makes it so that there is much more material in the X- and Y-directions that can essentially constrain the expansion and contraction due to changes in temperature. Further, because of the partially symmetric geometry of the block, all stresses in the X- and Y- directions are identical and as such the primary results presented will be the development of stresses in the X-direction only.

First looking at the σ_{xx} stress fields for the 3D block reveals that very distinct patterns arise, and they obviously coincide with the heating and cooling of the block as calculated by the original thermal analysis. Screenshots of two crucial timesteps are shown in Figure 46, with the core of the overall block being represented by the nearest vertical edge.
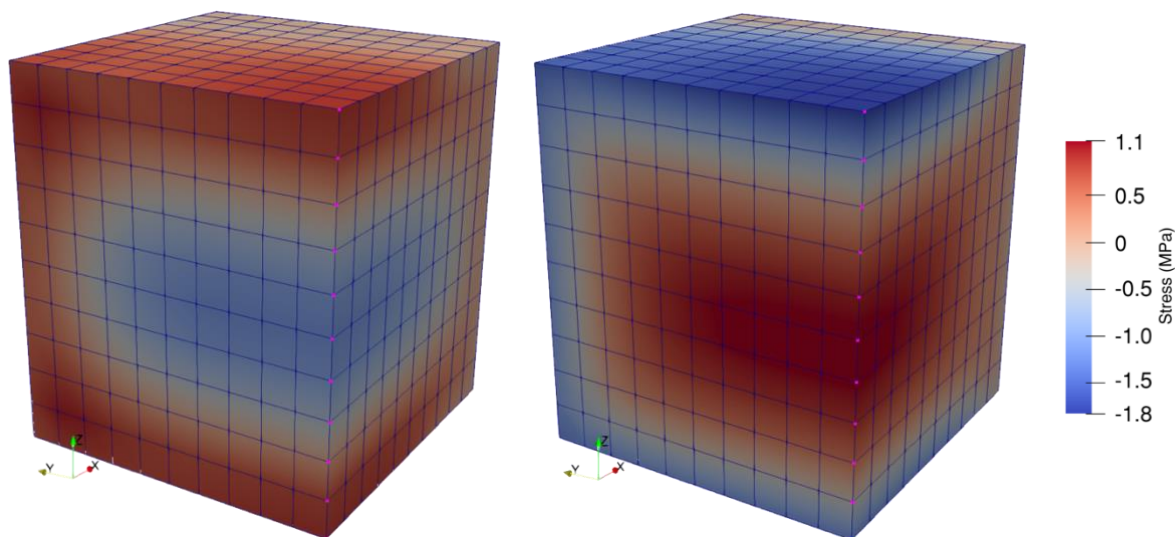

Figure 46. σ_{xx} stress fields for two extreme timesteps; (left) peak of temperature rise at 44 days; (middle) peak of cooling at 400 days; (right) color scale for both blocks.

Those two timesteps were selected because they represent the two extreme stress values experienced at the core of the block for maximum compressive and tensile stress. They also visualize the fact that the mechanical analysis can be broken down into two phases when looking into the evolution of tensile stress. The first portion (Figure 46, left) represents the slow rise in temperature at the core while the hydration reaction keeps contributing more and more heat causing the core to expand against a cooler and more solidified outer surface. The cooler surrounding material restrains the core causing compressive stresses for the expanding core, while the outermost material experiences tensile stresses due to its unconfined expansion. The second portion (Figure 46, right) is the cooling phase when the fully expanded core begins to shrink but is now resisted by the also expanded outer surfaces. Thus, while the core contracts back to the original size it experiences tensile forces and also causes the outer surfaces to experience compressive forces.

Now understanding the overall pattern of stress evolution, the block can be reduced from a large volume with copious amounts of time dependent data into a smaller subset containing only the critical nodes with the extreme stresses. Knowing that thermal expansion and contraction are the only driving factor for the tensile stresses, it is obvious the higher stresses will occur where the steepest temperature gradients arise. Looking back to the thermal analysis, this should be at the core of the block and this is confirmed by the stress profiles shown in Figure 46 above. Thus, the 3D block can effectively be reduced down to the vertical column of nodes at the center of the block to determine maximum tensile stresses for the block at both the core and the outer surfaces. For better visualization, this reduced set of eleven critical nodes have been highlighted in pink on the 3D block as shown in Figure 47.
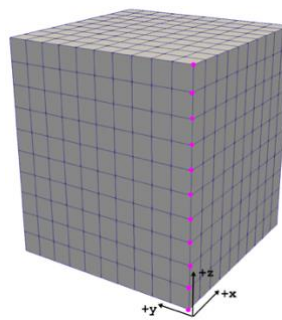

Figure 47. Isoparametric view of the 3D block with critical nodes highlighted in pink.

Looking at the stress development over time for the centermost node of the block, where temperature rise is the greatest, shows a significant variation in σ_{xx} stresses between the expansion and contraction phases. The time dependent curve for this specific node is shown in Figure 48
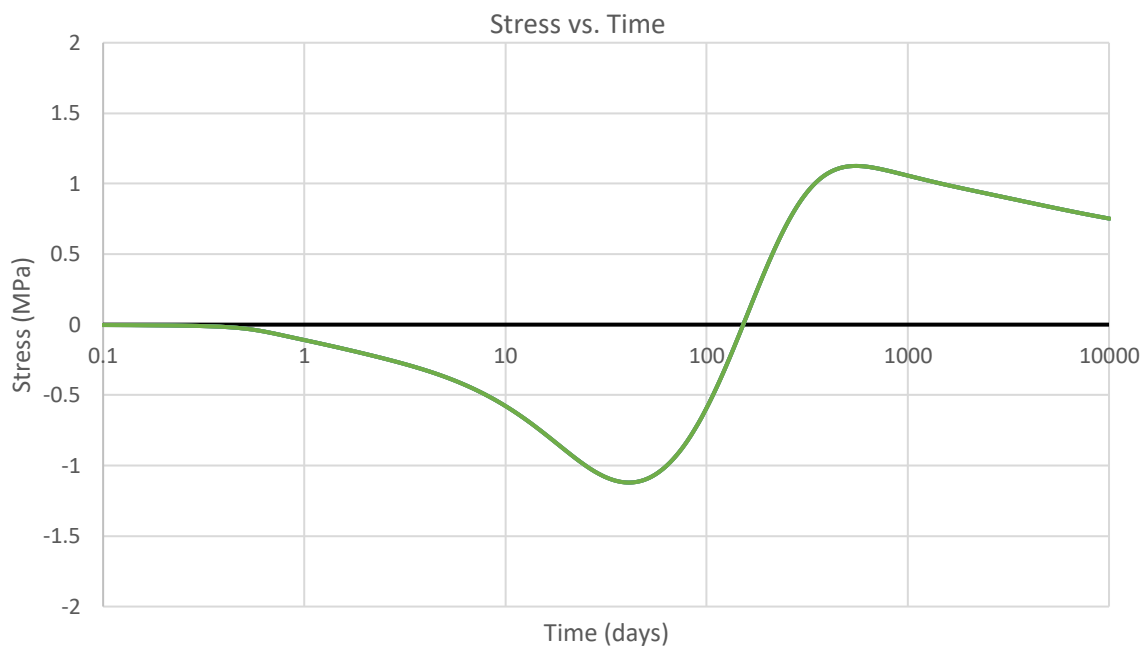

Figure 48. σ_{xx} stress versus time for the centermost node at the core of the block.

The time-dependent stress curve shows that during the expansion phase, the core is experiencing compressive stresses for approximately 147 days until the block begins to cool and shrink, thus leading to the onset of tensile stresses. The tensile stress reaches a maximum value of 1.13 MPa after approximately 546 days meaning that the block is now steady-state with no further change in temperature and no further stresses due to thermal effects. From then on, the stress logarithmically trends towards zero because of the relaxation within the viscoelastic concrete creep material model.

Now, plotting the stress development over time for the node at the top surface of the block should show a pattern somewhat inverse to the behavior at the center as previously explained. The stress versus time curve for the node on the top surface is shown in Figure 49. Highly similar behavior occurs at the bottommost node as well, but because boundary conditions were simplified and don't model any X/Y axes interaction between the seafloor and the block, more accurate results are expected for the node on the top surface.
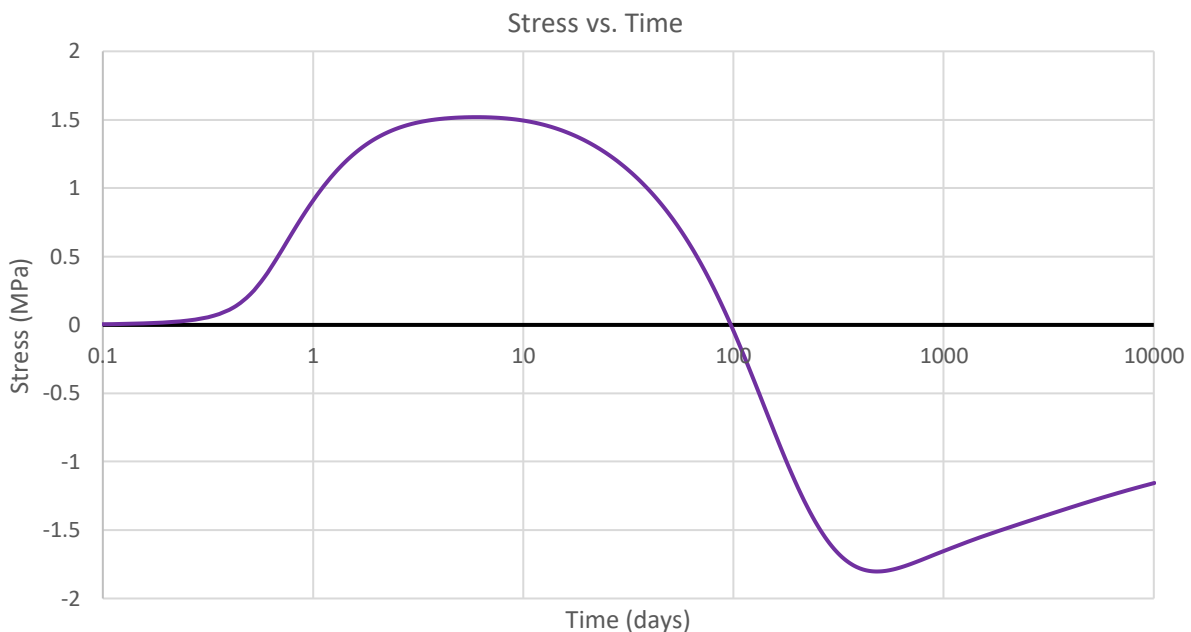

Figure 49. σ_{xx} stress versus time for the topmost node at the core of the block.

Finally, superimposing the two curves (Figure 50) should serve as maximum stress envelope for the tensile stresses arising throughout the whole block in either the X- or the Y-axis because these are the most critical nodes.
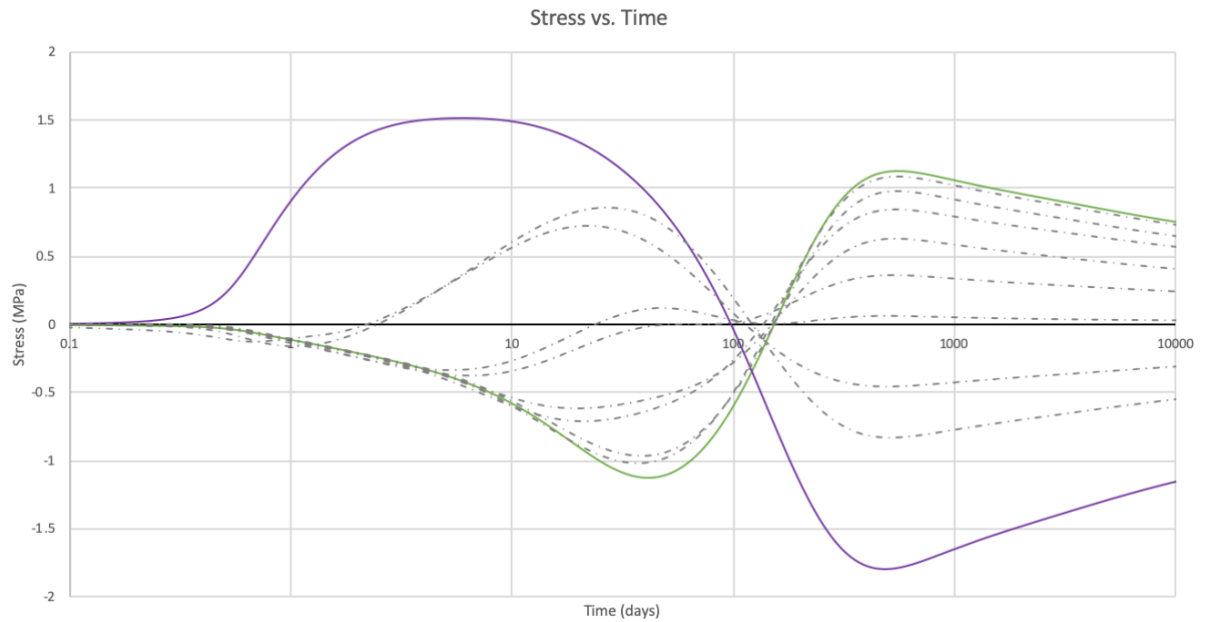
Figure 50. σ_{xx} stress versus time for all 11 critical nodes at the center of the block.

One final way to visualize the evolution of stress throughout the centermost column of elements deemed the most crucial portion of the block is via a series of contour plots distinguishing stresses by a color gradient. Eight screenshots were collected from ParaView using timesteps deemed best to visualize the overall pattern of stress evolution across the height of the block and they are set side by side in Figure 51 with a common scale. The pattern shows the inverse pattern that the core has with the upper and lower surfaces of the block.

Figure 51. Selective stress profiles at eight timesteps for the centermost column of elements.
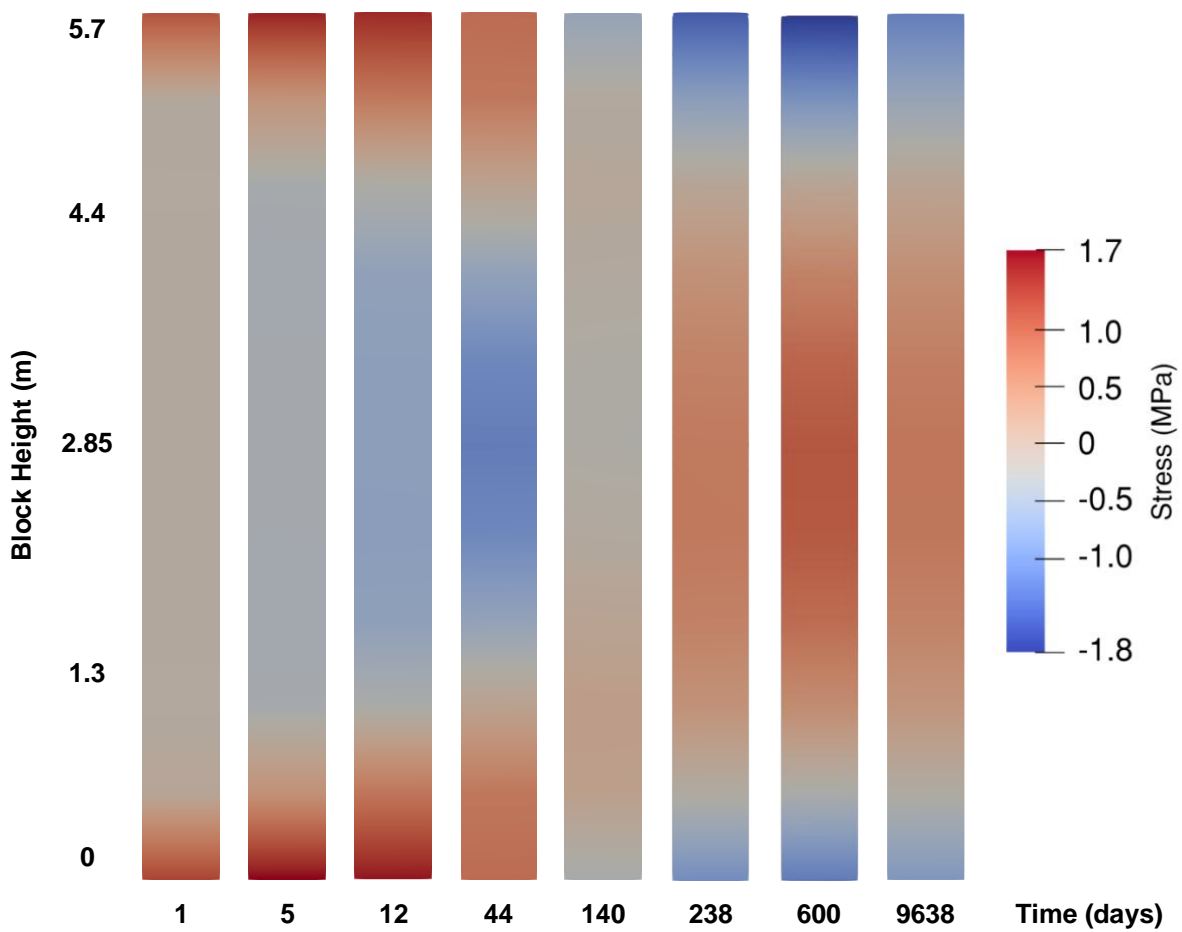
Summarizing the stress results from the thermomechanical analysis, the maximum compressive stress of 1.8 MPa occurs at the center of the block on the top surface 476 days after concrete casting. The maximum tensile stress of 1.64 MPa occurs at the center of the block on the bottom surface 4 ¼ days after concrete casting or 1.52 MPa at the center of the block on the top surface after 5 ¾ days. It should be noted that boundary conditions were most simplified at the base and no interface was modeled to represent any interactions between the concrete block and the seafloor. Real-life conditions would introduce some restrictions at the bottom surface in the X/Y-axes due to friction at a bare minimum, which would reduce the experienced tensile stresses. The top surface has boundary conditions more closely representing the open-air conditions of real life.

When considering the compressive strength of the material, which has been experimentally tested to be 6.5 MPa (J. Oleson et al., 2004), the stress development due to temperature rise and fall within the block does not present issues in regard to compressive failures. Considering tensile stress development however, cracking would surely occur at the outer portions of the block during the thermal expansion phase, and then later at the core during the thermal cooling phase. The associated tensile stresses for those portions of the block rise well above the expected tensile strength of the material.

Although the tensile strength of the Roman seawater concrete hasn't been explicitly characterized with experimental testing, it can be reasonably estimated based on comparisons to modern concrete. A general rule of thumb for unreinforced concrete is that the tensile strength should be about 1/8 that of the compressive strength, which would mean the tensile strength of the Roman seawater concrete can be roughly estimated to be about 0.8 MPa. Tensile stresses throughout the block well exceed 0.8 MPa throughout the thermomechanical analysis.

Further analysis could be conducted to extend the scope of the project to focus more on the occurrence and locations of cracking. This could be done by properly characterizing the tensile strength of the Roman seawater concrete and then implementing a damage based viscoelastic material within the OOFEM code. This would introduce cracks to reduce the effective area of the block when the tensile stress reaches the material's defined strength to give a more accurate result in regard to development of tensile stresses.

7.   CONCLUSIONS

Based on the thermal analysis of the Roman seawater concrete FE model, temperature rise would be drastic at the core of the concrete block with a peak temperature rise of 59.5 °C. This value very closely matches the calculated temperature rise of 59.3 °C given completely adiabatic conditions, which proves that the large volume of the concrete structure plays a significant role in the development of temperature throughout the block. When comparing to the Jackson et al. study that this thesis aimed to validate, their calculated temperature rise of 66 °C (M. D. Jackson, Chae, et al., 2013) is not far off from the results of this study, which improved upon some of their assumptions in regard to material characterization and boundary conditions.

The three extensions of the primary thermal analysis also clarified how select changes to either mix design or construction procedures would affect the temperature development throughout the block. Mixing the experimental mortar with seawater instead of freshwater resulted in a difference in peak temperature of 12.6 °C and shows that there is no significant benefit to mixing with freshwater only. Modeling the concrete block with a time-dependent geometry that simulated a thirteen day long concrete pouring procedure reduced the peak temperature rise from 59.5 °C down to 54.8 °C, which is a significant decrease but still a very large overall increase in temperature. Finally, modeling a 10 wt% substitution of slaked lime for quicklime caused an additional temperature rise of 5.5°C making the peak temperature at the core of the block 91 °C.

The thermomechanical analysis successfully calculated and allowed for visualization of the stress development throughout the block over time and how they relate to the evolution of temperature. The stresses can be broken into two distinct phases where the first phase occurs when the increase in temperature causes thermal expansion and the second phase when the cooling of the block causes thermal contraction. The first phase shows a maximum compressive stress of 1.12 MPa at the core and a maximum tensile stress of 1.64 MPa at the bottom surface. The second phase shows a maximum compressive stress of 1.80 MPa at the top surface and a maximum tensile stress of 1.13 MPa at the core. The time and location dependent rise of high tensile stresses would surely cause cracking at the outer portions of the concrete block during the thermal expansion phase and at the inner core during the thermal contraction phase.

Further efforts to characterize the tensile strength of the Roman seawater concrete could be incorporated into a similar thermomechanical FE analysis utilizing damage based viscoelastic material models to better understand crack propagation.

8. REFERENCES

Adam, J.-P. (1994). Roman building: materials and techniques, trans. *A. Mathews, London*.

Ahrens, J., Geveci, B., & Law, C. (2005). Paraview: An end-user tool for large data visualization. *The Visualization Handbook*, *717*.

Bazant, Z. P., & Baweja, S. (2000). Creep and shrinkage prediction model for analysis and design of concrete structures: Model B3. *ACI Special Publications*, *194*, 1–84.

Brandon, C. J., Hohlfelder, R. L., Jackson, M. D., & Oleson, J. P. (2014). *Building for eternity: the history and technology of Roman concrete engineering in the sea*. Oxbow Books.

Casson, L. (1977). Ships and Seamanship in the Ancient World, *15*, 14.

Celik, K., Hay, R., Hargis, C. W., & Moon, J. (2019). Effect of volcanic ash pozzolan or limestone replacement on hydration of Portland cement. *Construction and Building Materials*, *197*, 803–812. https://doi.org/10.1016/J.CONBUILDMAT.2018.11.193

Céské Lupkové Závody. (n.d.). Mefisto L05 Data Sheet.

Cowper, A. D. (1927). Lime and Lime Mortars. *Dept. Sci. and Indus. Research Bldg. Research Bd. Spec. Rpt*, *9*, 81.

Damiani, V., Baudo, R., De Rosa, S., De Simone, R., Ferretti, O., Izzo, G., & Serena, F. (1987). A case study: Bay of Pozzuoli (Gulf of Naples, Italy). In *Ecological Effects of In Situ Sediment Contaminants* (pp. 201–211). Springer.

DeLaine, J. (1997). *The Baths of Caracalla: A Study in the Design, Construction, and Economics of Large-scale Building Projects in Imperial Rome*. Journal of Roman Archaeology. Retrieved from https://books.google.cz/books?id=-HQMAQAAMAAJ

DeLaine, Janet. (2002). Bricks and mortar: exploring the economics of building techniques at Rome and Ostia. In *Economies beyond agriculture in the classical world* (pp. 242–280). Routledge.

Faria, R., Azenha, M., & Figueiras, J. A. (2006). Modelling of concrete at early ages: Application to an externally restrained slab. *Cement and Concrete Composites*, *28*(6), 572–585.

Fedele, L., Insinga, D. D., Calvert, A. T., Morra, V., Perrotta, A., & Scarpati, C. (2011). 40 Ar/39 Ar dating of tuff vents in the Campi Flegrei caldera (southern Italy): toward a new chronostratigraphic reconstruction of the Holocene volcanic activity. *Bulletin of Volcanology*, *73*(9), 1323–1336.

Gazda, E. K., & McCann, A. M. (1987). Reconstruction and function: port, fishery, and villa. *McCann et Al*, 137–159.

Hassibi, M. (1999). An overview of lime slaking and factors that affect the process. In *3rd International Sorbalit Symposium, New Orleans* (pp. 1–20).

Heap, M. J., Kushnir, A. R. L., Griffiths, L., Wadsworth, F., Marmoni, G. M., Fiorucci, M., … Reuschlé, T. (2018). Fire resistance of the Mt. Epomeo Green Tuff, a widely-used building stone on Ischia Island (Italy). *Volcanica*, *1*, 33–48. https://doi.org/10.30909/vol.01.01.3348

Hohlfelder, R. L., Brandon, C., & Oleson, J. P. (2008). The Roman Maritime Concrete Study: A Brief Summary of Fieldwork from 2002 to 2005. *Memoirs of the American Academy in Rome. Supplementary Volumes*, *6*, 297–304. Retrieved from http://www.jstor.org/stable/40379308

Houston, J. R., Maxwell, R. S., & Carroll, S. A. (2009). Transformation of meta-stable calcium silicate hydrates to tobermorite: reaction kinetics and molecular structure from XRD and NMR spectroscopy. *Geochemical Transactions*, *10*(1), 1. https://doi.org/10.1186/1467-4866-10-1

Jackson, M. D., Chae, S. R., Mulcahy, S. R., Meral, C., Taylor, R., Li, P., … Vola, G. (2013). Unlocking the secrets of Al-tobermorite in Roman seawater concrete†. *American Mineralogist*, *98*(10), 1669–1687. https://doi.org/10.2138/am.2013.4484

Jackson, M. D., Moon, J., Gotti, E., Taylor, R., Chae, S. R., Kunz, M., … Monteiro, P. J. M. (2013). Material and Elastic Properties of Al-Tobermorite in Ancient Roman Seawater Concrete. *Journal of the American Ceramic Society*, *96*(8), 2598–2606. https://doi.org/10.1111/jace.12407

Jackson, M., R. Mulcahy, S., Chen, H., Li, Q., QinfeiLi, Cappelletti, P., & Wenk, H.-R. (2017). *Phillipsite and Al-tobermorite mineral cements produced through low-temperature water-rock reactions in Roman marine concrete. American Mineralogist* (Vol. 102). https://doi.org/10.2138/am-2017-5993CCBY

Jakobsson, S. P., & Moore, J. G. (1986). Hydrothermal minerals and alteration rates at Surtsey volcano, Iceland. *Geological Society of America Bulletin*, *97*(5), 648–659.

Jeong, J.-H., Zollinger, D., Lim, J.-S., & Park, J.-Y. (2012). Age and Moisture Effects on Thermal Expansion of Concrete Pavement Slabs. *Journal of Materials in Civil Engineering*, *24*, 8–15. https://doi.org/10.1061/(ASCE)MT.1943-5533.0000342

Lancaster, L. C. (2005). *Concrete vaulted construction in Imperial Rome: innovations in context*. Cambridge University Press.

Lewis, J. D. (1972). Controlled airlifting in sand-filled harbours. *International Journal of Nautical Archaeology*, *1*(1), 169–170.

M Neville, A. (1997). Properties of Concrete. John Wiley & Sons, Inc.

Manzano, H., Dolado, J. S., Guerrero, A., & Ayuela, A. (2007). Mechanical properties of crystalline calcium-silicate-hydrates: comparison with cementitious C-S-H gels. *Physica Status Solidi (A)*, *204*(6), 1775–1780.

Massazza, F. (2002). Properties and applications of natural pozzolanas. *Structure and Performance of Cements*, 326–352.

Massazza, Franco. (1998). Pozzolana and pozzolanic cements. *Lea's Chemistry of Cement and Concrete*, *4*, 471–636.

Meteostat. (n.d.). Climate Data - Naples, Italy. Retrieved from https://meteostat.net/en/station/16289

Meyer, C. (2009). The greening of the concrete industry. *Cement and Concrete Composites*, *31*(8), 601–605.

Mitsuda, T., Sasaki, K., & Ishida, H. (1992). Phase evolution during autoclaving process of aerated concrete. *Journal of the American Ceramic Society*, *75*(7), 1858–1863.

Moropoulou, A., Bakolas, A., & Aggelakopoulou, E. (2001). The effects of limestone characteristics and calcination temperature to the reactivity of the quicklime. *Cement and Concrete Research*, *31*(4), 633–639.

National Lime Association. (n.d.). Properties of Typical Commercial Lime Products. https://www.lime.org/documents/lime_basics/lime-physical-chemical.pdf.

Oh, J. E., Clark, S. M., & Monteiro, P. J. M. (2011). Does the Al substitution in C–S–H (I) change its mechanical property? *Cement and Concrete Research*, *41*(1), 102–106.

Oleson, J., Brandon, C., Cramer, S., Cucitore, R., Gotti, E., & Hohlfelder, R. (2004). *The ROMACONS Project: A Contribution to the Historical and Engineering Analysis of Hydraulic Concrete in Roman Maritime Structures*. International Journal of Nautical Archaeology (Vol. 33). https://doi.org/10.1111/j.1095-9270.2004.00020.x

Oleson, J. P., Bottalico, L., Brandon, C., Cucitore, R., Gotti, E., & Hohlfelder, R. L. (2006). Reproducing a Roman maritime structure with Vitruvian pozzolanic concrete. *Journal of Roman Archaeology*, *19*, 29–52.

Patzák, B. (2012). OOFEM - an object-oriented simulation tool for advanced modeling of materials and structures. *Acta Polytechnica*, *52*(6), 59–66.

Pellenq, R. J.-M., Kushima, A., Shahsavari, R., Van Vliet, K. J., Buehler, M. J., Yip, S., & Ulm, F.-J. (2009). A realistic molecular model of cement hydrates. *Proceedings of the National Academy of Sciences*, *106*(38), 16102–16107.

Rowland, I. D., & Howe, T. N. (2001). *Vitruvius:'Ten Books on Architecture'*. Cambridge University Press.

Ryan, J. F. (1929). The story of Portland cement. *Journal of Chemical Education*, *6*(11), 1854.

Sabbioni, C., Bonazza, A., & Zappia, G. (2002). Damage on hydraulic mortars: the Venice Arsenal. *Journal of Cultural Heritage*, *3*(1), 83–88.

Sabir, B. ., Wild, S., & Bai, J. (2001). Metakaolin and calcined clays as pozzolans for concrete: a review. *Cement and Concrete Composites*, *23*(6), 441–454. https://doi.org/10.1016/S0958-9465(00)00092-5

Seatemperature.org. (n.d.). Pozzuoli Sea Temperature.

Shi, C. (2001). An overview on the activation of reactivity of natural pozzolans. *Canadian Journal of Civil Engineering*, *28*(5), 778–786. https://doi.org/10.1139/l01-041

Shi, C., & Day, R. L. (1993). Acceleration of strength gain of lime-pozzolan cements by thermal activation. *Cement and Concrete Research*, *23*(4), 824–832.

Šmilauer, V., Baquerizo, L., Matschei, T., Havlásek, P., Silva, W. R., & Hájková, K. (2016). ConTemp - A virtual thermo-mechanical simulator for hydrating reinforced concrete blocks with extension to service life. In *International RILEM Conference on Materials, Systems and Structures in Civil Engineering*.

Taylor, R., Richardson, I. G., & Brydson, R. M. D. (2010). Composition and microstructure of 20-year-old ordinary Portland cement–ground granulated blast-furnace slag blends containing 0 to 100% slag. *Cement and Concrete Research*, *40*(7), 971–983.

Vola, G., Gotti, E., Brandon, C., Oleson, J. P., & Hohlfelder, R. L. (2011). Chemical, mineralogical and petrographic characterization of Roman ancient hydraulic concretes cores from Santa Liberata, Italy, and Caesarea Palestinae, Israel. *Periodico Di Mineralogia*, *80*(2), 317–338.

Waller, V., De Larrard, F., & Roussel, P. (1996). Modelling the temperature rise in massive HPC structures. In *4th International Symposium on Utilization of High-Strength/High-Performance Concrete* (pp. 415–421). RILEM SARL Paris.